Progress in Energy and Combustion Science 100 (2024) 101131

Contents lists available at ScienceDirect

Progress in Energy and Combustion Science

journal homepage: www.elsevier.com/locate/pecs

Alkali metal release in thermochemical conversion of biomass and coal: Optical measurements and modeling

Zhihua Wang [a,*], Siyu Liu [a], Wubin Weng [a], Yong He [a], Marcus Aldén [b], Zhongshan Li [b,**]

[a] State Key Laboratory of Clean Energy Utilization, Zhejiang University, 310027, Hangzhou, China
[b] Division of Combustion Physics, Lund University, P.O. Box 118, S-22100, Lund, Sweden

ARTICLE INFO

Handling Editor: Christof Schultz

Keywords:
Alkali metals
Optical measurement
Release characteristics
Modeling
Biomass
Coal

ABSTRACT

Alkali metals, mainly K and Na, which are present in solid fuels such as biomass and coal, play an important role during their thermal conversion, e.g., in combustion or gasification. At high temperatures, alkali elements will be released in gas phase as alkali atoms, alkali chlorides, alkali hydroxides and alkali sulphates. In biomass/coal-fired boilers, the release of these alkali species can cause problems such as corrosion, slagging and fouling, threatening the safe operation of the facilities. The information on the release dynamic is important for developing proper models for alkali metal transformation in solid fuel combustion and gasification. Therefore, accurate quantitative measurements of the release of different alkali species during thermal-chemical conversion processes of biomass/coal are important. In this paper, we review literatures published over the last few decades in the field of quantitative optical measurements of alkali metals performed in combustion/gasification processes, and the release modeling based on those optical measurements. Firstly, the current situation of biomass and coal utilization is discussed, including the speciation of alkali metals in biomass/coal and their adverse effects on facilities. Secondly, requirements for optical measurements as well as several quantitative optical techniques are introduced including the general principles, typical setups, calibration methods and major advantages and drawbacks. In contrast to off-line techniques, these optical techniques provide nonintrusive measurements with high temporal and spatial resolution, which are indispensable for alkali release modeling. Furthermore, the alkali release behaviors based on optical measurements in thermochemical conversion processes are discussed. Based on the experimental results, the kinetic data for alkali release were summarized. Alkali release modeling was fulfilled relying on the knowledge of alkali release mechanisms and the kinetic data. In addition, simulations of alkali metal release with computational fluid dynamics during the biomass/coal combustion processes are also discussed, providing valuable information for industrial processes. Finally, typical examples of industrial applications of optical measurement methods in solid fuel thermochemical conversion processes as well as waste incineration and other processes are presented.

1. Introduction

1.1. Biomass and coal

Energy supply is always an important issue for the economic and social development of human society. The usage of biomass and coal through thermochemical conversion processes has played important roles in heat and power supply. Fig. 1 shows the global primary energy consumption in the past 30 years and an outlook of energy consumption for the coming decades according to the statistics and estimation from Energy Institution (EI) [1] and British Petroleum (BP) [2], respectively. As can be seen, the utilization of coal accounts for nearly one-third of fossil fuel consumption, which means it's still the major primary energy in the current world. However, due to global warming and climate change, greenhouse gas (GHG) emissions from each country need to be strictly regulated according to the Paris Agreement at the Conference of Parties 21 (COP21) in 2015. The CO_2 generated from fossil fuel consumption is the major contributor to GHG emissions. Currently, many countries declare to reduce GHG emissions and intend to achieve "zero carbon emission" or "carbon neutral emission" around 2050–2060. Therefore, it can be predicted that the global energy supply and

* Corresponding author.
** Corresponding author.
E-mail addresses: wangzh@zju.edu.cn (Z. Wang), zhongshan.li@forbrf.lth.se (Z. Li).

https://doi.org/10.1016/j.pecs.2023.101131
Received 30 May 2023; Received in revised form 4 August 2023; Accepted 22 September 2023
Available online 30 November 2023

List of acronyms

AAS	Atomic absorption spectroscopy
AES	Atomic emission spectroscopy
BAS	Broadband absorption spectroscopy
BFB	Bubbling fluidized bed
CFB	Circulating fluidized bed
CFD	Computational fluid dynamics
CLC	Chemical looping combustion
CPD	Chemical percolation devolatilization
CPFAAS	Collinear photofragmentation and atomic absorption spectroscopy
DNS	Direct numerical simulation
EDC	Eddy dissipation concept
EFR	Entrained flow reactor
FB	Fluidized bed
FGM	Flamelet generated manifolds
FOAM	Fiber-optic alkali monitor
FWHM	Full width at half maximum
ICCD	Intensified charge-coupled device
ICP	Inductively coupled plasma
LAI	Laser absorption imaging
LAT	Laser absorption tomography
LES	Large eddy simulation
LIBS	Laser-induced breakdown spectroscopy
LIF	Laser-induced fluorescence
LIPF	Laser-induced photofragmentation fluorescence
LOS	Line-of-sight
MSW	Municiple solid waste
PaSR	Partially stirred reactor
PCFB	Pressurized circulating fluidized bed
PFF	Pulverized fuel furnace
PCB	Pulverized coal boiler
PF-TDLAS	Photofragmentation tunable diode laser absorption spectroscopy
PLIF	Planar laser-induced fluorescence
PMT	Photomultiplier tube
TDLAS	Tunable diode laser absorption spectroscopy
XRD	X-ray diffraction

Uppercase symbols

A_K	Pre-exponential factor of potassium release (s^{-1})
A_{Na}	Pre-exponential factor of sodium release (s^{-1})
A_{21}	Einstein coefficient for spontaneous emission (s^{-1})
$(B_F)_{max}$	Maximum fluorescence radiance
C	Constant relating to efficiency of optical components
C_M	Radial concentration distribution of alkali metals (mg/m^3)
$E_i^{(j)}$	Upper-level energy of species i
E_K	Activation energy of potassium release (kJ/mol)
E_{Na}	Activation energy of sodium release (kJ/mol)
I	Transmitted light intensity
I_0	Incident light intensity
L	Optical path length (m)
M_{KOH}	Molecular weight (kg/kmol)
$M_{flux,t}$	Alkali flux at time of t (mg/s)
N	Number density ($molecule/m^3$)
p	Pressure (bar)
p_{KOH}	Vapor pressure of KOH (bar)
Q	Quenching rate of atoms at excited state (s^{-1})
Q_{KOH}	Total mass of KOH released (mg)
R	Universal gas constant (8.314 J/mol K)
S	Signal intensity
T	Temperature (K)
$W_{Na,at}$	Total flow of atomic sodium (mol/s)
X_{KCl}	Concentration of KCl (ppm)

Lowercase symbols

c	Speed of light (m/s)
d_o	Initial diameter of particles (mm)
$g_i^{(j)}$	Statistical weight of species i at upper energy level j
h	Planck constant (6.62×10^{-34} J s)
k	Boltzmann constant (1.38×10^{-23} J/K)
k_v	Rate constant of devolatilization stage (s^{-1})
k_c	Rate constant of char combustion stage (s^{-1})
$k_{c,Na}$	Rate constant of sodium release during char combustion stage (s^{-1})
l	Depth of fluorescence volume in observation direction (m)
n_T	Atom concentration (ppm)
r	Radius (m)
t	Time (s)
u	Velocity (m/s)

Greek symbols

αL_{max}	Maximum absorption of fragment potassium atoms
γ	Photofragmentation efficiency
λ	Wavelength (mm)
υ	Frequency (GHz)
ρ	Density (kg/m^3)
σ	Absorption cross-section of target species (m^2/molecule)
Γ	Mass diffusivity of KOH in the medium (m^2/s)
Φ	Quantum yield of photofragmentation

consumption patterns will dramatically change in the near future, characterized by a reduction in fossil fuel utilization and an increase in the utilization of renewables and low-carbon, or even carbon-free fuels. As a type of renewable fuel, biomass has similar properties to coal, especially low-rank coal, which means its utilization does not require a complete replacement of the existing facilities for fossil fuels. Besides, biomass can supply stable energy sources compared with intermittent wind and solar power, which is beneficial for the power grid. It can be deduced biomass energy will definitely play a more and more important role in the future. According to the BP energy outlook 2023 [2], the proportion of renewables in global primary energy consumption will reach 34.8 % in 2050, where bioenergy accounts for 27.3 % of renewables.

Biomass refers to all solid organic materials derived from sources such as plants and their products, animal biomass, and waste. When biomass is used as fuel, the carbon inside reacts with oxygen and generates CO_2, whose amount is equivalent to the amount absorbed through photosynthesis. Thus, biomass is regarded as a carbon-neutral fuel and becomes more and more attractive as an alternative fuel to fossil fuels in thermochemical conversion processes, e.g., combustion and gasification. An important issue that cannot be ignored is the time lag between the direct CO_2 release while utilizing biomass in combustion and gasification processes and its eventual consumption by existing forests and newly growing plants. This temporary portion of CO_2 emissions also contributes to climate change [3]. One of the obvious mitigation methods is to improve the efficiency of thermal conversion processes or even adopt alternative low-carbon-emission conversion techniques, but there is still a long way to go. Another strategy is to utilize biomass residues and waste instead of standing trees harvested from forests as fuel. This approach does not deplete current carbon stocks. Through planting new fast-growing crops as a supplement, the emitted CO_2 can be quickly consumed. These fast-growing crops can also

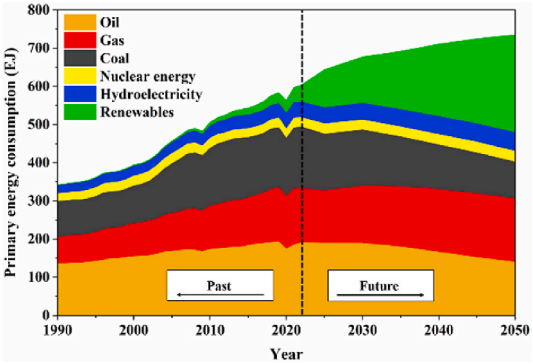

Fig. 1. Global primary energy consumption in the past 30 years and an outlook. (Data from EI Statistical Review of World Energy 2023 [1] and BP energy outlook 2023 [2]).

serve as a reliable source of biomass fuel. Additionally, by combining this approach with carbon capture and storage (CCS), there is a potential possibility to achieve negative CO_2 emissions in combustion and gasification [4,5].

Considering biomass is worldwide distributed and can be obtained from wood and woody residues, agricultural residues, aquatic plants, waste, etc. [6], their properties vary a lot. However, in general, biomass has very high moisture contents and low carbon content, causing lower heating values and lower energy density compared with conventional fossil fuels. At the same time, biomass usually has a variety of minor constituents, such as chlorine, sulfur, phosphorus, nitrogen, and ash-forming metals like alkali metals, and many challenges connected with biomass utilization are caused by these constituents [7]. One of the major challenges while utilizing biomass is its high amount of alkali metals, especially potassium, whose release during thermochemistry processes can cause serious problems such as fouling, slagging, and corrosion. These problems pose a significant obstacle to the safe and effective utilization of biomass in the industry [8]. Knowledge about the alkali release characteristics during utilization processes is an indispensable step toward addressing these issues.

Some low-rank coals with large reserves but enriched with alkali metals (mainly sodium), such as Zhundong coal in China, and Loy Yang coal in Australia, are also facing similar problems arising from alkali metals as biomass does. Coal is a kind of fossil fuel with complex components that vary from each other. Due to the rich global reserve and low price, it has been used for a long time in different industries, such as steel, power, chemistry, paper and textile, etc. Most of these utilizations are based on thermochemical conversion processes. The striving to get rid of the use of fossil fuels is underway, however, it is something that takes time. As can be seen from Fig. 1, the consumption of coal keeps growing in the past 30 years. In the power generation industry, coal remains the dominant fuel with a stable share of around 35 % [1]. Additionally, coal accounts for the largest primary energy consumption in the Asia-Pacific region with a share of nearly 50 %. Keep improving the safety and efficiency of coal utilization is still a meaningful issue for the current global energy system. The huge reserves of high-alkali coal can largely meet the demand for coal supply, but it is necessary to solve alkali-induced problems. Understandings on alkali release behavior in combustion and gasification processes of coal is one of the key factors to overcome these problems.

1.2. Alkali metals

1.2.1. Alkali content in biomass and coal

The content of alkali metals, i.e. potassium (K) and sodium (Na), in biomass and coal varies a lot among different fuel species. Most coals have an alkali content below 0.01 % by weight. However, in some low-rank lignite and sub-bituminous coal, such as Zhundong coal, the sodium amount can be up to 0.3–0.7 % by weight and over 10 % expressed by Na_2O in ash. The variation in alkali content of biomass is greater than that of coal. Biomass usually contains a very high level of potassium, as potassium is the main nutrient for plant growth. Since the potassium in the soil will be absorbed by plants through the root system as a nutrient and transported to all areas of the plant, like leaves, trunk, bark, etc., the alkali content level varies greatly depending on biomass category and growing environments. Table 1 lists the alkali content in different species of coal and biomass. As can be seen, the potassium content in herbaceous and agricultural residues is generally higher than that in wood and woody residues. Even among wood and woody biomass, there are differences in potassium content, with bark typically having higher potassium content compared to wood. Besides, the influence of the growing environment on the alkali content in biomass is also significant. While most plants contain more potassium than sodium, marine algae have a significantly higher content of sodium than potassium. Many studies found that the variations contents of alkali and other minor elements like Al, Si, and Ca would affect the release behavior of alkali metals. Therefore, the variation of alkali content, as well as other ash-forming elements in biomass and coal, is also expressed by ash composition as shown in Table 2. Similar to the raw fuel, the content of alkali elements in the ash also exhibits varying features depending on the fuel type. The K_2O and SiO_2 contents in the ash of herbaceous and agricultural biomass like grasses and straws are more than twice as much as those of wood and woody biomass, while the CaO content is much lower. The Zhundong coal and Loy Yang coal have similar Na_2O content, but there is a significant difference in the content of Al_2O_3 and CaO.

1.2.2. Original chemical forms of alkali species in biomass and coal

Generally, the alkali species in biomass and coal can be divided into two types, i.e., organic compounds and inorganic compounds. Further determination of their forms in biomass and coal can be investigated using sequential extraction procedures with water, ammonium acetate solution and hydrochloric acid solution, respectively [30,31]. The water-soluble (H_2O-soluble) compounds of alkali metals are those present as ions held by water inside the biomass and coal pore structure existing as water-soluble salts. The ammonium acetate-soluble (NH_4Ac-soluble) compounds are those present as exchangeable ions which are organically boned with carboxyl groups of biomass and coal. The hydrochloric acid-soluble (HCl-soluble) compounds are those present as coordinated metal ions which are organically bonded with nitrogen- or oxygen-containing functional groups of biomass and coal. The acid-insoluble compounds are those present as silicate minerals. Generally, inorganic alkali salts in biomass and coal are water-soluble compounds and organic alkali species may dissolve in water or ammonium acetate solution. Minerals containing alkali metals will dissolve in hydrochloric acid solution or be insoluble in any solution. The alkali content of different occurrence forms in coal varies with coal rank. Typically, water-soluble alkali decreases with the degree of coalification while insoluble-alkali compounds show the opposite tendency. As for biomass, alkali metals are primarily organically associated or present as alkali salts and their contents vary with different types of biomass [32,33]. Werkelin et al. [34] analyzed the chemical forms of ash-forming elements in eighteen varieties of woody biomass and found potassium and sodium were mainly present as water-soluble substances. Vassilev et al. [35] found that the content of water-soluble alkali in herbaceous and agricultural biomass was much more abundant than that in wood and woody biomass. Besides, the amount of water-soluble alkali in coal was normally lower than in biomass.

Alkali release characteristics during combustion and gasification processes are strongly related to its chemical forms in raw fuels. It is generally believed that with increasing combustion temperature, the release ability of alkali metals will be enhanced, among which, the release of alkali metals mainly comes from water-soluble and NH_4Ac-soluble alkali metals, while the HCl-soluble and insoluble alkali metals

Table 1
Alkali content in the raw materials of different biomass and coal. (wt.%, dry basis).

Biomass groups	Biomass sub-groups	Species	K	Na	Reference
Wood and woody biomass	Wood	Spruce	0.021	0.0005	[9]
		Pine	0.04–0.09	0.015–0.03	[9,10]
		Birch	0.032	0.0004	[9]
		Beech	0.016	0.0045	[9]
		Aspen	0.14	0.0016	[9]
		Poplar	0.709	–	[11]
		Willow	0.341	0.008	[12]
	Bark	Spruce	0.20	0.002	[9]
		Pine	0.32	0.003	[9]
		Birch	0.17	0.0014	[9]
		Aspen	0.47	0.0012	[9]
	Twigs	Spruce	0.36	0.01	[9]
		Pine	0.304	0.0037	[9]
		Birch	0.303	0.0043	[9]
		Aspen	0.59	0.0022	[9]
	Needles	Spruce	0.43	0.0049	[9]
		Pine	0.48	0.0027	[9]
	Shoots	Spruce	1.46	0.0015	[9]
		Pine	0.88	0.0035	[9]
	Leaves	Birch	0.94	0.0035	[9]
		Aspen	2.39	–	[9]
	Sawdust	Pine	0.05	0.002	[13]
		Bamboo	0.03	0.004	[14]
		Sawdust	0.013	0.002	[15,16]
Herbaceous and agricultural biomass	Straw	Corn straw	1.31	–	[11]
		Barley straw	1.67	0.008	[9]
		Rice straw	2.42	0.007	[17]
		Wheat straw	1.32	0.039	[13,18]
		Flax straw	0.515	0.013	[13]
	Grass	Switchgrass	0.64	0.030	[9]
		Reed canarygrass	0.348	0.015	[13]
		Kenaf grass	0.72	0.052	[13]
		Miscanthus	0.64	0.014	[13]
		Cane	0.97	0.018	[13]
	Other residues	Corn cobs	0.82	0.024	[9]
		Rice husks	0.64	0.029	[9]
		Sunflower shells	1.005	0.023	[9]
		Walnut shells	0.98	0.023	[9]
		Plum pits	0.64	0.006	[9]
		Rapeseeds	0.577	0.014	[13]
Aquatic biomass	Algae	Freshwater algae	0.59–1.08	0.23–0.51	[19]
		Marine algae	0.39–1.03	0.40–10.86	[19]
Waste	Black liquor		0.62	22.7	[20]
	Sewage sludge		0.33	0.68	[21]
	Municipal solid waste mixture		0.95	0.72	[22]
Coal	Lignite	Zhundong coal	0.044	0.74	[23,24]
		Loy Yang coal	0.005	0.09	[25,26]
		Beulah coal	–	0.57	[27]
		San Miguel coal	–	1.97	[27]
	Sub-bituminous	Eagle Butte coal	0.04	0.1	[27]

Table 2
Ash composition of different biomass and coal (wt.%).

	K_2O	Na_2O	SiO_2	Al_2O_3	CaO	MaO	Reference
Wood and woody biomass	10.75	2.85	22.22	5.09	43.03	6.07	[28]
Grasses	24.59	1.25	46.18	1.39	11.23	4.02	[28]
Straws	24.49	1.35	43.94	2.71	14.13	4.66	[28]
Other residues	28.25	3.05	24.47	4.90	16.58	6.62	[28]
Waste	3.45	1.90	35.73	15.41	18.30	1.90	[28]
Zhundong coal	0.40	10.87	10.79	9.62	36.82	9.20	[23]
Loy Yang coal	0.77	11.30	12.90	31.40	5.60	12.20	[29]

are almost not released. The above four chemical forms of alkali metals can be converted into each other during thermochemical conversion processes. Zhang et al. [18] studied potassium occurrence and release characteristics and found that NH_4Ac-soluble potassium would convert into water-soluble potassium as the temperature rises. At higher combustion temperatures, water-soluble alkali metals can react with silico-aluminate mineral composition inside the fuel forming insoluble types of alkali metals [31].

1.2.3. Release and transformation of alkali species during thermochemical conversion

Understanding the alkali release and transformation behavior during thermochemical conversion processes is the premise for the technology development concerning alkali-related operation problems. Potassium is the most important alkali metal in biomass while sodium is the most important one in coal. Compared with coal, a much higher proportion of alkali species bonded in biomass will be released to gas phase, due to its

mobile alkali composition forms [36]. During the combustion/gasification process, a portion of the alkali metal in the fuel is released in the form of vapor phase, where it remains gas phase until condensing on the surface of the heat exchanger after cooling down. The chemical forms of the released alkali metals are varied depending on fuel compositions and environmental conditions. Inorganic alkali metals in fuels, such as alkali chloride, can be directly released into the atmosphere. Organic alkali metals will be oxidized and decomposed into alkali atoms and alkali hydroxides. In addition, a portion of the alkali metals may react with substances such as Si and Al in the fuel, resulting in the formation of aluminosilicates which are difficult to release. During the cooling process, the released alkali components will condense, contributing to aerosol formation and causing operational problems such as deposit formation. The fate of the alkali metals before condensation would depend on their interactions with sulfur, chlorine, oxygen, and radicals in the gas phase environment. Chlorine and sulfur in the fuel can increase the mobility of sodium and potassium and thus facilitate alkali release as alkali chlorides and alkali sulfates during combustion. Adequate oxygen in the environment could oxidize alkali atoms into alkali hydroxides. On the contrary, in a reducing atmosphere, the presence of H radicals could reduce alkali hydroxides back into alkali atoms. In addition, reaction pressure and temperature will also affect alkali transformation paths and rates [37]. Under low temperatures, both potassium and sodium have a very low release level, while the release increases with temperature rising. Although the release characteristics of potassium and sodium are generally similar and can be analogized, their behaviors may vary slightly due to differences in the physical properties of their species. A relatively higher release of sodium compared with potassium has been reported because of the lower sublimation temperature of NaCl than KCl [38]. A schematic diagram of alkali release and transformation during biomass and coal combustion process is shown in Fig. 2, including typical optical methods that can be utilized to achieve online measurements of the critical gaseous alkali species. Detailed release mechanism based on experimental results are discussed in Section 3.1.

1.3. Alkali metal caused problems

In biomass and coal thermochemical conversion processes, part of alkali metals will release as gas phase into the hot flue, resulting in a variety of problems such as slagging and fouling, agglomeration, and corrosion. Fig. 3 shows images of slagging, agglomeration, and corrosion caused by high alkali biomass. Those problems significantly affect the heat transfer efficiency of the boiler, and even threaten the safe utilization of industrial facilities [39].

Alkali-induced slagging and fouling are attributed to the low melting temperature of alkali compounds formed in thermochemical conversion processes [7]. Wu et al. [44] compared slagging and deposition tendencies between coals with different alkali content. The results are shown in Fig. 4. Obviously, coal with higher alkali content is easier to cause slagging. In addition, speciation of alkali metals is of great importance in terms of slagging propensity since it will affect ash fusion temperature [45–48]. Studies on biomass show that biomass with high K_2O, P_2O_5, SO_3, Cl_2O content is classified as low acidity biomass and has

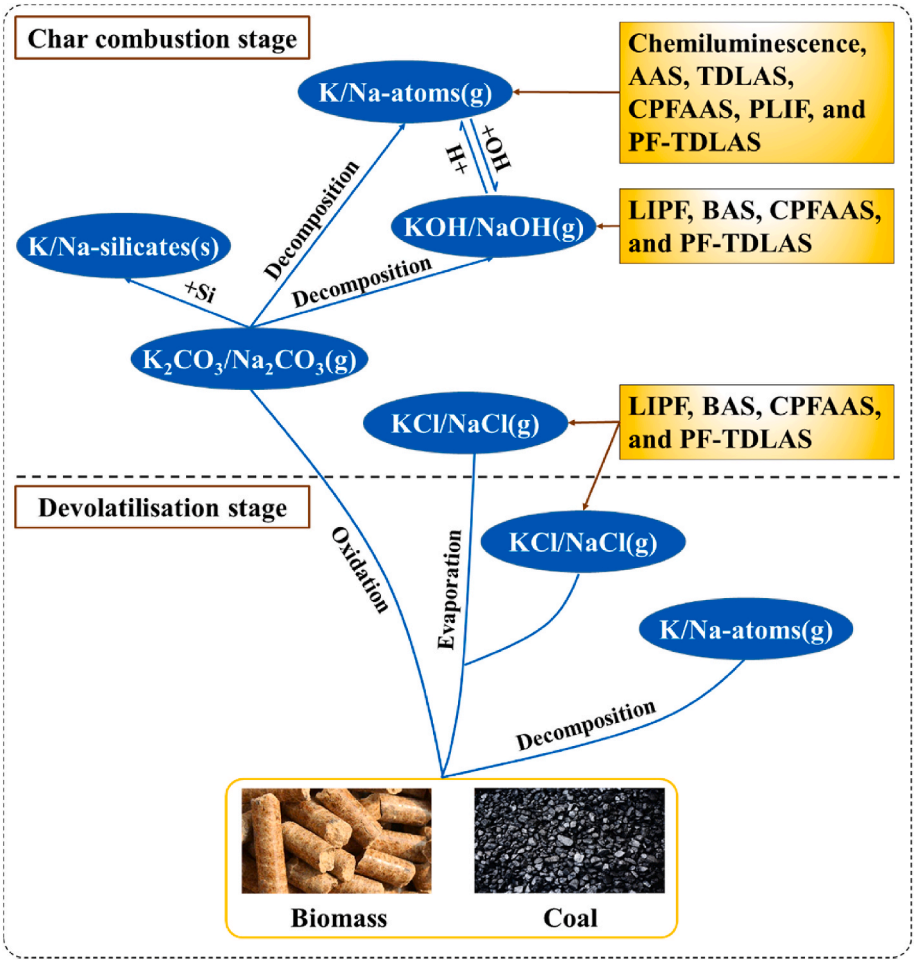

Fig. 2. Alkali transformation during biomass and coal combustion process. Main gaseous alkali species are involved accompanied by corresponding *in situ* optical techniques.

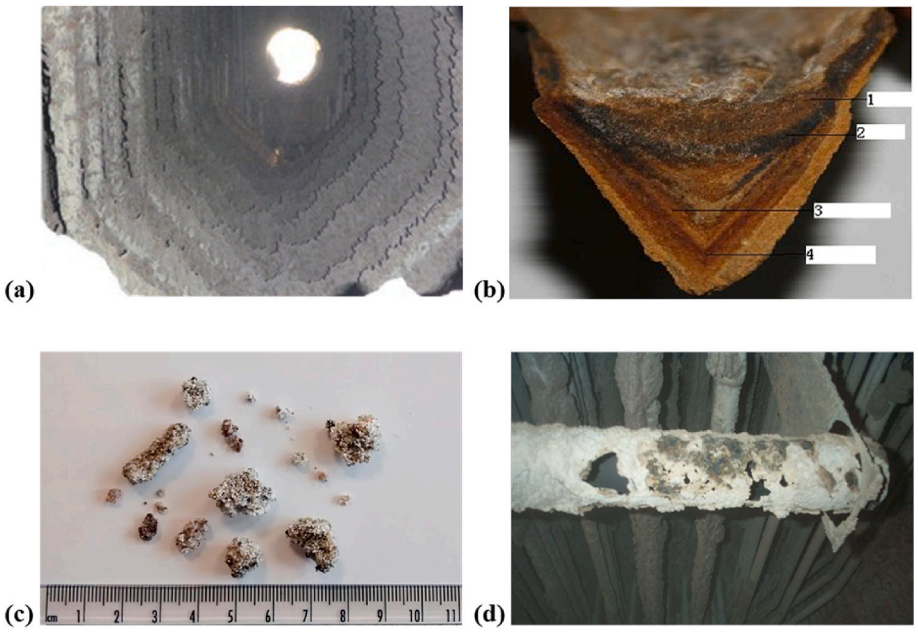

Fig. 3. (a) and (b) Images of alkali-induce slagging. Reproduced from Li et al. [40] Copyright (2013): Elsevier. and Niu et al. [41] Copyright (2014): Elsevier. (c) Image of agglomeration of bed materials in a fluidized bed (FB) boiler. Reproduced from Morris et al. [42] Copyright (2018): Elsevier. (d) Images of alkali-induced corrosion. Reproduced from Bowie et al. [43] Copyright (2006): Elsevier.

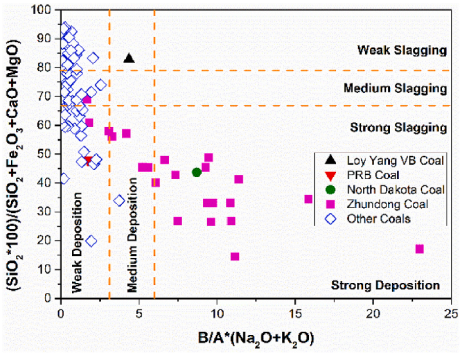

Fig. 4. Slagging and deposition tendency between coals with different alkali content. The B/A value refers to the ratio of basic to acidic oxides. Reproduced from Wu et al. [44] Copyright (2016): Elsevier.

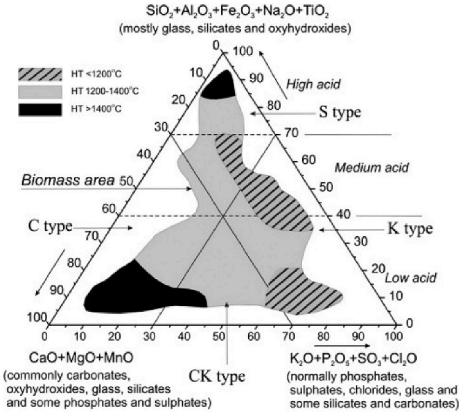

Fig. 5. Ash-fusion temperatures of 60 varieties of biomass with different ash compositions. HT represents hemispherical temperature. Reproduced from Vassilev et al. [47] Copyright (2015): Elsevier.

a higher slagging propensity, while biomass with high Na_2O, SiO_2, Al_2O_3, Fe_2O_3, TiO_2 content is categorized in high acidity biomass and has a lower slagging propensity as shown in Fig. 5.

A detailed mechanism based on the experimental results was proposed to account for the formation and growth of the slagging layer [41]. This issue is mainly associated with alkali chlorides and alkali sulfates [49,50]. During thermal conversion processes, alkali compounds will directly release in the form of alkali vapor. Chlorine is shown to be a major factor in slagging formation, as it facilitates the mobility of potassium to form potassium chlorides, which are among the most stable, gas-phase, alkali-containing species [33]. Another important factor is sulfur which promotes the transformation to alkali sulfates. Due to the low melting temperatures, alkali chlorides and sulfates condense on the heating surface at lower flue gas temperatures, causing the formation of an initial sticky layer. Fine particles containing alkali metals, chlorine, and sulfur deposit on the initial layer, and capture coarse large particles. The fine particles undergo re-enrichment to maintain their ability of capturing large particles. Thus, slagging structures characterized by multilayers were observed, as shown in Fig. 3(b). The slag layer eventually bonds tightly to the surface and causes a serious safety risk to the facilities.

In addition, alkali inherent in fuel and ash may lead to bed agglomeration in fluidized bed (FB) units, which may result in defluidization and even in a costly shutdown of the whole facility [51]. Two principal mechanisms of agglomeration were put forward: i.e. coating-induced agglomeration and melt-induced agglomeration [42]. Coating-induced agglomeration is defined by the interaction of alkali metals in fuel ash with silica in the bed material to form an alkali silicate melt. Melt-induced agglomeration is defined by the presence of sufficient amounts of alkali metals and silica in the fuel ash which together form a eutectic melt. Prediction of agglomeration propensity and path requires knowledge about alkali behavior under high temperatures. Agglomeration may also occur in chemical looping combustion (CLC) [52]. Different from that in FB, agglomeration was caused mainly through the melt-induced path, since the oxygen carrier generally doesn't contain silicon.

Alkali-induced corrosion is mainly related to alkali chlorides, which are highly corrosive, especially under high temperatures. Alloy

materials like chromium (Cr) have been frequently added in Fe- and Ni-based alloys to prohibit high-temperature corrosion. However, alkali chlorides are known to easily react with Cr to form chromium chlorides and Cl_2, which destroys the protective chromium oxide layer on stainless steels [53]. Then Cl_2 can directly react with the bare metal surface, leading to the corrosion of the materials. One of the possible ways to mitigate high-temperature corrosion is to transfer alkali chlorides to alkali sulfates, which are less problematic [54,55].

1.4. Scope of article

As introduced above, alkali-induced problems affect the safe and efficient utilization of biomass and coal. To mitigate these issues, knowledge about alkali behaviors during thermal conversion processes is necessary. Besides, kinetic data for alkali release during fuel combustion and gasification processes are needed to develop alkali release mechanisms as well as models for numerical simulations. The alkali release behaviors are closely related to fuel compositions and reaction environments. The alkali content and chemical forms inherent in raw fuels, the presence of chlorine, sulfur, silicon, aluminum, calcium, etc., reaction temperatures and operating conditions will all affect alkali release fates. Optical diagnostics can provide in situ quantitative data with a temporal resolution, which provides insights into the whole reaction process with the above variables and an effective way to acquire kinetic data. In this work, we review the optical diagnostic methods for various alkali species measurements (Chapter 2). The development of release mechanisms as well as modeling works based on optical measurements are then summarized in Chapter 3. In Chapter 4, we put emphasis on the industrial applications of these optical techniques. Finally, an outlook for the further development and applications of these optical techniques is released in Chapter 5.

2. Optical measurement methods and applications

For optimized utilization of biomass and coal, a comprehension understanding of the release and reaction of alkali metals is needed. Typical off-line methods such as X-ray diffraction (XRD) and inductively coupled plasma (ICP) can analyze the contents of alkali metals in the solid phase after time-consumed pretreatment. But the time-resolved release dynamic can be hardly obtained especially along with the thermochemical process. Although the amount of alkali metals can be determined before and after the reaction process, it is still far away from the requirement for the development of kinetic modeling. *In situ* or online measurements of alkali metal release during the thermochemical reaction process are needed. Nonintrusive optical methods can provide qualitative and quantitative information on alkali metal release with high temporal and spatial resolution, which have been quickly developed in the past thirty years.

Optical techniques based on absorption or emission spectroscopy are the most commonly used methods for monitoring alkali species like atoms and molecules. In addition, plasma induced by high energy laser pulse has also been employed to measure the release of total alkali elements during the combustion process. A summary of the cutting-edge optical methods developed and applied for *in situ* alkali measurements during thermal conversion processes of biomass and coal is shown in Table 3. The principles and applications of these techniques are introduced in the subsequent section. Additionally, Fig. 6 summarized the optical methods with an emphasis on their emerging years and spatial resolution ability. As can be seen, many methods with spatial resolution have been developed in recent ten years. It is worth mentioning that some long-standing methods have been developed to achieve spatial resolution, such as TDLAS. This, on the one hand, is due to the rapid advancement of imaging technology. But more importantly, it is pivotal to acquire spatial-resolved information, as this information is crucial for the development and validation of alkali metal release mechanisms, chemical kinetic models, and numerical simulation methods.

Table 3
Overview of main features of quantitative optical methods for alkali monitoring.

Method	Detected species	Detected phase	Calibration[a]	Lower detection limits[b]	Spatial resolution in lab-scale	Spatial resolution in large-scale	Application in large-scale
AAS	Alkali atoms	Gas phase	No	1 ppb	LOS	LOS	/
TDLAS	Alkali atoms	Gas phase	No	0.8 ppb	LOS (except LAI[c])	LOS	PCB, EFR
BAS	Alkali hydroxides, alkali chlorides	Gas phase	No	500 ppm for KOH, 250 ppm for KCl	LOS	LOS	CFB, BFB
CPFAAS	Alkali atoms, alkali hydroxides, alkali chlorides	Gas phase	No	100 ppb for KOH, 500 ppb for KCl, 1 ppb for K-atom	LOS	LOS	Oxy-fuel combustor fired coal and gas fuel
PF-TDLAS	Alkali atoms, alkali hydroxides, alkali chlorides	Gas phase	No	18 ppb for KOH, 32 ppb for KCl, 6 ppb for K-atom	LOS (except PF-LAI[c])	LOS	EFR, oxy-fuel combustor
AES	Alkali atoms	Gas phase	Yes	0.1 ppm	Single point, 2D	Single point	PFF, MSW incinerator
LIF	Alkali atoms	Gas phase	Yes	8 ppm	2D	No report yet	No report yet
LIPF	Alkali hydroxides, alkali chlorides	Gas phase	Yes	250 ppb for KOH, 500 ppb for KCl	Single point, 2D	Single point	EFR, PCB, FB, PFBC
LIBS	Total alkali elements	Gas phase and particle phase[e]	Yes	29 ppb for Na, 72 ppb for K	Single point, 1D	Single point	Grate boiler, recovery boiler, blast boiler, cement plant, glass furnace

[d] Through low laser fluence.
[a] Requirement for a separate calibration procedure. No: no calibration required; Yes: calibration required.
[b] The detection limits of absorption-based methods were estimated with an optical path length of 1 cm.
[c] LAI can provide 2D resolution.

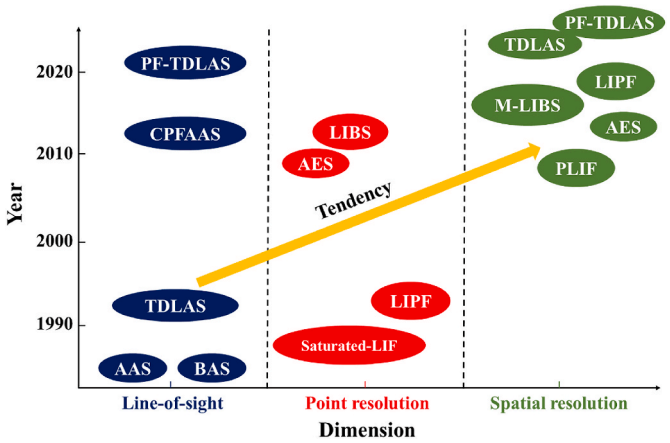

Fig. 6. A summary of optical methods employed in alkali measurements during thermal conversion processes of biomass and coal.

2.1. Requirements for quantitative measurements

Quantitative monitoring of key atomic/molecular species is of crucial importance in composing predictable kinetic models. To achieve accurate measurements, the following requirements are to be considered.

(1) Calibration

Usually, it is challenging to obtain the concentration of alkali metals directly from an optical signal. Thus, a calibration of the optical signals to species concentrations is needed. In general, a basic calibration function f can be expressed as follows:

$$S = f(c, \lambda, x_i) \tag{1}$$

where S is the signal intensity collected by the detector, c is the concentration of target species, λ is the detected wavelength, and x_i is the magnitude of ith variable, e.g., the optical path length etc.

Depending on the specific features of each technique, detailed calibration methods vary a lot. For absorption measurements, the concentration determination is based on the Beer-Lambert law. Thus, techniques based on absorption can be considered as calibration-free methods since the relationship between the concentration and the signal can be derived, if the variables such as absorption cross-section of target species and the optical path length can be determined before measurement. For emission-based measurements, calibrations are generally needed to obtain the geometry parameters of the system. It is necessary to confirm that the same arrangement of optical components, e.g., light source, mirrors, lens, and detectors, are adopted for the calibration and experiment processes. Particularly, the electrical settings of the detectors should be consistent.

In some cases, geometry parameter is not the only one to be determined during calibration procedure. For example, in laser-induced fluorescence (LIF) measurements, the fluorescence quenching also needs to be considered. The fluorescence quenching is caused by de-excitation of the excited species through collisions with other molecules/atoms, which depends on collision partners, temperature and pressure. The determination of the quenching rate, although mandatory for most quantitative LIF measurements, is a delicate task in LIF measurements. In some special cases, it can be replaced by adopting calibration methods such as using simultaneous absorption measurement to calibrate the fluorescence signal [11,25,56].

For measurements of the alkali metal emission at high alkali concentrations, self-absorption needs to be considered and the Beer-Lambert law is to be adopted [57]. Some detailed discussions about different calibration approaches of specific applications will be introduced in Section 2.2, 2.3, and 2.4.

(2) Determination of spectroscopic parameters

Although absorption based methods do not require calibration procedures, prior knowledge on the spectroscopic parameters such as the absorption cross-sections and broaden widths are needed. This is crucial for obtaining accurate results, especially when atomic absorption spectroscopy technique is adopted. Those parameters vary with the reaction conditions such as environmental temperatures and pressures. Under some situations, the incident laser light can also have an impact on these parameters. For example, Thorin et al. [58] found that the shape of atomic absorption cross-section at potassium D1 line increased from a full width at half maximum (FWHM) of 0.19 to 0.26 cm^{-1} after laser photofragmentation. Since the experimental conditions vary a lot, it is necessary to measure the spectroscopic parameters separately before experiments.

(3) Knowledge of gas temperatures

As we mentioned above, the absorption cross-section and broaden width depend on the gas temperature. Therefore, knowledge about temperatures is another key requirement in optical diagnostics. In fact, not only measurements based on absorption techniques rely on the knowledge of temperatures. The optical signals based on emission techniques are also closely related to temperatures. For spontaneous emission method, the emission intensity depends on the number density of the alkali atoms at the upper stage, which in turn depends on the temperature. For laser-induced fluorescence and laser-induced photofragmentation fluorescence, the required quenching rate in the calibration expression is also related to the temperatures. Thus, the temperature dependence should also be determined in the calibration process.

(4) Signal-to-noise ratio

The raw signal is the readout by the detector during optical measurements. Only signals originating from the target species provide useful information for quantitative measurements. Background signals, detector noises, and interferences from other matrix components such as polycyclic aromatic hydrocarbons (PAHs) will be regarded as noises during the measurements. The noise should be subtracted properly from the total signal. However, in some cases, spectral interferences due to other gaseous species in complex matrices are hard to avoid. Thus, the signal-to-noise ratio (S/N) is an important parameter to evaluate the feasibility and precision of the measurements. Optical filters are one of the most common optical components used to improve the signal-to-noise ratio by suppressing noise at other wavelengths. Under some circumstances, the polarizer can also be a good choice to discriminate polarized signals from scattering light. More strategies to improve S/N will be discussed in the introductions of specific optical techniques.

(5) Detection limits

The detection range of the selected optical technique needs to meet the requirement of measurement environments. That is, the lowest and highest concentrations occur during the thermochemical conversion process should be covered in this range. For absorption measurements, the chosen wavelength usually plays an important role in the determination of the detection range. For instance, 769.9 nm is the most common wavelength adopted for potassium measurement using tunable diode laser absorption spectroscopy (TDLAS) due to its high sensitivity. However, optically thick conditions will arise at a relatively high potassium concentration which limits the dynamic range of this method. The 404.4 nm, corresponding to 4s → 5p transition of potassium, can extend the detection range in this case due to the relatively smaller

absorption cross-section [59]. For emission measurements, the detector response has a great effect on the detection range. A suitable electrical setting is crucial in avoiding saturation of the detector while having enough signal-to-noise ratio.

(6) Discrimination of gas and particle phase for alkali species

In general, alkali metals bonded as silicates and aluminosilicates will slowly release along with the burnout process and the residues will remain in the fly ash. Alkali species such as atomic alkali, alkali chlorides, alkali hydroxides, and alkali sulfates that lead to slagging and corrosion will mainly release in the gas phase. Thus, monitoring of the release of gas-phase alkali metals is critical in most cases. The optical techniques introduced below including absorption, emission, and plasma spectroscopy are capable of measuring gas phase alkali metals under thermochemical conversion processes. For some special situations, such as the initial alkali release of the thermochemical process, both alkali element concentrations in gas phase and solid phase can be detected. Techniques with the ability of phase discrimination are important in understanding the characteristics of alkali metals transformation from solid phase to gas phase and this will be introduced in Section 2.4.

2.2. Absorption method

Absorption spectroscopy techniques are based on the Beer-Lambert law,

$$-\ln(I/I_0) = \sigma NL \quad (2)$$

where $-\ln(I/I_0)$ is the absorbance derived from I_0 and I which are the intensity of the light before and after passing the absorbing species, respectively, σ is the absorption cross-section, N is the number density of the species, and L is the optical path length.

The absorption spectroscopy techniques, widely used in the study of alkali metals in the thermochemical conversion of biomass and coal, include atomic absorption spectroscopy (AAS) and tunable diode laser absorption spectroscopy (TDLAS), which are used for the measurement of alkali-atom, and broadband absorption spectroscopy (BAS), collinear photofragmentation and atomic absorption spectroscopy (CPFAAS) and photofragmentation tunable diode laser absorption spectroscopy (PF-TDLAS), which are commonly employed for the measurement of gas phase alkali chloride and alkali hydroxide.

2.2.1. Atomic absorption spectroscopy (AAS)

Thanks to the strong absorption at resonant wavelength, the concentration of alkali atoms in combustion environments can be measured with high sensitivity by atomic absorption spectroscopy. This technique has been widely adopted in the study of alkali-atom reactions in flames. A typical schematic of AAS optical system is comprised of an absorption light source and a monochromator. A typical light source could be a tungsten-strip filament lamp, a hollow cathode lamp or an alkali vapor lamp. As the light passed the gas environment with alkali atoms, the light at the absorption lines of the corresponding alkali atom, such as the D lines of sodium at 588.9/589.6 nm and potassium at 766.5/769.9 nm, would be absorbed. The intensity of the light at different wavelengths can be obtained by a monochromator. Based on the intensity of the light after passing the measurement zone with and without alkali atoms, the absorbance, $-\ln(I/I_0)$, can be obtained, and the concentration of the alkali atom can be calculated with a known optical path length and absorption cross-section of the corresponding spectral lines using the Beer-Lambert law, as presented in Equation (2).

In 1965, Kaskan [60] determined sodium and potassium atomic concentration in various lean $H_2/O_2/N_2$ steady flat flames using AAS, where a tungsten-strip filament lamp was used as the light source, and the absorption of the resonance lines at 588.9/589.6 nm for sodium and at 766.5/769.9 nm for potassium was adopted. The measurement was conducted at different distances from the surface of the burner where the flat flame was located. A strong decay of the concentration of sodium and potassium atom was observed to the downstream of the flame (cf. Fig. 7), and the decay was faster as the flame was leaner. Since the alkali atom decay rate depended on the oxygen concentration in the hot gas, the alkali reaction, $A + O_2 + M \rightarrow AO_2 + M$, was proposed, where A represents alkali atoms. Using the same technique, McEwan and Phillips [61] conducted similar work in lean $H_2/O_2/N_2$ flames and confirmed the reaction, $A + O_2 + M \rightarrow AO_2 + M$. The authors determined the termolecular rate constant of the reaction to be about 3×10^{-33} cm^6 $molecule^{-2}s^{-1}$ for potassium and 2×10^{-33} cm^6 $molecule^{-2}s^{-1}$ for sodium. Using AAS, Carabetta and Kaskan [62] measured oxidation reaction rates of sodium, potassium and cesium atoms in lean $H_2/O_2/N_2$ flames. The flames had a pressure varied from 100 to 1520 Torr and a temperature range from 1420 to 1600 K. The average reaction rates for sodium, potassium and cesium atoms were determined to be 0.82×10^{-33} cm^6 $molecule^{-2}s^{-1}$, 1.02×10^{-33} cm^6 $molecule^{-2}s^{-1}$, 2.1×10^{-33} cm^6 $molecule^{-2}s^{-1}$, respectively. The authors also concluded that in the lean flames, the AO_2 may not be the final product.

Moreover, Carabetta and Kaskan [63] investigated the sodium chemi-excitation process in flames using direct atomic absorption spectroscopy. The process mostly occurs through the reactions of $Na + O + O \rightarrow Na^* + O_2$ and $Na + H + H \rightarrow Na^* + H_2$. In this work, low pressure (50–100 Torr) flames were adopted to have an expanded reaction zone. The concentration of atomic sodium at different distances from the burner was measured, and together with the concentration of O, H and OH in the flame, the rate constants for the Na + O + O and Na + H + H recombination were evaluated to be about 1×10^{-29} cm^6 $molecule^{-2}s^{-1}$ and 4×10^{-31} cm^6 $molecule^{-2}s^{-1}$, respectively. Fenimore [64] investigated the interaction of NaOH and SO_2 in the flue gases produced by fuel-lean hydrogen-air flames. About 1 ppm sodium was introduced into the flames, and the concentration of atomic sodium at different distances from the burner was measured through the absorption at 588.9 and 589.6 nm. As SO_2 was added into the flame, the decay of the sodium atom concentration from the flame reaction zone to the downstream increased. Based on the comparison of the sodium atom concentration in the flames with and without SO_2 seeding, the gas-phase NaOH–SO_2 reaction was proposed, i.e., $NaOH + SO_2 \leftrightharpoons NaSO_2 + OH$. Durie et al. [65] focused on the gas phase reaction of sodium species and sulfur species in hydrocarbon flames. About 0.1 ppm sodium was introduced into the flame. Using AAS, the effects of SO_2 addition on the sodium atom concentration in the flame were investigated. Different from the formation of $NaSO_2$ in fuel-lean hydrogen flames, in this work,

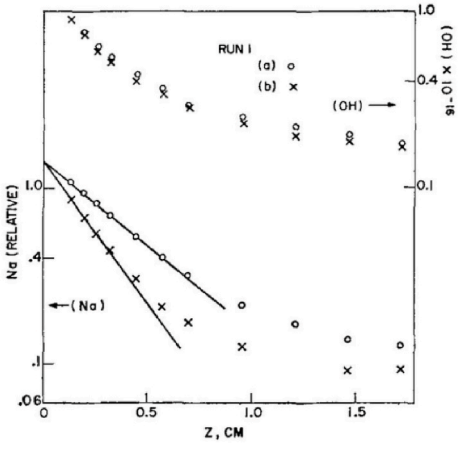

Fig. 7. Decay of sodium atoms and OH radicals in two lean flames as a function of the distance from the burner. The hot gas having 2.36 and 4.45 % oxygen for mark (a) and (b), respectively. Reproduced from Kaskan et al. [60] Copyright (1965): Elsevier.

$NaSO_3$ was suggested as the product in the fuel-lean flame and NaS_2 in the fuel-rich flame.

To improve the understanding of the fundamental reaction kinetics of alkali atoms with various species, such as O_2, N_2O, and HCl, besides in the flames, numeral studies have been conducted in a cell heated by an oven at about 800 K. In the cell, alkali-atom could be produced by UV photodissociation of alkali halide molecules, such as alkali iodide salt. The decay of the alkali atom concentration occurred due to the recombination reactions and could be detected using time-resolved AAS. Using the decay rate, the reaction rate between alkali atom and corresponding species was obtained. Husain et al. [66,67] and Vinckier et al. [68] investigated the recombination reaction between Na/K and O_2. In the work of Husain et al. [67], besides the potassium atom absorption lines at 766 nm and 769 nm, the concentration measurement based on the unresolved Rydberg doublet at 404 nm was also carried out, which showed a much low absorption intensity. The reaction rates of the third-order reactions between Na + O_2 + M at around 800 K was determined to be about 6×10^{-31}, 1×10^{-30}, and 2×10^{-30} $cm^6 molecule^{-2} s^{-1}$ as the third body was, He, N_2, and CO_2, respectively [66]. Vinckier et al. [68] obtained the reaction rate of Na + O_2 + He in the reactor with a temperature range of 392–777 K. The rate had a temperature (T) dependence and was 8.6×10^{-31} $(T/300\ K)^{-1.04}$ cm^6 $molecule^{-2} s^{-1}$. Meanwhile, the reaction rate constant for reaction K + O_2 + M at about 800 K was determined by Husain et al. [67] to be AT^{-1} cm^6 $molecule^{-2} s^{-1}$ with a small temperature dependence, where A was about 9.8×10^{-28}, 1.7×10^{-27}, and 4×10^{-27} for third body of He, N_2, and CO_2, respectively. Based on the measurement in the environment with a temperature range of 680–1010 K, the temperature dependence of the third-order rate constant of the K + O_2 + N_2 reaction was further investigated by Husain et al. [69] with a value of $6.63 \times 10^{-23} T^{-2.6}$ $cm^6 molecule^{-2} s^{-1}$. Using the same method, Husain et al. have also studied the absolute rate constant of the reaction between K atom and N_2O [70] and various halogenated reactants, CH_3F, C_2H_5F, C_6H_5F, CH_3Br, C_2H_5Br, HCl, and HBr [71]. Moreover, the reaction between an alkali-metal atom and a halogen molecule has been widely investigated as the collision process of these molecules are relatively simple with theoretical descriptions. Edelstein and Davidovits [72] measured the reaction rate between the alkali-metal atoms, including Na, K, Rb, and Cs, with I_2 molecules, in a cell heated by an oven at about 600 °C using the time-resolved AAS.

Besides conventional light sources such as a tungsten-strip filament lamp, Slack et al. [73] used a 404 nm laser as a light source for the potassium atom concentration measurement. The laser was generated by a tunable dye laser pumped by a frequency doubled Nd:YAG laser. The work was conducted in laminar flat methane flames with potassium seeding up to 360 ppm. The measured potassium atom concentration showed a small decay with distance from the burner under fuel-rich conditions, and a rapid decay under fuel-lean conditions. The addition of potassium accelerated the OH concentration decay especially for the flames at higher equivalence ratios. The experimental results were used to evaluate potassium reaction mechanisms and a mechanism with the most satisfactory agreement was provided.

Recently, Sorvajärvi et al. [74] used direct atomic absorption spectroscopy to measure the K atoms released from burning biomass fuels in a single particle reactor at temperatures from 850 to 1050 °C. High amount of potassium atom was measured during the devolatilization stage with a peak value over 200 ppb generated from the decomposition of alkali-organic compounds and KCl. During the char combustion stage, the potassium atom concentration strongly depended on the temperature. About 50 ppb potassium atom was detected at 1050 °C, while no potassium atom was observed at 850 °C.

2.2.2. *Tunable diode laser absorption spectroscopy (TDLAS)*

Different from traditional atomic absorption spectroscopy, tunable diode laser absorption spectroscopy (TDLAS) uses a narrow continuous-wave laser as the light source, which has a much higher spectral power-density and spatial/time resolution than those incoherent radiation sources such as a tungsten-strip filament lamp. Due to its relative simplicity, free of calibration, and high accuracy, TDLAS has been widely adopted in combustion diagnostics, especially in industry, where other laser-based methods are challenging to implement. Comprehensive reviews of the TDLAS-based sensors and their applications were given by Goldenstein et al. [75] and Bolshov et al. [76]. The application of TDLAS can achieve a significant improvement in the detection sensitivity of alkali atoms. A typical optical setup for the TDLAS measurement is shown in Fig. 8 [77], which is mainly comprised of tunable diode lasers and photodiodes as detectors. The wavelength of the tunable diode laser scans across the absorption line of the alkali atom, and the absorption of the light as a function of wavelength can be obtained for the calculation of atomic alkali concentration. An absorption curve of potassium atoms at 769.9 nm measured by TDLAS is presented in Fig. 9 [78]. Due to lack of a feasible diode laser at the wavelength for sodium atoms, the TDLAS system for atomic sodium measurement has so far not been reported.

As a pioneer work, Groll and Niemax [79] used a tunable diode laser centered at 766 nm measuring the concentration of potassium atoms produced in a commercial laminar air-acetylene analytical flame and in a graphite-tube atomizer. Schlosser et al. [78] employed Fabry-Pérot (FP) and vertical-cavity surface-emitting lasers (VCSEL) in measuring the concentration of potassium atoms in the flue gas of a pressurized coal combustion system under various pressures. The absorption lines of potassium atoms at 767.5 and 769.9 nm were adopted. The effect of the pressure on the spectral broadening and line shift was determined. In the measurement, a detection limit of 10 ng m^{-3} with a time resolution of 1.7 s was achieved. Based on the *in situ* detection of the trace atomic potassium in combustion plants, Schlosser et al. [80] developed a method in evaluating the residence-time distribution of flue gas. In this work, certain amount of alkali compounds was injected in a short pulse, and alkali atoms as a tracer were produced from the decomposition of the alkali compounds after fuel combustion. By monitoring the atomic alkali at certain positions, the residence-time of the flue gas was determined.

However, due to the strong absorption of potassium atoms at 769/766 nm, especially under the measurement condition with a long optical path length, optically thick conditions occurred. This challenges the accurate quantification using TDLAS measurement as the absorption center becomes optical opaque. As shown in Fig. 10 reported by Qu et al. [77], a truncated absorption peak was obtained under high concentration situations. Thus, the wings of the absorption profile were used for the absorption fitting through a fitting routine described by Qu et al. [77] to achieve a quantitative measurement under the optically thick conditions.

Besides the fitting of the wings of the absorption profile, another way

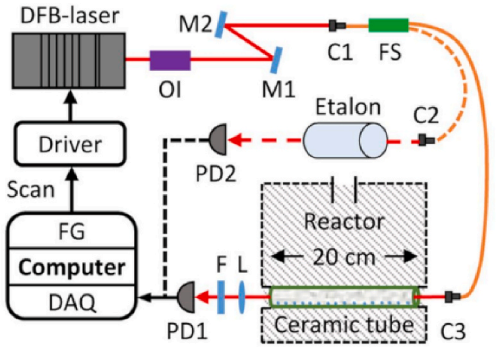

Fig. 8. Schematic of typical TDLAS setup for the measurement of potassium atoms. Note: OI (optical isolator); M (mirror); C (collimator); FS (fiber splitter); L (lens); F (optical filter); PD (photodetector). Reproduced from Qu et al. [77] Copyright (2016): ACS.

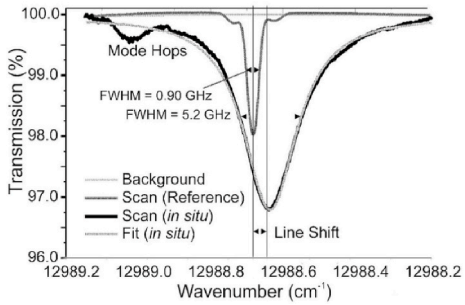

Fig. 9. Absorption of potassium atoms at 769.9 nm in the flue gas at atmosphere pressure and 1170 K, and in a low-pressure reference cell with pure potassium vapor at the room temperature. Reproduced from Schlosser et al. [78] Copyright (2002): Elsevier.

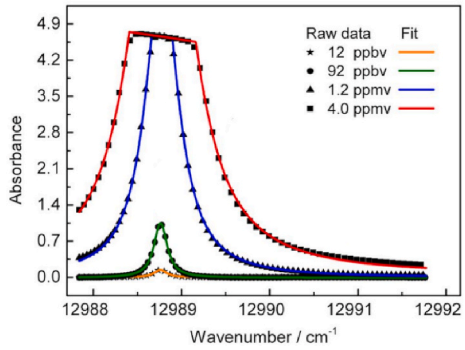

Fig. 10. Absorbance of potassium atoms at 769 nm as a function of wavelength under the conditions with different potassium concentrations. Reproduced from Qu et al. [77] Copyright (2016): ACS.

to avoid the optically thick condition is to choose a weaker absorption line of potassium, such as the line at 404 nm, which is about 30 times weaker in line intensity. Gustafsson et al. [81] performed measurement of potassium atoms using frequency-modulation absorption spectroscopy using the 404.8 nm line. Recently, Weng et al. [59] used both absorption lines, at 404 and 769 nm, for potassium quantification, which significantly increased the dynamic range of the measurement. The potassium atom concertation varying from several ppb up to 20 ppm could be accurately measured with an optical path length of 100 mm.

TDLAS is typically considered as a line-of-sight (LOS) technique, where the measured concentration is an average along the laser path. Hence, the concentration information with spatial resolution is missing. However, considering potassium atoms are excited during the atomic absorption process in TDLAS measurements, and the corresponding fluorescence from the excited potassium atoms when de-excite back to the ground states can be observed. Thus, by combining TDLAS and simultaneous fluorescence imaging, Gao et al. [82] reported one-dimensional quantitative measurements of potassium atoms in hot flue gases from laminar flames. In addition, laser absorption imaging (LAI) [83] is another strategy for acquiring spatially resolved information. In this method, the laser beam was split into several beams to measure the line-of-sight concentration along each beam path. The spatial-resolved concentration is then derived through laser absorption tomography (LAT) technique which reconstructs the three-dimensional distribution from several two-dimensional projections at different angles using inversion algorithms [84]. If the measured target is cylindrical symmetry, the reconstructed process can be further simplified using only one projection. This method was recently adopted by Thorin et al. to measure the concentration distribution of atomic potassium in high temperature environments and the results agreed well with their previous results obtained by point measurements [85].

Since atomic potassium was considered as a key species in the potassium thermochemistry, accurate measurements of potassium atoms using TDLAS were widely applied in different combustion environments. Leffler et al. [86], Weng et al. [87,88] and Berdugo Vilches et al. [89] investigated the potassium species balance between potassium atoms and other species, such as KCl, KOH and K_2SO_4, in various combustion environments. Leffler et al. [86] conduced measurements in KCl/KOH seeded methane/air laminar flames with various equivalence ratios. The hot gases produced by the flames were measured to be around 1500 K and the addition of potassium varied from ~3 ppm to ~30 ppm. The concentration of potassium atoms in the flame increased with equivalence ratio. For instance, it increased from 0.3 ppm to 5 ppm as the equivalence ratio increased from 0.8 to 1.3 with the addition of ~20 ppm KOH in the flame. Similar results were obtained by Weng et al. [87] for the gases at about 1750 K provided by flames with different equivalence ratios and the addition of ~20 ppm KOH or KCl (cf. Fig. 11). The authors presented the positive correlation between potassium atom concentration and gas temperature which varied from ~1100 K to ~1900 K. When SO_2 was added into the hot flue gases which contained ~20 ppm KOH or KCl, the concentration of potassium atom decreased especially under the conditions of low temperature, such as 1100 K, attributed to the sulfation of KOH/KCl [88]. Combining the measurement of the OH concentration in the hot gas, it was found that potassium atoms enhanced the consumptions of OH radicals and could inhibit the oxidation of CO in the hot flue gas produced from methane-air flames [89].

Qu et al. [77] and Weng et al. [90] adopted TDLAS for measurement of potassium atoms released from burning biomass and coal pellets. The measurement provided important information to the study of the fate of potassium during the thermal conversion process of solid fuels. As reported by Qu et al. (Fig. 12) [77], pelletized wood and wheat straw were burned in a laboratory reactor at 1123 K. For both fuels, significantly high amount of potassium atom with a concentration of around 3 ppm was released during the devolatilization stage. During char combustion, the detected potassium atom was much less than the devolatilization stage. The peak concentration was about 0.1 ppm, and the position closer to the pellet surface provided a higher potassium atom concentration. Weng et al. [90] measured the release of potassium atom from pelletized wood, straw and coal burning in the hot gas environments provided by laminar flames at about 1700 K. Like the results from Qu et al. [77], the release had its maximum during the devolatilization stage for both wood and straw. Coal had much weaker potassium atom release during the devolatilization stage due to lower volatile content. Sepman et al. [91] measured the concentration of potassium atoms using a TDLAS system at 770 nm in a biomass entrained-flow gasifier. The measurement was conducted together with the CO, H_2O, and temperature measurements using different TDLAS systems. Much lower

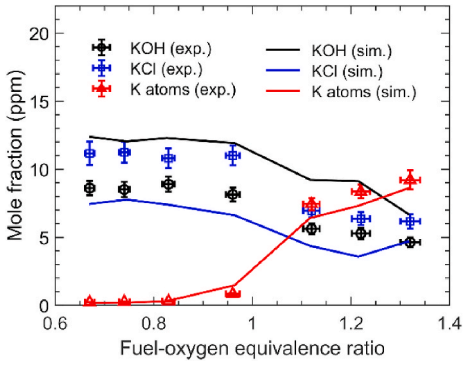

Fig. 11. Concentration of KOH, KCl, and K atoms in the 1800 K hot environments provided by flames as a function of fuel-O_2 equivalence ratio with seeding of KCl salt. Reproduced from Weng et al. [87] Copyright (2020): Elsevier.

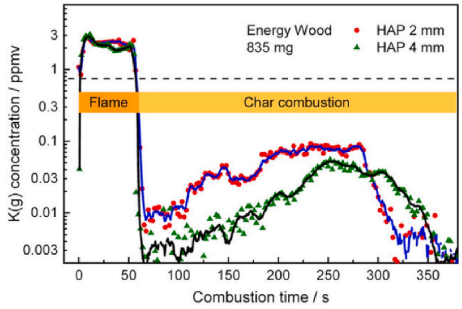

Fig. 12. Concentration of potassium atoms released from burning wood pellet as a function of the burning time. HAP: height above pellets. Reproduced from Qu et al. [77] Copyright (2016): ACS.

potassium atom concentration was measured in the combustion (~0.01 ppm) than in the gasification mode (~0.1 ppm) of the reactor, and the potassium atom concentration presented a similar varying trend to the measured temperature. Later, Sepman et al. [92] fired softwood with artificial air with varying oxygen concentrations in the entrained-flow reactor. It showed that the concentration of potassium atoms was very sensitive to the equivalence ratio. Furthermore, Qu et al. [93] have applied TDLAS for the measurement of the concentration of potassium atoms at four different locations of an entrained-flow reactor. The study was used to understand the thermochemical conversion progress of the biomass fuels in the reactor. The potassium atom concentration decreased with residence time, and an excellent agreement in the measurement and thermodynamic equilibrium calculation was obtained in the gas having a long residence time. Thorin et al. [85] applied LAI method to measure the distribution of potassium atoms above a burning wheat straw pellet. The optical setup mainly consists of a diode laser, a pair of lens (L1 and L2), and a high-speed camera, as shown in Fig. 13. The laser beam diameter was expanded to 44 mm through the lens-pair and projected onto the camera. By applying the Abel transform, the potassium atom distribution was obtained with a spatial resolution of 2 mm and a time resolution of 0.1 s.

2.2.3. *Broadband UV absorption spectroscopy (BAS)*

Alkali molecules, such as KCl and KOH, have broadband absorption spectra, mainly in the ultraviolet region, which can be used for the concentration measurement based on the Beer-Lambert law. A typical optical setup is shown in Fig. 14. It mainly contains a UV light source, such as a deuterium lamp or a Xeon lamp, and a spectrometer. To make a reliable quantification, it is essential to obtain accurate spectrally resolved UV absorption cross-sections of different alkali molecules. Quite some efforts have been spent in obtaining the absorption spectrum of different alkali compound vapors at different temperatures in graphite-furnaces or flames.

Koirtyohann and Pickett [95], Culver and Surles [96], Furuta et al. [97], Pritchard and Reeves [98], Allain and Mauras [99] and Daminelli [100] reported UV absorption spectra of NaCl and KCl vapor at high temperatures, such as 1800 °C [98]. The vapor of NaCl and KCl has similar absorption spectrum, which is negligibly dependent on temperature. The broadband UV absorption located between 210 and 300 nm and its peak position was at around 250 nm. At the wavelength close to 200 nm, another strong absorption peak appeared. Furuta et al. [101] and Daidoji [102] reported UV absorption spectra of NaOH and KOH in flames. Different from NaCl and KCl, NaOH and KOH have extra broadband UV absorption peak located between 300 and 350 nm.

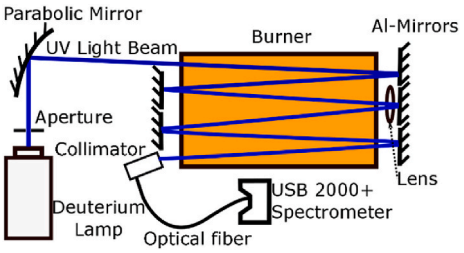

Fig. 14. A typical schematic of the UV absorption spectroscopy setup. Reproduced from Weng et al. [94] Copyright (2018): OSA.

To obtain the absolute UV absorption cross-section of NaCl and KCl, Davidovits and Brodhead [103] and Leffler et al. [104] introduced known amount of NaCl and KCl vapor in a sealed quartz tube at varying temperatures up to around 1100 K, and based on the Beer-Lambert law, the absorption cross-section value was calculated with known optical path length (L). Typical UV absorption cross-sections of KCl are shown in Fig. 15. Davidovits and Brodhead [103] reported that, at the wavelength about 250 nm, NaCl had a peak absorption cross-section about 3.5×10^{-17} cm^2/molecule at temperature between 850 and 950 °C, and KCl had a peak value about 2.0×10^{-17} cm^2/molecule at temperature

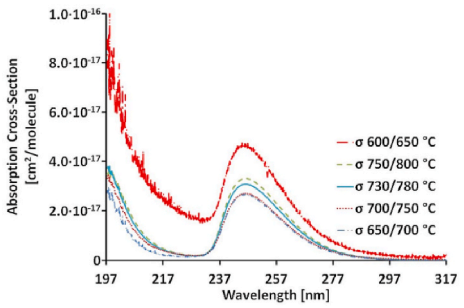

Fig. 15. UV absorption cross-section of KCl at different temperatures in the wavelength range of 197–317 nm. Reproduced from Leffler et al. [104] Copyright (2017): AIP.

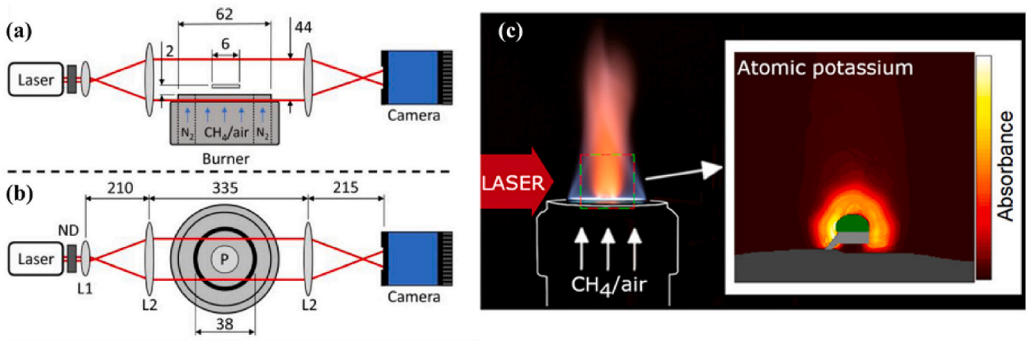

Fig. 13. Schematic of the LAI setup with (a) front view and (b) top view. A lens-pair (L1 and L2) was used to expanded the laser beam. (c) Photograph of the burning wheat pellet during char combustion stage and the atomic potassium distribution above it. Reproduced from Thorin et al. [85] Copyright (2023): ACS.

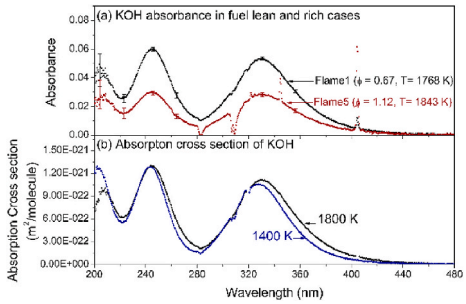

Fig. 16. Typical absorbance and derived UV absorption cross-section of KOH at different temperature in different flames. Reproduced from Weng et al. [59] Copyright (2019): ACS.

between 841 and 951 °C. Leffler et al. [104] presented that KCl had an absorption cross-sections of 2.9×10^{-17} cm^2/molecule at 246.1 nm and 3.4×10^{-17} cm^2/molecule at 197.6 nm at the temperature between 700 and 800 °C. The authors also concluded that the absorption cross-section of KCl almost had negligible dependence on temperature. Similarly, Forsberg et al. [105] introduced known amount of KCl and NaCl into a gas cell kept at around 1100 K to obtain the absorption cross-section, which was about 1.8×10^{-17} and 1.75×10^{-17} cm^2/molecule, respectively, near 250 nm.

Rowland and Makide [106] estimated the UV absorption cross-section of NaOH based on the work of Daidoji [102], with the obtained absorbance of NaOH in the flame and corresponding known amount of NaOH solution that was seeded into the flame. The peak absorption cross-section of NaOH near 230 nm was about 1.75×10^{-17} cm^2/molecule and near 330 nm was about 1.0×10^{-17} cm^2/molecule. It showed that the cross-section value of NaOH was close to that of NaCl and KCl. Recently, Weng et al. [94] obtained the UV absorption cross-section of NaOH, KOH, NaCl and KCl in hot flue gases provided by flames at the temperature from 1200 to 1850 K relying on the data obtained by Leffler et al. [104] at 1100 K. For the first time, the UV absorption cross-section of KOH has been obtained by Weng et al. [94]. At 1400 K, KOH had the absorption cross-sections of 1.7×10^{-17} and 1.3×10^{-17} cm^2/molecule at wavelengths of 244.3 and 327.3 nm, respectively. Further on, Weng et al. [59] developed a new method to derive the UV absorption cross-section of KOH at high temperature, based on the knowledge of the chemical balance between KOH and atomic K in different flames and the accurate quantification of potassium atoms using TDLAS as described in Section 2.2.2. At the temperatures of 1400 and 1800 K, the absorption cross-section of KOH was determined to be about 1.26×10^{-17} cm^2/molecule at 246.2 nm and 1.05×10^{-17} cm^2/molecule at 327.3 nm (cf. Fig. 16).

Broadband UV absorption spectroscopy has been widely adopted for the quantitative measurements of NaCl, KCl, NaOH, and KOH in different combustion environments based on their absorption cross-sections. The quantitative measurements facilitate the investigation of alkali metal thermochemistry. Leffler et al. [86] and Weng et al. [87] provided experimental data for the understanding of K−Cl chemistry in flames. The studies mainly focused on the chemical balance between KOH, KCl, and K atoms. The results showed that the balance between KOH/KCl and K atoms strongly depended on flame equivalence ratio. Much less KOH/KCl was measured in fuel-rich flames as a notable part of potassium was in the form of potassium atoms. The balance between KOH and KCl was almost unaffected by flame equivalence ratio but mainly depended on temperature. More KOH was converted from KCl at a higher temperature through the fast reaction, $KCl + H_2O \leftrightharpoons KOH + HCl$ [87]. Berdugo et al. [89] presented the influence of KOH and KCl on CO and H_2 oxidation in combustion environments through the measurement of KOH, KCl, and K atoms and OH radicals. It was found that KOH could inhibit the oxidation of CO and H_2 as the consumption of OH radical was enhanced by the K atoms decomposed from KOH.

Alkali chloride presented in flue gases can cause problems of slagging, fouling and corrosion. Converting alkali chloride to alkali sulfate through sulfation is regarded as a promising way to mitigate these problems as alkali sulfate is less corrosive and its melting point is much higher than alkali chloride. Thus, the gas phase sulfation process of alkali chloride and also alkali hydroxide has been conducted in several studies. Li et al. [107] and Weng et al. [88] investigated the gas-phase sulfation of KCl and KOH by SO_2 in hot flue gases through monitoring the concentration of KCl and KOH as different amounts of SO_2 were added with a typical result in Fig. 17. Both KCl and KOH could be sulfated by SO_2 in gas phase to K_2SO_4 especially at a relative low temperature such as 1100 K. KOH could be sulfated more rapidly than KCl.

Moreover, Leffler et al. [108,109] and Allgurén and Andersson [110] applied this technique to monitor the KCl vapor concentration in running furnaces and big test units. Allgurén and Andersson [110] investigated the chemical interactions between potassium, chlorine, sulfur and carbon monoxide in a 100-kW test unit which fired propane in an air-fuel or oxy-fuel mode.

2.2.4. Collinear photofragmentation and atomic absorption spectroscopy (CPFAAS)

CPFAAS is a technique combining photofragmentation and atomic absorption spectroscopy to measure the concentration of alkali compounds, such as NaOH, NaCl, KOH, and KCl. Compared with broadband absorption spectroscopy, CPFAAS shows to be more sensitive and species selective. This technique was originally applied in the investigation of reaction of metal atoms with other molecules (O_2, N_2O). For example, Husain et al. [66] generated atomic sodium from the photofragmentation of NaI with the excimer laser or flash lamp, and the decay of the concentration of atomic sodium after the photofragmentation was monitored by time-resolved atomic absorption spectroscopy with a hollow cathode lamp to study the atomic sodium reaction process.

Sorvajärvi et al. [74,111,112] developed CPFAAS to measure the concentration of alkali salts, where two collinear light beams were used (cf. Fig. 18), one was used to photodissociate the alkali salt and the other was used to measure the concentration of alkali atom fragments. For the KCl vapor measurement, Sorvajärvi et al. [111] used a pulsed UV laser at 245 nm with a 10 Hz repetition rate and a 5 ns pulse duration to photodissociate KCl to generate ground-state potassium atoms. A diode laser tunable around the potassium atom absorption line near 766.5 nm was used as the probe laser to measure absorption by the potassium atoms generated from KCl photodissociation. Based on the measured absorption, the concentration of KCl could be derived with a detect limit of about 1 ppb through the expression [112],

$$X_{KCl} = -\ln\left(1 - \alpha L_{max}\frac{A_f}{E}\frac{hc}{\gamma\lambda_f}\frac{1}{\sigma_K}\right)\frac{kT}{p}\frac{1}{\sigma_{KCl}L} \tag{3}$$

where X_{KCl} is the KCl concentration, αL_{max} is the maximum absorbance of fragment potassium atoms, A_f, E and λ_f are the cross-section area, input energy and wavelength of the fragmenting laser, h is the Planck constant, c is the speed of light, γ is the photofragmentation efficiency, k is the Boltzmann constant, T, p and L are the sample temperature, pressure and length, and σ_K and σ_{KCl} are the absorption coefficient of K atom and KCl at the wavelength of the probing laser and fragmenting laser, respectively.

Since the photofragmentation was achieved using a wavelength-selected UV light source, only selected molecular was detected. Sorvajärvi et al. [74] used two pulse lasers having a wavelength of 266 nm and 320 nm to selectively measure the concentration of KCl and KOH, since 266 nm light source could only photodissociate KOH molecule. This technique was applied to simultaneously detect the KCl and KOH vapor released from burning biomass fuels in a single particle reactor [74]. It was well presented that KCl/KOH was mainly released during char combustion stage. At a low temperature (850 °C), KCl was the dominant potassium species. About 10 ppm KCl was detected. At a

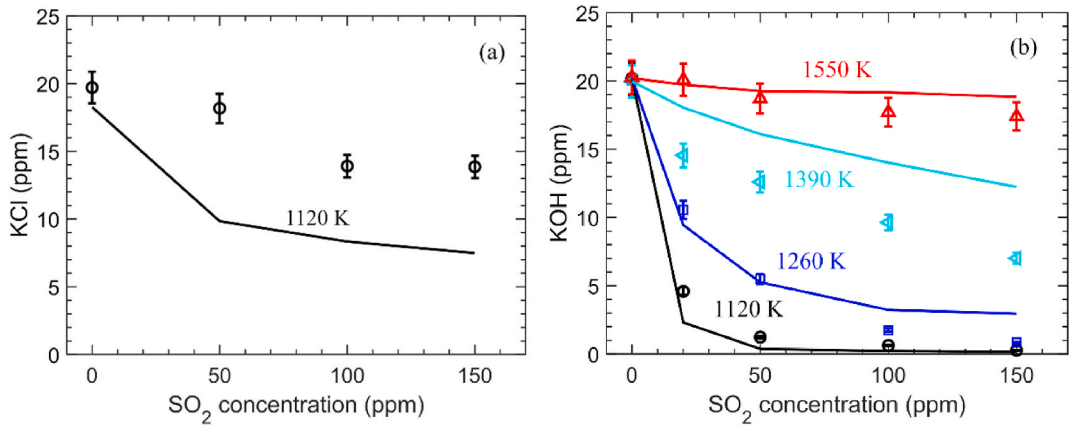

Fig. 17. The concentration of (a) KCl and (b) KOH as a function of SO_2 concentration in the hot flue gas from experiment (dot) and simulation (line). Reproduced from Weng et al. [88] Copyright (2020): Elsevier.

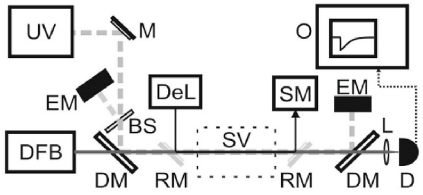

Fig. 18. Typical schematic of CPFAAS setup. Note: UV (ultraviolet laser); DFB (probe laser); M (mirror); AP (aperture); BS (beam splitter); DM (dichroic mirror); EM (energy meter); L (lens); D (detector); A (amplifier); O (oscilloscope). Reproduced from Sorvajärvi et al. [111] Copyright (2012): OSA.

higher temperature, such as 1050 °C, about 5 ppm KOH was detected.

Moreover, Sorvajärvi et al. [113] used CPFAAS to investigate the rate constant and thermochemistry of $K + O_2 + N_2 \leftrightharpoons KO_2 + N_2$ at the temperature of 748–1323 K after the dissociation of KCl by a 266 nm fragmentation laser. The constant was summarized to be about $1.07 \times 10^{-30}(T/1000\ \mathrm{K})^{-0.733}\ \mathrm{cm^6 molecule^{-2} s^{-1}}$. Lehmusto et al. [114] applied CPFAAS to explore the high-temperature corrosion reaction between KCl and metals at 550 °C through the online detection of gaseous KOH. Viljanen et al. [115] introduced this method to simultaneously monitor the concentration of KCl and KOH to investigate the K–Cl–S chemistry in a pilot-scale combustor with fragmentation lasers at 266 nm and 355 nm. The study showed that both Cl/K and S/K ratios played an important role in the sulfation process.

2.2.5. *Photofragmentation tunable diode laser absorption spectroscopy (PF-TDLAS)*

The transmitted probe laser intensity in CPFAAS depends on the product of atomic alkali line strength, atomic alkali concentration, and the optical path length. Since the probe laser wavelength is often fixed at the absorption line center of the alkali atoms, the product becomes large under optically thick conditions, causing the transmitted signal below the detector's threshold. In this case, the CPFAAS technique is no longer capable of monitoring concentrations of KCl, KOH, and K atoms. Although the probe laser wavelength could be detuned from the line center, the concentration calculation based on Equation (3) requires accurate knowledge of the atomic absorption line shape. To solve this problem, recently, Thorin and Schmidt [58,116] combined photofragmentation spectroscopy and tunable diode laser absorption spectroscopy (PF-TDLAS) to monitor the concentration of KOH, KCl, and K atoms. The PF-TDLAS technique employed TDLAS rather than AAS for the measurement of potassium atoms. Since the photofragmentation location could be flexibly chosen within the line shape, the measurement of alkali atoms and compounds could be possible even in optically thick situations. A typical schematic of photofragmentation positions selected in an optically thick situation and in a weak absorption situation is shown in Fig. 19.

For simultaneously monitoring the concentration of KCl, KOH, and K atoms, Thorin et al. [58] adopted two pulse lasers at the wavelength of 355 nm and 266 nm to dissociate potassium hydroxides and potassium chlorides, respectively. The generated potassium-atom fragments and background potassium atoms were both measured by an external-cavity diode laser (ECDL) scanning over 0.158 nm across the potassium D1 line. Two detectors with high bandwidth and low bandwidth were used to separately monitor the photolysis-induce potassium atoms and the background potassium atoms. Detailed setup of the PF-TDLAS technique is shown in Fig. 20. The detection limits of 9/16 ppb and 310/630 ppb under combustion conditions and gasification conditions were achieved for KOH/KCl.

Moreover, Thorin et al. [117] applied the PF-TDLAS technique in a 140 kW pilot-scale entrained-flow gasifier to measure the KOH, KCl, and K atom release behaviors. Two types of biomass, i.e., forest residues and a mixture of forest residues and wheat straw, were studied during the gasification process (at air-to-fuel equivalence ratio of 0.5) and the combustion process (at air-to-fuel equivalence ratio of 1.3), respectively. The position of photofragmentation pulses was detuned 7.3 $\mathrm{cm^{-1}}$ away from the potassium D1 line center, which successfully achieved KOH/KCl measurements with the background potassium concentration up to ~100 ppm under the gasification case. Recently, Viljanen et al. [118] used the PF-TDLAS technique to figure out the alkali fate in a 100 kW Oxy-fuel reactor. The optical system was similar to that in Fig. 20, where a DFB laser scanning over the potassium D2 line at 766 nm was

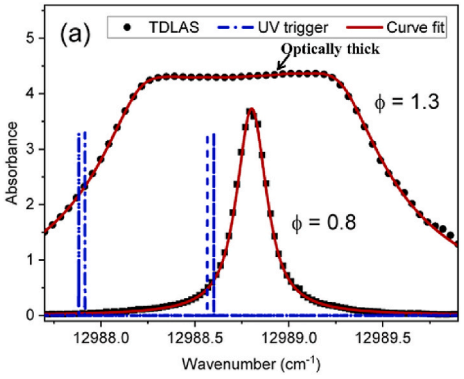

Fig. 19. The schematic of photofragmentation positions selected in a relatively low concentration situation and an optically thick situation. Reproduced from Thorin et al. [58] Copyright: (2021): OSA.

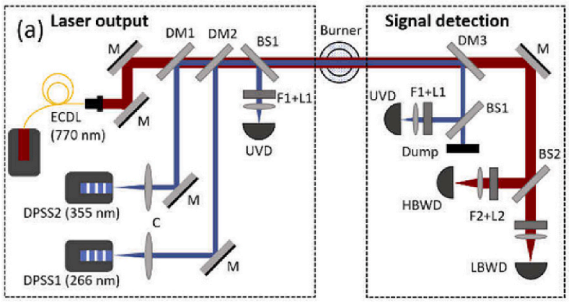

Fig. 20. Schematic diagram of the experimental setup of PF-TDLAS. Note: ECDL (probe laser); DPSS (fragmentation laser); C (collimating lens); DM (dichroic mirror); BS (beam splitter); UVD (UV detector); F (optical filter); L (lens); HBWD (high bandwidth detector); LBWD (low bandwidth detector); Dump (UV beam dump); B (burner); Reproduced from Thorin et al. [58] Copyright: (2021): OSA.

adopted as the probe laser. Propane was injected into the reactor as fuel and KCl solution was seeded into the reactor to provide potassium. In addition, SO_2 was also injected to analyze the sulfation process. While the concentrations of KOH, KCl and K atoms were monitored by PF-TDLAS, a surface ionization detector was employed to monitor the total alkali concentration in gas phase and in particles through online sampling and analysis of the flue gas. By continuous monitoring of various alkali species and gas temperature, the fate of potassium sulfation and KCl nucleation were observed in their work. Besides, by replacing the conventional TDLAS with the LAI method mentioned above (cf. Section 2.2.2), PF-TDLAS method has the potential to be applied to KOH/KCl imaging. Thorin came up with the idea and the PF-LAI method has been preliminarily validated capable to measure the distribution of atomic K, KOH and KCl above heating KCl samples and burning wheat straw pellets [119].

2.3. Emission

Emission spectroscopic techniques are based on the intensity of the detected fluorescence signal emitted from target species excited using different approaches. Techniques including chemiluminescence, laser-induced fluorescence (LIF), and laser-induced photofragmentation fluorescence (LIPF), have been developed and used for the measurement of alkali species like atoms, alkali chlorides and alkali hydroxides.

2.3.1. Atomic emission spectroscopy (AES)

Chemiluminescence is the emission from the species excited by chemical reactions rather than radiation [120]. It is widely used due to lower requirements on devices and system arrangement than others, such as laser-based optical techniques.

In 2007, Jones et al. [121] examined the behavior and the fate of potassium in biomass combustion using emission spectroscopy of potassium atoms. In their study, the emission signal of potassium was used to represent K release characteristics. A typical three-stage evolution process of potassium release was observed. Two release models were developed to simulate the first two stages and this will be specifically introduced in Section 3.2.1. Then, the catalytic effect of potassium on biomass combustion was investigated. For comparison, potassium was first removed from the biomass through water-washing and demineralization process and then doped into the sample. Simultaneous observations of the K emission signal and the close-up view of willow sample combustion were carried out. The results indicated the burnout process of char residue was extremely slow without potassium but resumed to the initial speed after re-doping K, which suggested the catalytic effects of potassium on char combustion.

Mason et al. [122] applied emission spectroscopy to measure the potassium release from biomass pellets suspended in a methane flame. The emission signal from the atoms in the excited state was collected by a photo-detection device equipped with a band-pass interference filter with the center wavelength at 766 nm. The experimental results are shown in Fig. 21(a). It is difficult to quantify the potassium release using this method, but a relationship between the peak release rate and the initial potassium content is derived (cf. Fig. 21(b)). In addition, potassium release fraction of different combustion stages can be calculated using this emission spectroscopy. In their work, they found the peak release of potassium occurred in the char stage, which agreed well with the results from Hsu et al. [57]. Later in 2017 [123], they used the same system to measure the potassium release from a single pellet under high temperatures and extended their work [124] in modeling the phase transformation of potassium species to gas phase. The effects of additives on potassium release were also estimated in their subsequent work [125].

Striūgas et al. [126] used an ICCD camera mounted with different filters to record Na*, K* and Ca* chemiluminescence during biomass pellet combustion and thus the two-dimension alkali release characteristics were obtained during combustion. They investigated the emission signals of different biomass types at different temperatures. The results were in good agreement with Mason et al. [122].

Weng et al. [127] used emission from Na* and K* chemiluminescence to investigate the potassium and sodium release from single wheat straw particles in the size range of 224–250 μm burning in the hot flue gas produced by a flat flame McKenna burner. The arrangement of the devices and optical elements is shown in Fig. 22(a) and the experimental images are shown in Fig. 22(b). The release characteristics from the ignition to the early stage of the char oxidation of the moving burning particles were obtained by an ICCD camera with spatial resolution. The camera was equipped with corresponding band-pass filters. They found that sodium and potassium started to release as volatiles ignited and the signal of sodium and potassium stayed at high intensity until the onset of the char oxidation process since sodium and potassium continued to release during char burning period. In 2019, Weng et al. [128] extended their work to more types of biomass, i.e., pine wood, wheat straw, rice husk, and grape pomace. The CH*, Na*, and K* emission signals were used to represent the volatile combustion intensity, sodium release intensity and potassium release intensity, respectively (cf. Fig. 22 (b)). During the volatile combustion stage, as shown in Fig. 22 (c), the release of Na and K increased which was mainly governed by the volatile combustion intensity. At the end of the volatile combustion stage, the Na* and K* emission signals were still in existence, which indicated the release of alkali metals from char combustion. In order to eliminate the effect of volatiles, Weng et al. employed Na*/CH* and K*/CH* ratios to represent the sodium and potassium release characteristics as well. They found the ratio of alkali signal to CH* was stable during the volatile combustion stage and abruptly increased which indicated the initiation of the char oxidation stage (cf. Fig. 22 (c)).

Recently, He et al. [129] measured the temporal release of total potassium elements from single biomass pellet combustion using flame emission spectroscopy and the experimental setup is shown in Fig. 23(a). The calibration of the emission signals was achieved by seeding KCl solutions into the flame with a series of known concentrations. Then, they analyzed the effects of biomass composition and moisture content on potassium release. In addition, the temperature of biomass pellet was also acquired using thermal radiation from the pellet. The experimental results are shown in Fig. 23(b). Both temporal release of potassium and temperature can be used to distinguish the combustion stage, i.e., devolatilization, char combustion and ash stage.

In general, methods based on chemiluminescence detection require simple systems that consist of cheap equipment. It can be predicted that these methods are of great advantage in some harsh situations. However, these methods usually do not have the ability of alkali species discrimination as well as spatial resolution. Even with a camera, the received emission signal is actually the projection of the line-of-sight

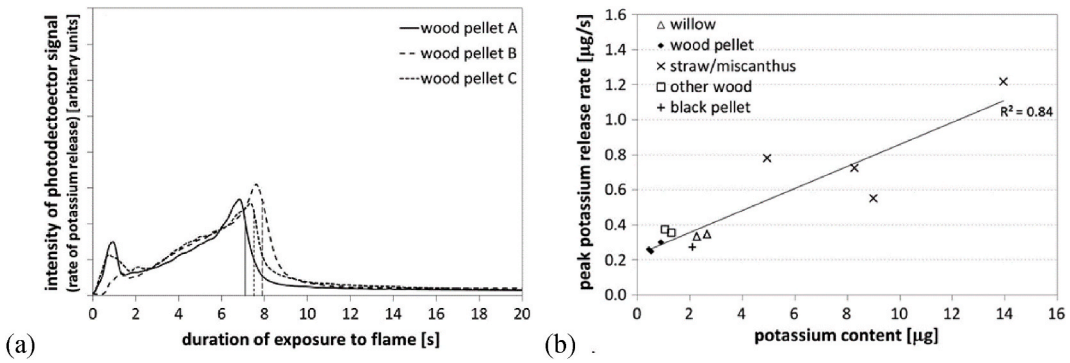

Fig. 21. (a) Emission signal of potassium atoms during wood pellet combustion and (b) the relationship between the peak potassium release rate and the initial potassium content in biomass. Reproduced from Mason et al. [122] Copyright (2016): Elsevier.

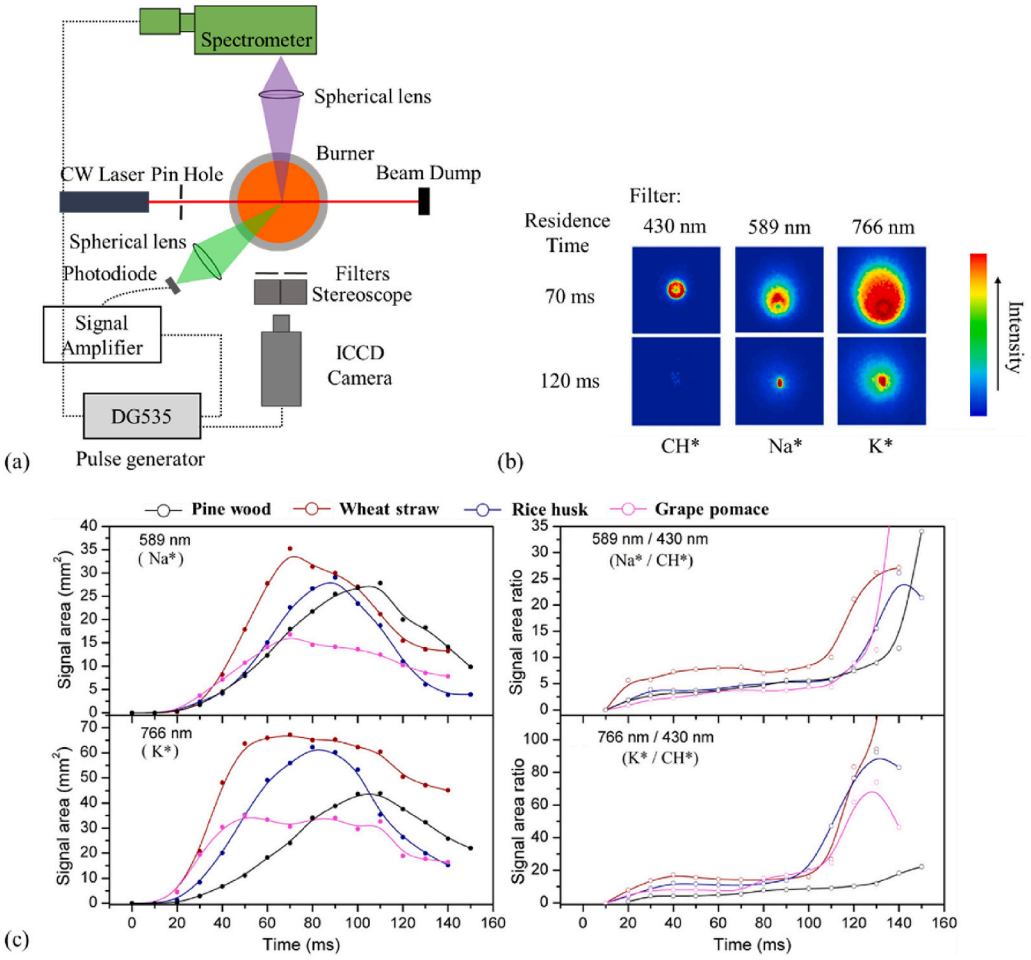

Fig. 22. (a) The arrangement of chemiluminescence measurements using an ICCD camera and (b) chemiluminescence images of CH*, K*, and Na* from burning pulverized wheat straw particles obtained with the ICCD camera equipped with corresponding filters. Reproduced from Weng et al. [127] Copyright (2018): Elsevier. (c) Respective emission signal of Na* and K* during particle combustion processes and emission signal ratios of Na* to CH* and K* to CH*. Reproduced from Weng et al. [128] Copyright (2019): Elsevier.

signal on the two-dimensional plane. Calibration of these emission signals is also a tough task. Besides, under the situation with high alkali concentrations, self-absorption will affect the signal significantly which decreases the accuracy of this method. These shortcomings require the use of other measurement methods to compensate.

2.3.2. *Laser-induced fluorescence (LIF)*

Laser-induced fluorescence (LIF) is one of the most widely used optical techniques for the investigation of thermochemical conversion processes. This technique is based on the fluorescence emission from atoms or molecules that have been selectively excited by laser radiation [130]. The main issue for quantitative LIF measurement is to convert the fluorescence signal into the concentration of alkali atoms.

When the laser radiation intensity is high enough, the selected transition can be saturated and the fluorescence signal is independent of incident laser intensity, quantum efficiency and collisional energy

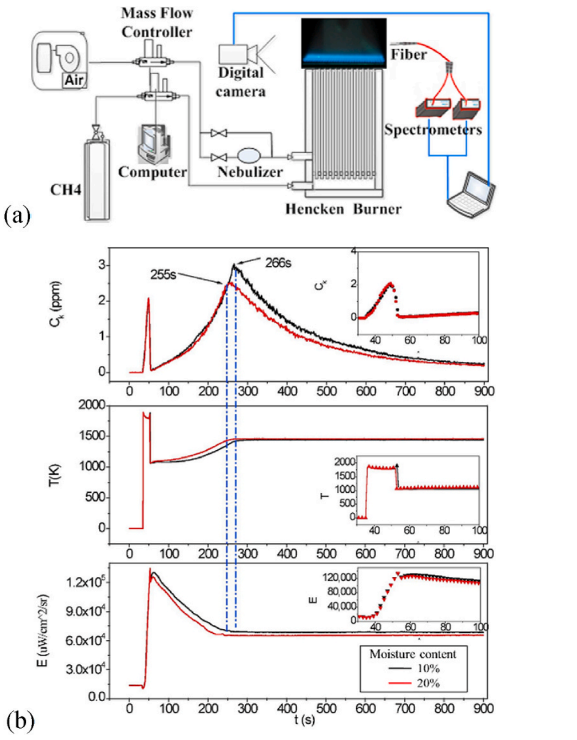

Fig. 23. (a) The experimental setup of flame emission spectroscopy and (b) K release behavior, flame temperature as well as thermal radiation of burning camphorwood pellets with different moisture contents (10 % and 20 %). Reproduced from He et al. [129] Copyright (2019): Elsevier.

transfer. Then, a simplified theoretical curve between the saturated LIF signal and atomic alkali metal concentration could be obtained conveniently. Smith et al. [131] derived the relationship between atomic sodium concentrations and saturated LIF signals as:

$$(B_F)_{\max} = \frac{l}{4\pi} A_{21} h\nu_0 \frac{n_T}{2} \tag{4}$$

where $(B_F)_{\max}$ is the maximum fluorescence radiance, l is the depth of the fluorescence volume in the observation direction, A_{21} is the Einstein coefficient for spontaneous emission, h is the Planck constant, ν_0 is the frequency and n_T is atomic concentration. Atomic sodium concentration can be easily obtained by measuring $(B_F)_{\max}$ and substituting it into Equation (4). Smith et al. [131] measured the atomic sodium concentration in air-hydrogen and air-acetylene flames to prove this method works.

Hynes et al. [132] also measured atomic sodium concentration using saturated LIF technique. Atomic Na concentrations of different oxygen-rich hydrogen flames were obtained as well as the concentration of OH radicals. Chemistry equilibrium was assumed to calculate concentrations of H, O and H_2. This study extended the former work of Smith et al. [131] by analyzing the correlation between Na atom concentration with [H], [O], [OH], and [H_2] and establishing the rate constants of Na, NaOH, NaO_2, and NaO reactions with different flame species.

Saturated LIF measurement has been theoretically and experimentally verified as a feasible method to measure atomic sodium concentration during combustion processes. However, two main disadvantages restrict its applications in the actual solid fuel combustion processes. On the one hand, the sodium or potassium concentrations in coal and biomass are sometimes of high levels where optically thick conditions would happen. The high alkali metal concentration between the measurement point and the detection device will cause reabsorption of fluorescence which leads to a difficult calibration process [133]. On the other hand, the need for high laser intensity limits the spatial resolution since only point measurements are allowed.

The 3s→3p atomic transition (D line) of alkali metals is the most commonly selected wavelength for both atom excitation and signal detection. The resonant light may cause severe scattering and decrease the signal-to-noise ratio. Weiland et al. [133] examined several alternative one- and two-photon LIF techniques to select the best strategy for use in a fluidized bed coal gasifier and combustor. All measurement cases and the relative signal intensity are listed in Table 4. They found that the single-photon excitation of Na of the 3s → 4p transition near 330 nm and detection of the 3d→3p fluorescence at 818 nm was the optimum strategy. They also employed a KrF excimer laser producing light at 248 nm to dissociate sodium salt. The dissociation process created atomic sodium which can be subsequently measured using LIF technique. More detailed information about the dissociation process and the excimer laser will be demonstrated in Section 2.3.3.

The experiments introduced above mainly focused on the investigation of the atomic alkali measurement methods and the reaction chemistry of the dominant alkali metal species in different flames with corresponding alkali seeding. However, the measurements of atomic alkali metal under the combustion condition of actual biomass or coal particles are more complicated, especially the scattering caused by the volatiles released during the devolatilization stage, which largely decreases the signal-to-noise ratio. In addition, the thermochemical conversion processes of biomass and coal are usually unsteady and vary from sample to sample. The LIF techniques should have the capacity for temporal and spatial resolution.

Planar laser-induced fluorescence (PLIF) is a well-established two-dimensional (2D) method with its strength of imaging capacity, high sensitivity, and high spatial resolution. A typical PLIF system consists of a tunable laser, a pair of cylindrical lenses which are used to form the laser sheet and an intensified charge-coupled device (ICCD) camera orthogonal to the direction of the propagating light sheet.

van Eyk et al. [25] established a quantitative PLIF method to measure atomic sodium release from a burning brown coal particle suspended in a flat flame as shown in Fig. 24. One of the key issues in quantitative PLIF measurements is the fluorescence calibration. In their research, the PLIF signal was calibrated using simultaneous absorption measurement. A certain amount of aqueous solution of Na_2CO_3 was seeded in the burner to achieve the calibration process. Sodium D1 line at 589.59 nm was excited by a Nd:YAG pumped dye laser and then the fluorescence signal was recorded by an ICCD camera. Two water cells placed in the laser path before and after the burner, respectively, were used to record the absorption intensity. The relationship between the fluorescence signal and laser absorption was built. Consequently, the atomic sodium concentration was calculated using the Beer-Lambert law. The results of their study provided, for the first time, 2D quantitative data on atomic sodium release above a burning coal in char combustion and ash stage. A peak that corresponds closely to the end of char combustion was observed before decaying. An atomic sodium release model was then proposed in a first-order kinetics model that will

Table 4
Electronic transition of atomic sodium and relative fluorescence signal intensity [133].

Excitation transition	Wavelength (nm)	Fluorescence transition	Wavelength (nm)	Normalized signal intensity
3s → 3p	589	3p → 3s	589	Too high to measure using PMT
3s → 5s	2 × 602	3p → 3s	589	60
		5s → 3p	615	2.4
		3d → 3p	818	9.0
		4d → 3p	568	0.5
3s → 4d	2 × 578	3d → 3p	818	0.75
		4d → 3p	568	0.35
3s → 4p	330	4p → 3s	330	75
		3d → 3p	818	300

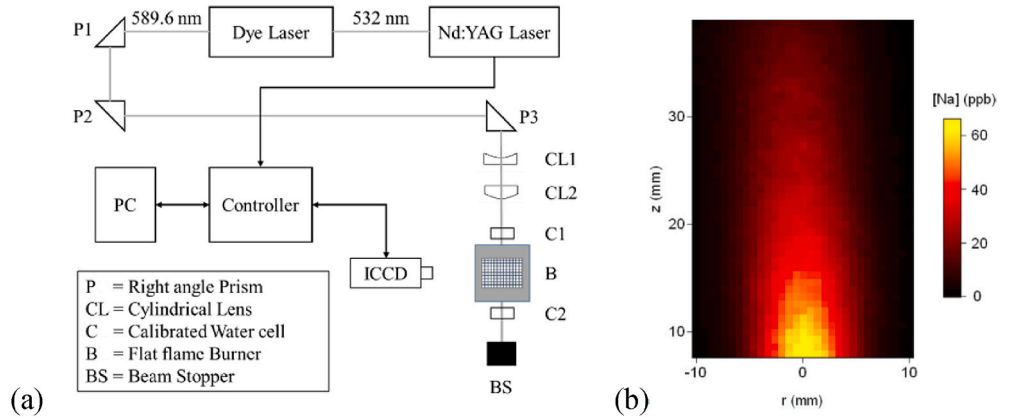

Fig. 24. (a) A typical setup for PLIF measurement of atomic sodium and (b) 2D distribution of alkali atoms. Reproduced from van Eyk et al. [25] Copyright (2008): Elsevier.

be discussed in detail in Section 3.2.1. In the same environment, simultaneous measurement of sodium atom concentration, coal particle diameter, and temperature was conducted. Two-color pyrometry was applied to measure particle temperature with two CCD cameras [134]. They also measured atomic sodium release from water-bound and organically-bound sodium [29]. It is worth mentioning that the total sodium release was also calculated in their study by the measured atomic sodium concentration and chemical equilibrium calculations.

The atomic sodium release data during the devolatilization stage was not included in the work of van Eyk et al. [25,134,135] because of the strong Mie scattering between the incident laser and volatiles. Wang et al. [56] employed non-resonant fluorescence to measure the atomic sodium release from a burning coal pellet for the whole combustion process i.e., devolatilization stage, char burnout stage, and ash reaction stage. A laser pulse at the wavelength of 330.274 nm was used to induce fluorescence (3s → 4p) from atomic sodium. An ICCD camera was used to record the fluorescence signal at 589 nm (3p → 3s) from the measurement region. The noise from Mie scattering was effectively avoided through non-resonant laser-induced fluorescence. The quantitative PLIF technique was also calibrated using laser absorption. The images of atomic sodium release in the devolatilization stage, char burnout stage and ash reaction stage are shown in Fig. 25(a) ~ (c), respectively. The temporal concentration profile of Na at a position 14 mm above the pellet is shown in Fig. 26. Two release peaks were observed in the whole combustion process (cf. Fig. 26), one is in the devolatilization stage, the other one is in the char burnout stage. The ash reaction stage has a long decay line along with time. A two-step atomic sodium release model was established which shows a better predictive ability in the devolatilization stage than van Eyk et al. [135].

The PLIF technique was also applied for measurements of atomic potassium in biomass thermochemical conversion process. Liu et al. [11] measured the atomic potassium release from a burning biomass pellet suspended in a methane/air flat flame. Potassium atoms were excited by

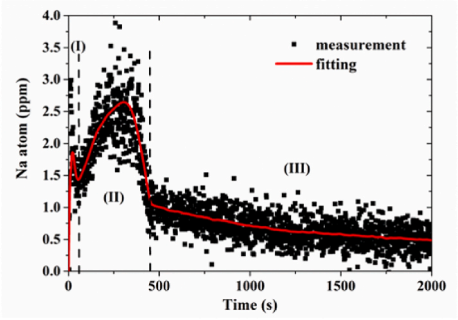

Fig. 26. The temporal concentration profile of Na at a position 14 mm above the pellet. Reproduced from Wang et al. [56] Copyright (2017): Elsevier.

a 769.9 nm incident laser sheet to induce fluorescence from the $4^2s_{1/2} \rightarrow 4^2p_{1/2}$ transition. The Mie scattering was well filtered by a polarizer mounted before the ICCD camera. A better signal-to-noise ratio was achieved at the cost of signal intensity as shown in Fig. 27. Different from the atomic sodium release from coal, the combustion time of biomass was much shorter under the same weight and diameter condition (cf. Fig. 27(b)). Only one release peak was observed during corn straw combustion while two peaks were found in the combustion process of poplar. Diameters and surface temperatures were measured at the same time to derive a kinetic model of atomic potassium release.

2.3.3. *Laser-induced photofragmentation fluorescence (LIPF)*

Laser-induced fluorescence (LIF) has been successful in quantitative measurement of alkali atoms with temporal and spatial resolution, but understanding of the reaction mechanism requires more quantitative information on other alkali species as well. Alkali compounds consist of molecules with only repulsive excited electric states, i.e., the excited

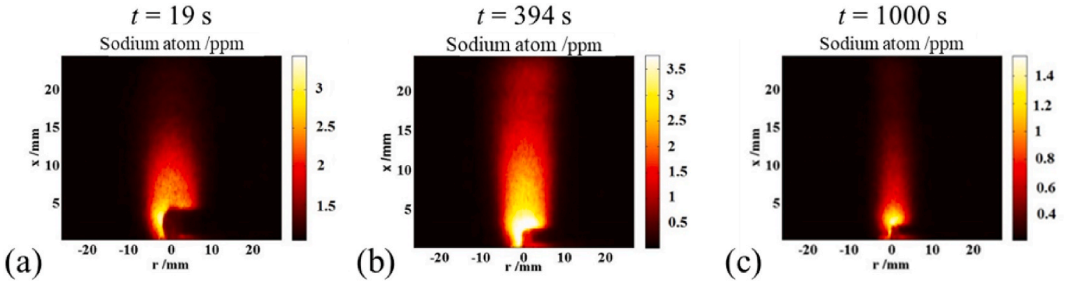

Fig. 25. Images of atomic sodium release in (a) devolatilization stage, (b) char burnout stage and (c) ash reaction stage. Reproduced from Wang et al. [56] Copyright (2017): Elsevier.

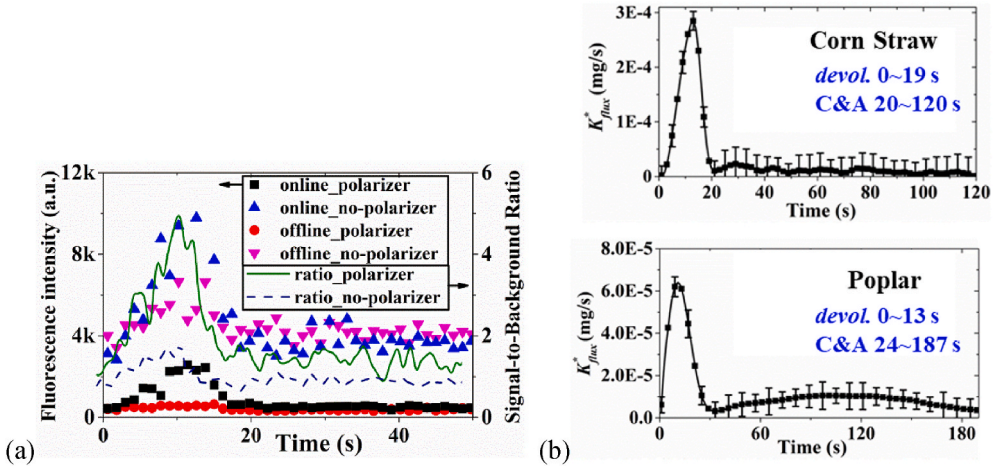

Fig. 27. (a) Fluorescence intensity and signal-to-noise ratio with and without polarizer. (b) Atomic K flux at a position 18 mm above the burning corn straw and poplar pellet, respectively. Reproduced from Liu et al. [11] Copyright (2019): Elsevier.

molecules will spontaneously dissociate into atoms. Thus, most applications of conventional LIF were not suitable in this case since the quantum yield for fluorescence will be immeasurably small [136]. However, incident laser light at a suitable ultraviolet wavelength regime can dissociate alkali molecules into atoms at excited states. Detection of fluorescence from these excited fragmented alkali atoms provides an alternative strategy for molecular alkali measurements.

Laser-induced photofragmentation fluorescence (LIPF) is one of the advanced optical techniques which employs UV laser light to create atomic fragments at the excited state and calculated the alkali compounds concentration through atomic fluorescence. UV laser pulses from an excimer laser [86,137,138] and a frequency-tripled Nd:YAG laser [139] (355 nm) are the most commonly used in LIPF technique. The following reactions show the LIPF process:

$$MX + h\nu \rightarrow M^* + X \tag{5}$$

$$MX_n + 2h\nu \rightarrow M^* + nX \tag{6}$$

$$M^* \rightarrow M + h\nu \tag{7}$$

where M represents alkali metals and X represents radicals such as Cl and OH. Measurements of the spontaneous fluorescence from M* provide qualitative and quantitative information on MX. Both Equation (5) and Equation (6) express the excitation process for one photon and two photons, respectively, while Equation (7) represents the process to produce atomic fluorescence. The fluorescence intensity depends on the exciting UV laser wavelength, laser power, and the alkali compound properties. The requirement for the relationship between the fluorescence signal and the concentration of alkali compounds is one of the most important issues in quantitative LIPF measurements.

Oldenborg et al. [136] presented an assessment of LIPF technique for the determination of gas-phase alkali species in terms of discrimination potential, sensitivity, and quantitative behavior. The discrimination of alkali compounds with different alkali metals is easy to achieve via different emission wavelengths, i.e., 589 nm for Na and 766 nm for K. The different threshold wavelengths for alkali compounds make it possible to distinguish alkali chlorides and alkali hydroxides. The threshold wavelengths for some important compounds of alkali reactions are listed in Table 5. The relationship between the number density of the alkali compounds and fluorescence intensity is expressed as Equation (8):

$$S(\lambda, T) = CN\sigma(\lambda, T)\varphi(\lambda, T)\frac{A_{21}}{A_{21} + Q(T, P)}I \tag{8}$$

where S is the signal intensity at a wavelength λ and temperature T. C is the constant relating to the efficiency of optical components, the solid angle of the detector and its quantum yield. N is the number density of the target compound and σ is the absorption cross-section of the compound. φ is the quantum yield to produce the fragment in the observed electronic state. A_{21} is the Einstein coefficient for spontaneous emission. Q is the quenching rate of the atoms at the excited state which depends on temperature and pressure. I is the laser intensity. It is obvious in Equation (8), that the quenching rate is essential to obtain the absolute concentration of the target compound. In the work of Oldenborg et al. [136], the quenching rate was set as 4×10^{-10} m^3 $molecule^{-1}s^{-1}$.

Table 5
Excitation wavelength for LIPF of common alkali compounds [136,140].

Alkali compound	Excited state of metal atom	One-photon threshold wavelength (nm)
NaCl	Na(3p)	195.9
	Na(4p)	155.5
NaOH	Na(3p)	219.8
NaO	Na(3p)	262.7
Na_2O	Na(3p)	264.6
NaO_2	Na(3p)	326.6
Na_2SO_4	Na(3p)	178.5
KCl	K(4p)	206.8
KOH	K(4p)	233.1
KO	K(4p)	276.9
K2O	K(4p)	266.4
KO_2	K(4p)	353.2
K_2SO_4	K(4p)	188.3

Oldenburg et al. [136] demonstrated the potential of LIPF in online measurements of alkali compounds. On this basis, Helbel et al. [141] measured NaCl release from coal in a drop-tube furnace. They investigated the effects of elevated temperatures on NaCl release from different types of coal. However, the absolute concentration of NaCl release was not obtained due to the lack of quenching rate. Chadwick et al. [138] simultaneously monitored NaOH and NaCl release during pyrolysis and gasification of Loy Yang coal using emission wavelengths of 819 nm and 589 nm, respectively. In their work, they used an ArF excimer laser (output wavelength at 193 nm) to dissociate NaOH and NaCl at the same time. Both of them would produce fluorescence at 589 nm while NaOH dissociation would also produce fluorescence at 819 nm. Thus, the discrimination of NaOH and NaCl was achieved with a detection limit of 0.1 ppb, which is adequate for most situations. The Monte Carlo simulation was used in their method to modify the influence of radiation trapping and quenching phenomena [142]. They found that under the inert atmosphere (pyrolysis conditions), NaCl was the dominant Na species and the NaOH concentration increased with oxygen content,

which agreed with chemical kinetics predictions. Later in 1996, Chadwick et al. [143] further investigated the sodium species release during Loy Yang coal combustion and gasification process using the above method. In 1997, Chadwick et al. [139] developed a new LIPF method using 355 nm multiple-photon photofragment fluorescence to measure gas-phase NaOH. The principle of this method is shown in Fig. 28. The fluorescence intensity is proportional to the square of the laser power since multiple-photo excitation is employed in this method. The detection limit of this method is 0.5 ppm which is less sensitive compared with the excimer laser approach. They also proposed a theoretical calculation of wavelength needed to measure different types of alkali compounds using Nd:YAG laser. The calculated wavelengths are listed in Table 6.

In the past 30 years, Monkhouse and Gottwald et al. [36,140,144–150] did a lot of work on the measurements of alkali compounds in both lab-scale and industrial-scale flue gas. They investigated the influence of fluorescence quenching [144] on the detection of alkali compounds as well as the effects of operating conditions [150], gas composition [150] and fuel additives [147,148]. The measurement conditions of industrial scale mainly focused on fluidized beds with different fuel types [146] and operating parameters [140,145,149]. The fate of alkali species in gasification has been investigated [151], in which few measurements of alkali release concentration were conducted before. More information on their works in industrial boilers will be introduced in Chapter 4 in detail.

Leffler et al. [86,137] developed the LIPF method by capturing the fluorescence image using an ICCD camera. This method gives a two-dimension distribution of alkali species and could be useful in the fundamental investigation of biomass and coal combustion. Recently, Weng et al. [152] combined LIPF technique with broadband absorption spectroscopy to measure the potassium species release from single burning pulverized biomass particles. The results show that KOH represented 60 % of the total potassium release in the char combustion stage.

2.4. LIBS spectroscopy

2.4.1. Laser-induced breakdown spectroscopy (LIBS)

Laser-induced breakdown spectroscopy (LIBS) has been widely used for the total potassium/sodium element measurements due to the relatively simple and robust approach. In LIBS system, a high-energy laser is focused at the measurement point generating a spark of high-temperature plasma. During cooling down, characteristic spectrum emission can be detected by a spectrometer and the signal intensity represent the amount of alkali metal release information. During the LIBS process, all the alkali-containing species will be converted into a plasma state. Therefore, the LIBS technology is a kind of element detection technology that cannot distinguish the different compound species. Nd:YAG laser is the mostly used laser source to induce plasma at solid or gas phase. A typical experimental arrangement of LIBS is shown in Fig. 29.

Table 6
Calculation wavelength required for multiple-photon absorption detection of gas-phase alkali compounds. (D_0: dissociation energy) Reproduced from the Chadwick et al. [139] Copyright (1997): OSA.

Alkali compound	D_0 (kcal/mol)	Threshold wavelength (nm)	Convenient photolysis source
NaCl	97.5 ± 2	293 ± 6	Nd:YAG fourth harmonic/266 nm
NaOH	81.5 ± 3	350 ± 10	Nd:YAG third harmonic/355 nm
Na_2SO_4	111 ± 5	257 ± 15	Nd:YAG fourth harmonic/266 nm
KCl	89.7 ± 2	319 ± 6	Nd:YAG fourth harmonic/266 nm
KOH	97.5 ± 2	386 ± 6	Nd:YAG third harmonic/355 nm
K_2SO_4	103 ± 5	277 ± 15	Nd:YAG fourth harmonic/266 nm

Hsu et al. [57] employed the LIBS technique in elemental Na/K detection and measured the dynamic release behavior of brown coal and wood pellet. The relationship between LIBS signals and alkali concentrations was established through seeding a series of alkali solutions into the flame (cf. Fig. 30(a)). However, the nonlinearity of the calibration curve was found because of the self-absorption by atoms of the outer plasma region and the flame region as shown in Fig. 31. The authors developed a quantitative method to modify the self-absorption using the Beer-Lambert law. The corrected LIBS signal shows a very good linear relationship with alkali concentration as shown in Fig. 30(b). The detection limits were estimated to be 29 and 72 ppb for sodium and potassium, respectively.

He et al. investigated the effects of O_2 and CO_2 concentrations on the total sodium and potassium element release of coal [24]. They found that both O_2 and CO_2 concentrations have little effect on the alkali release during devolatilization stage while increasing O_2 concentration promoted alkali metal release and increasing CO_2 concentration suppressed the release in char combustion stage, respectively. The authors also [153] measured the release of different chemical forms of sodium from a burning coal pellet by LIBS. It was found that the amount of sodium release was in an order of H_2O-soluble Na > NH_4Ac-soluble Na > HCl-soluble Na > insoluble Na. Moreover, the additive effects on sodium release during coal combustion were estimated [154]. Recently, the potassium release from two types of biomass, i.e., poplar and corn straw with different classes of potassium and the additive effects was investigated by their group [155] using LIBS technique. Different results were obtained for poplar and corn straw where poplar had two release peaks while corn straw only had one.

Fatehi et al. [38,156] adopted LIBS to measure the concentration of total potassium released from gasifying biomass. Potassium release at different temperatures was investigated in hot gas mixture of CO_2, H_2O

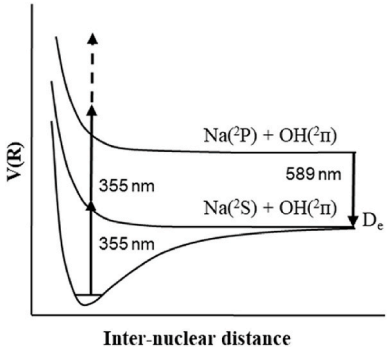

Fig. 28. Multi-photon absorption of NaOH and fluorescence of Na at 589 nm. Reproduced from Chadwick et al. [139] Copyright (1997): OSA.

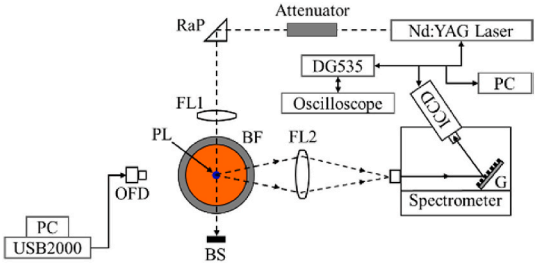

Fig. 29. A typical experimental arrangement for the LIBS technique. Note: RaP (right-angled prism); FL (focal lens); BF (burner and flame); PL (LIBS plasma); G (grating); BS (beam stopper); OFD (optical fiber detector). Reproduced from Hsu et al. [57] Copyright (2011): OSA.

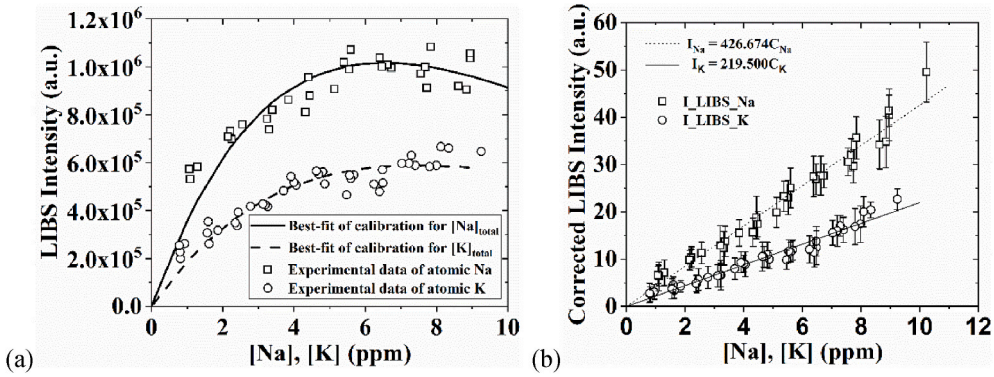

Fig. 30. (a) The relationship between LIBS signals and alkali concentrations in the flame before correction process of self-absorption. (b) Final calibration curves after signal trapping correction using Beer-Lambert law. Reproduced from Hsu et al. [57] Copyright (2011): OSA.

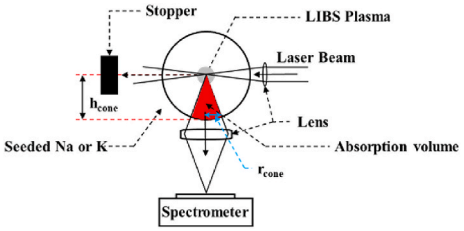

Fig. 31. Self-absorption (signal trapping) due to the outer region of the flame. Reproduced from Hsu et al. [57] Copyright (2011): OSA.

with different O_2 concentrations. The experimental data was subsequently used to determine the chemical kinetic constants of potassium release rate and propose a reaction path of biomass gasification.

Zhang et al. [10] investigated the effect of initial mass on potassium release from a single pinewood pellet. It is worth noting that, they calculated the potassium flux base on LIBS results and a computational fluid dynamics (CFD) model. The total amount of potassium release at different stages could be calculated by flux-time integrals. Liu et al. [157] developed a multi-point LIBS method to obtain the alkali flux directly from LIBS results which will be introduced in detail in Section 2.4.2.

Self-absorption leads to a non-linear relationship between the signal intensity and the alkali concentration under high concentration conditions. In general, the nonlinearity is corrected by using a modified Beer-Lambert law introduced in the work of Hsu et al. [57]. However, this would cause a poor accuracy at high alkali concentrations. Typically, the detection limits are below 10 ppm during alkali release measurements [10,24,57]. Viljanen et al. [158] improved the detection range of alkali metals by using a novel burner with a modified seeding apparatus and microwave-assisted LIBS (MW-LIBS). The upper limit of detection can be improved to over 200 ppm and the minimum detection concentration is around 10 ppb and 19 ppb for sodium and potassium, respectively. Recently, Zhao et al. [12] applied a developed calibration method which also extended the detection range to 200 ppm. They achieved this by applying the margin area of potassium D2 line (shadow area shown in Fig. 32 (a)) rather than the center wavelength that is commonly used. Fig. 32 (b) shows the linearity of this method.

The above-mentioned research activities mainly focused on gas-phase total potassium/sodium release during thermochemical conversion processes of coal and biomass. As mentioned in Section 2.1, alkali can also exist in a condensed phase in the droplets and fly ash particles. Yuan et al. [159] developed a phase-selective LIBS method to measure alkali release with the ability to distinguish the existence phase of alkali species since only breakdown emission from alkali in particle phase occurs with low laser intensity. Then they applied this method in the investigation of pulverized coal combustion and analyzed the process of sodium release, especially in the early stage of devolatilization from where they found that the ambient temperature had a dominant effect on the sodium transition from particle to gas phase.

2.4.2. *Multi-point laser-induced breakdown spectroscopy (M-LIBS)*

Studies mentioned in Section 2.4.1 employed a single-point LIBS measurement to obtain the temporally resolved release behavior of alkali metals. Thus, only alkali concentration at the measured point can be obtained. This limits the ability to acquire alkali flux which is an indispensable parameter to calculate the total alkali release.

As mentioned above, Zhang et al. [10] combined LIBS results with CFD simulations. A laminar CFD model was used to obtain the distribution of potassium. They validated simulation results with 11 pinewood particles of the same initial mass. The measurement points of these 11 particles were at different radial locations. Thus, the K flux and total

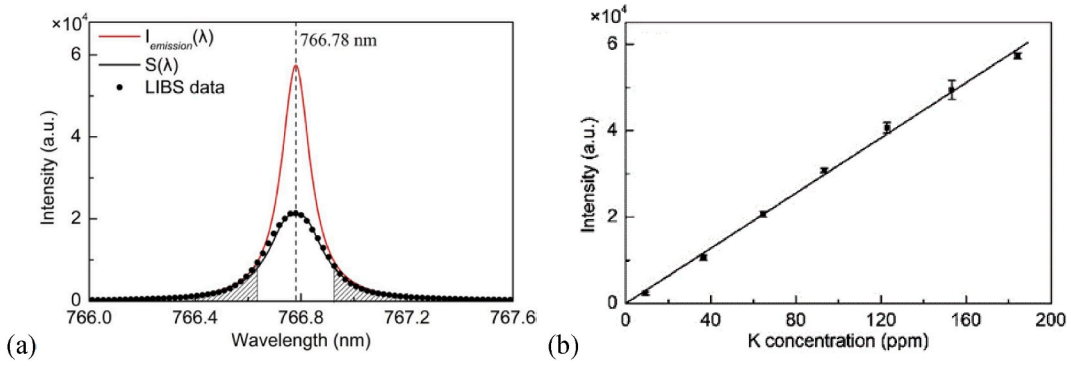

Fig. 32. (a) A typical example of the self-absorption effect for potassium in LIBS measurement. (b) Calibration profile of potassium using the margin area of K D2 line. Reproduced from Zhao et al. [12] Copyright (2020): ACS.

release amount could be calculated. However, the accuracy of this method depends on the CFD model which added more uncertainty to the results. Liu et al. [157] developed a multi-point LIBS method (M-LIBS) which measured nine points at the same height of different radii within 1 s. The multi-point measurement is achieved by mounting the focusing lens and signal collection optics on a translational platform. The radial concentration distribution (C_M) of alkali metals (M) can be derived from LIBS results of these points by a polynomial function fitting. By an integral function (Equation (9)), the alkali flux can be obtained. The arrangement of the M-LIBS method was shown in Fig. 33 (a).

$$M_{flux,t} = \int_0^{2\pi} \int_0^{\infty} u\, C_M\, r\, dr\, d\theta \tag{9}$$

The total amount of alkali release during the whole thermochemical conversion process and at each stage can be calculated from time-integration of the alkali flux. They measured the sodium release characteristics of a burning coal pellet using this method. As shown in Fig. 34, the temporal Na flux profile of the burning coal pellet clearly indicates the three stages of coal combustion, i.e. devolatilization stage, char burnout stage and ash reaction stage. The former two stages are separated by the trough (the green square) and the char burnout stage and ash reaction stage are separated by the intersection point of two blue trend lines (the red square). The sodium release proportion in different stages and the whole combustion process is derived by time integration. The results are in good agreement with the OES-ICP results which validates the feasibility of their method. Then they [160] studied the effects of mineral additives on sodium release inhibition and investigated the transformation of sodium in solid phase with the assistance of XRD results. In 2018, they employed this method in biomass combustion combined with K-PLIF measurement [11]. The release characteristics of elemental potassium and atomic potassium were investigated simultaneously. Recently, He et al. [161] measured the release behavior of potassium and zinc simultaneously from a burning hyperaccumulator pellet using the multi-point LIBS method. The total amount of potassium and zinc release of different chemical groups was studied in this work and H_2O-soluble K and NH_4Ac-soluble Zn were found to be the major released K and Zn compound groups, respectively.

3. Alkali metal release behavior and modeling

In Chapter 2, we introduced several optical methods that can be used for *in situ* measurements of various alkali metals in thermal conversion processes. In this chapter, we will present the progress in release mechanisms and release modeling of alkali metals based on measurements using optical methods.

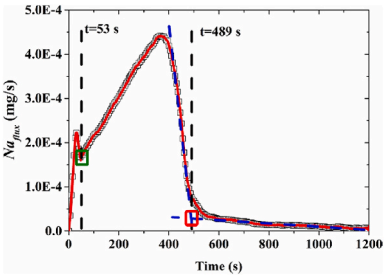

Fig. 34. Determination of three sodium release stages during a coal pellet combustion. Reproduced from Liu et al. [157] Copyright (2018): Elsevier.

3.1. Alkali metal release behavior

3.1.1. Release mechanism

Knowledge of alkali release mechanisms is of great importance to the understanding of the behavior of alkali metal release and transformation as well as the development of the release models. Numerous studies on alkali release mechanisms were conducted based on off-line sampling analyses [162–176]. With the rapid advancement of optical methods, access to the alkali release behaviors with temporal, spatial, and species resolutions promotes the development and validation of the release mechanism.

Earlier studies on the release mechanism based on optical measurement results were conducted by van Eyk et al. [135]. They measured the atomic sodium concentration above a burning Loy Yang coal pellet using Na-PLIF and investigated the sodium release behavior with different original chemical forms [29]. Based on the experimental results, they proposed a full mechanism for sodium release during the whole combustion process, including volatile release, char combustion, and ash stage (cf. Fig. 35). In their work, they found that ~33 % of water-bound sodium was released in the devolatilization stage, while no organically-bound sodium release was observed in this stage. Hence they deduced that the alkali release in this stage was due to the NaCl vaporization and the remaining portion (~67 %) of water-bound sodium was converted into organically-bound sodium. The organic sodium might be with a form of carboxylic acid sodium (−COONa). The study of brown coal showed that carboxylic acid groups would decompose and lead to a release of CO_2 during pyrolysis. However, since no organic sodium was observed to release in this stage, they believed that sodium was associated with the char structure (−CNa) to retain in char particle. In the char combustion stage, they proposed an oxidation/reduction cycle with sodium phenolate groups (−CONa) as the intermediate substance. The sodium phenolate groups play a role in catalyzing the char combustion. They thought that the rate-determining step for sodium release during char combustion was the formation of a reduced form of

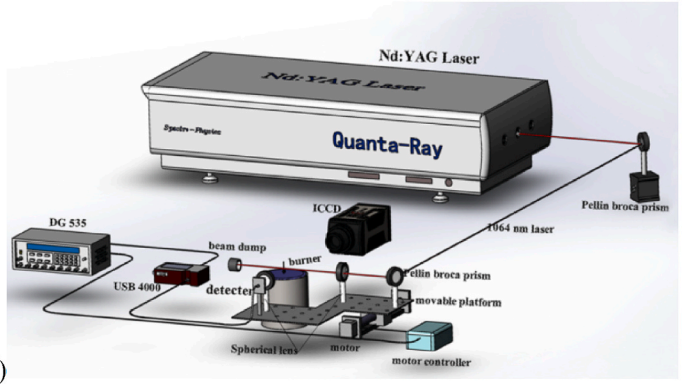

Fig. 33. (a) A typical arrangement of multi-point LIBS and (b) the schematic diagram of measured points. Reproduced from Liu et al. [157] Copyright (2018): Elsevier.

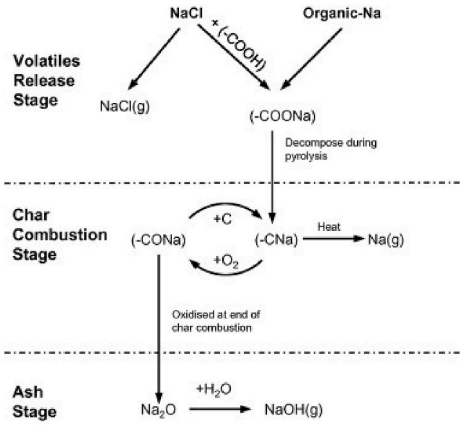

Fig. 35. Mechanism proposed by van Eyk et al. for sodium release during combustion of Loy Yang brown coal particle. Reproduced from van Eyk et al. [135] Copyright (2011): Elsevier.

sodium: CONa + C→-CNa + CO, which subsequently led to the rapid loss of sodium from the particle. The results from the online experimental in their work also showed that 60 % sodium release occurred at the ash stage. The most possible form of sodium in ash was Na_2O, which will react with H_2O in the ash stage and generate NaOH(g).

Zhang et al. [10] obtained the profile of K release during pinewood combustion process using the LIBS method and developed a nine-step mechanism of K transformation for all three stages (cf. Fig. 36). They divided potassium into two types, Char-K and inorganic K, and indicated that these two types of K would transform through five possible path (R1−R5, cf. Fig. 36) during the devolatilization stage. After the devolatilization stage, the K in the char particle presented as Char-K or potassium salts. The release of potassium from Char-K during char combustion stage was mainly from two pathways: thermal decomposition of Char-K (R6) and oxidation to inorganic K from Char-K (R7). However, they deduced that the release rate of K from the thermal decomposition of Char-K was much slower than that from Char-K oxidation to inorganic K, which was supported by the experimental results from their previous work [177] and brown coal pyrolysis [178]. Then, the generated inorganic K would decompose to release in gas phase (R8) or retain in ash by mineralization effect. A similar release mechanism was also proposed by Fatehi et al. [156] based on potassium release measurement using LIBS.

Liu et al. [11] developed the potassium release mechanism of biomass proposed by Zhang et al. [10] based on their optical measurements of burning poplar and corn straw pellets as shown in Fig. 37. They took into account the catalytic effect of potassium and an oxidation-reduction cycle of Char-K was involved in their mechanism. During the devolatilization stage, some organic K is directly decompose generating K(g) into gas phase (P1), while the other portion is retained in the fuel (P2). Inorganic-K is released into the gas phase through evaporation and decomposition (P3). Besides, inorganic-K will react with organic structures in the biomass and be transformed to Char-K (P4). They thought that in the char burnout stage, Char-K could be released through the path Char-K→CK→K (P6), rather than first oxidation into inorganic K proposed by Zhang et al. [10]. In the ash stage, the observed potassium release was due to the reaction between water vapor and potassium in ash (P8).

3.1.2. Factors affect release behaviors

The mechanisms proposed by van Eyk et al. [135] and Zhang et al. [10] differ a lot. For example, in the mechanism of van Eyk et al., the release of sodium in the devolatilization stage was all from water-soluble alkali metals, while in Zhang et al.'s mechanism, the potassium release may be due to the decomposition of organic K. The differences may attribute to several factors, such as the difference in fuel types, the original alkali chemical forms, and reaction conditions. Additionally, these factors can also affect the reaction path of alkali metal in a specific case. Optical methods provide a powerful way to investigate the effects of these factors, which are meaningful to the development of mechanism.

3.1.2.1. The effect of fuel type. The effect of fuel type is complicated since it would affect several factors at the same time. For example, the alkali content, the original chemical forms, the minor element compositions, etc. Weng et al. [90] compared the release profile of atomic potassium from burning wood, straw, and coal, respectively. As shown in Fig. 38, the atomic potassium release behaviors have a significant difference among the fuels characterized by the reaction duration, release intensity, peak values and peak positions. A much greater release was observed for wood and straw than for coal, due to a lower potassium content in coal. The same results were also observed by Chansa et al. [179] and Liu et al. [180]. Some studies attempt to compare the alkali release behavior of wood and straw, which represent two kinds of typical biomass [11,58,77,90]. Herbaceous biomass like straw is typically rich in both potassium and chlorine. The presence of Cl is known to promote the release of alkali metals [147,168,170]. Weng et al. [181] used LIPF to measure the KOH and KCl released from wood and straw

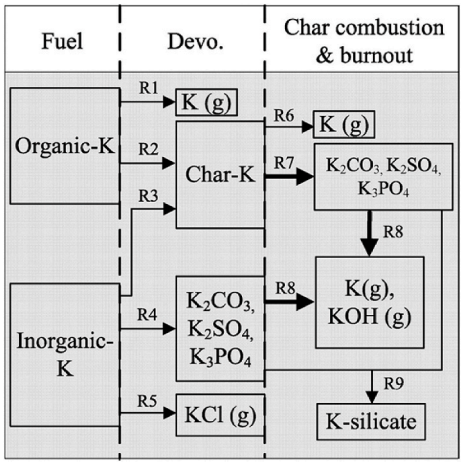

Fig. 36. Possible transformation during pinewood combustion. Reproduced from Zhang et al. [10] Copyright (2015): Elsevier.

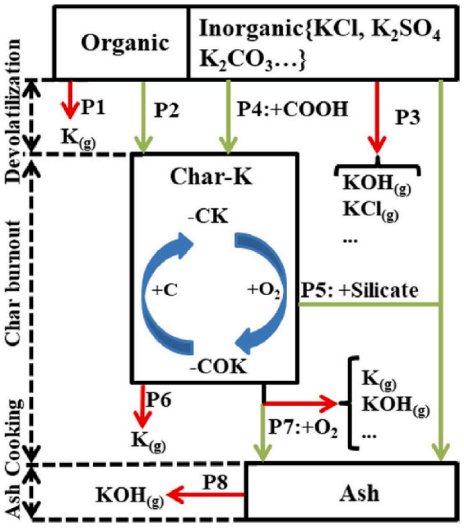

Fig. 37. A suggested potassium transformation mechanism during biomass combustion. Reproduced from Liu et al. [11] Copyright (2019): Elsevier.

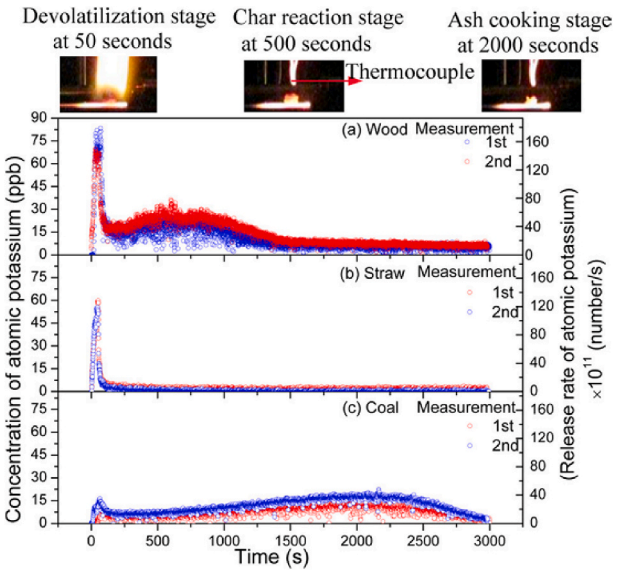

Fig. 38. Temporal profile of the atomic potassium concentration in the plume of burning (a) wood, (b) straw, and (c) coal at a measurement height of 2 mm above the pellet. Reproduced from Weng et al. [90] Copyright (2017): ACS.

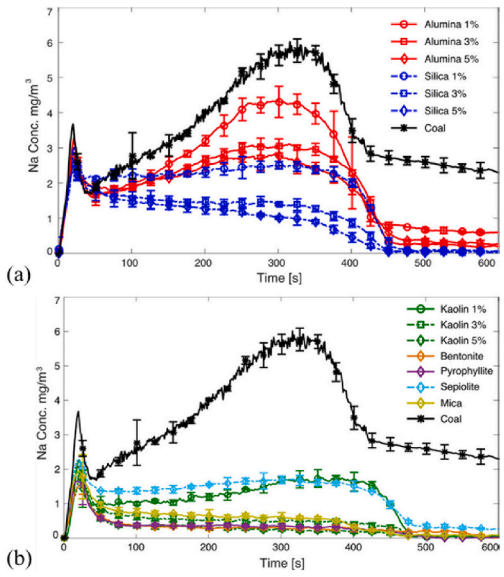

Fig. 39. The effects of additives on sodium release during coal combustion. (a) Synthetic additives; (b) natural mineral additives. Reproduced from He et al. [154] Copyright (2017): ACS.

pellets. Only KCl was observed for the burning straw pellet, while KOH was the dominant potassium species released from the wood, which indicated the presence of Cl in straw prompted potassium to release in the form of KCl. However, one interesting thing is, even though the alkali and chlorine content in straw was much higher than that in the wood samples used in their work, only 10 % of potassium in straw samples was released, which was less than the wood sample (about 37 %). This phenomenon was also observe by Qu et al. [77] and Thorin et al. [58]. One of the possible reason is the high amount of silicon in straw samples facilitates the forming of K-silicates, thus the potassium was retained in the ash. It is evident that the effect of minor elements on alkali metal release is crucial. However, there are relatively limited *in situ* investigations about the effect of inherent minor elements in fuel on alkali metal release. Nevertheless, numerous studies have been conducted on the additive effects [12,147,148,154,155,160,161] of alkali release using *in situ* optical methods. Interactions between alkali metals and elements such as Al and Si were also involved in these cases. Hereby, these studies can provide some insights into the minor element effects.

The additives include synthetic additives like silica (SiO_2) and alumina (Al_2O_3), and natural mineral additives like kaolin, mica, and pyrophyllite and generally contain a high amount of silicon (Si) or aluminum (Al). A comparison of the sodium release profile with and without additives during coal combustion processes is shown in Fig. 39. The inhibition effect of additives on alkali metal release is obvious. This is probably due to the form of insoluble sodium via reacting between the additives and water-soluble sodium [160]. These results implies Si and Al in biomass and coal can prohibit the alkali release.

3.1.2.2. The effect of alkali chemical forms. The effects of original chemical forms were investigated by several researchers [23,29,153,182]. These studies varied from fuel types (biomass and coal), optical method (PLIF, LIBS, and TDLAS) and target species (atoms or elements). van Eyk et al. [29] investigated the release behaviors of water-bound and organic sodium from burning Loy Yang brown coal. The release fate of sodium atoms during char combustion and ash stage was monitored by Na-PLIF. The results showed that ~67 % of the water-bound sodium would be released during the char and ash stages, whereas ~100 % of the organically-bound sodium would be released in these stages. He et al. [153] investigated release characteristics of sodium with different original chemical forms from burning Zhundong coal pellets using the LIBS method. They found that the relative contribution of various sodium forms to the total sodium release during each combustion stage was similar, with an order of H_2O-soluble Na > NH_4Ac-soluble Na > HCl-soluble Na > insoluble Na. Besides, ~64 % of total sodium released was observed from H_2O-soluble Na, which indicated washing might be an effective strategy to mitigate alkali-induced problems. Liu et al. [23] studied the release characteristics of different alkali forms using multi-point LIBS. The real-time sodium release flux could be determined in this setup. The experimental results are shown in Fig. 40. The results showed that the H_2O-soluble sodium dominate sodium

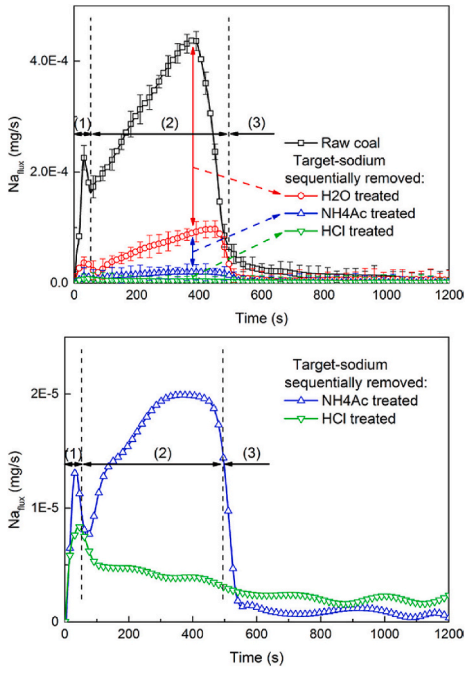

Fig. 40. Temporal sodium release profiles of raw and target-sodium sequentially removed Zhundong coal measured by multi-point LIBS. The NH_4Ac- and HCl-treated cases are zoomed in and shown on the bottom. Note: (1) devolatilization, (2) char burnout, and (3) ash cooking. Reproduced from Liu et al. [23] Copyright (2018): ACS.

release of all reaction stages and account for 76 % of the total sodium release. Besides, three kinds of sodium compounds, i.e., NaCl, NaOH, and Na_2SO_4 were then enriched into the coal sample to investigate their catalytic effects. The results showed that sodium additives can be used to catalyst coal combustion with an order of NaOH > Na_2SO_4 > NaCl.

The release behavior of different potassium forms from a burning biomass pellet was also investigated using the similar method. The results showed that the contribution of H_2O-soluble K, NH_4Ac-soluble K, and HCl-soluble K to the total K release were 58.2 %, 27.4 %, and 7.6 %, respectively [161]. Recently, Sun et al. [182] studied the release of potassium atoms from pulverized rice husk burning in tubular burner using the TDLAS method. The effects of O_2/N_2 and O_2/CO_2 atmosphere on potassium release were also investigated. The results are shown in Fig. 41. As can be seen, the atomic concentration decreased gradually after sequential extraction. After removing the water-soluble K, the organic K released slower but smoother, corresponding to a secondary reaction rate of potassium with ash. Besides, the atomic K concentration profiles along the burner's height indicated that the release of water-soluble K mainly occurred at the initial stage and was the fastest. The release of atomic K in O_2/CO_2 was slower and weaker than that in O_2/N_2 atmosphere, indicating an inhibition effect under oxy-fuel combustion conditions. The inhibition effect was observed more obviously between two raw rice husk combustion profiles, indicating O_2/CO_2 atmosphere had a more significant effect on the water-soluble potassium among the four different potassium forms.

3.1.2.3. The effect of reaction conditions. The changes in reaction conditions have a significant effect on the alkali release fates. Temperatures and reaction atmospheres are two of the most commonly considered factors. Increasing temperature promotes the release of alkali metals, and this is mainly achieved through two pathways. On the one hand, an increase in temperature promotes the direct evaporation of alkali chlorides [135]. On the other hand, the increased temperature facilitates the decomposition of both inorganic K and Char-K [11]. Sorvajärvi et al. [74] measured the release of atomic K, KOH, and KCl from spruce bark samples burning in a single particle reactor with 10 % O_2 and 90 % N_2. They found the release of these potassium species increased with increasing reactor temperature. Meanwhile, a higher amount of KCl was release in the devolatilization stage. Reaction atmospheres will also affect the alkali release behavior. Results from Thorin et al. [58] also showed that the potassium release in the fuel-rich was smaller than that in the fuel-lean flame. And the main species released changed from KOH to atomic K when the equivalence ratio changed from fuel-lean to fuel-rich.

Regarding the effects of reaction conditions, a special case that has to mention is the oxy-fuel combustion. Although biomass is considered a carbon-neutral fuel, there is still a direct CO_2 emission during their thermal conversion processes. Oxy-fuel combustion is a promising technology for efficient CO_2 capture, where pure oxygen mixes with recycled flue gas to act as an oxidizer for combustion. Thus, the main components in the gas products are CO_2 and H_2O. After simplified purification, the CO_2 can be easily captured and stored. A comparison of gas components of the inlet flue gas between combustion with air and oxygen is shown Table 7. As can be seen, the oxy-fuel combustion brings a significant change in the reaction atmosphere compared with air-fuel combustion, leading to the changes in characteristics of fuel combustion and influencing the release behavior of alkali metals.

Studies on alkali metal release in oxy-fuel combustion using optical methods are relatively rare and mainly focus on coal combustion. He et al. [24] applied LIBS to measure concentrations of elemental Na and K above the coal pellets burning with varied O_2 and CO_2 concentrations. The results of sodium release are shown in Fig. 42. The release of potassium and sodium exhibited a similar pattern. They found neither the stage duration nor the peak release intensity was observed to change with O_2 and CO_2 concentrations in the devolatilization stage. Therefore, they believed the alkali release in this stage was mainly caused by salt evaporation. Due to the similarly designed gas temperature, the evaporation intensity stayed constant with different concentrations. However, during the char burnout stage, the increasing O_2 concentration would promote the release of Na and K, while increasing CO_2 would inhibit their release. This implied in this stage, the release behavior was closely related to the char combustion. A higher O_2 concentration in the flame enhanced the char combustion by increasing the diffusion rate of O_2, while a higher CO_2 concentration showed the opposite tendency. An interesting result was observed in the ash stage. Due to the longest-lasting time, the alkali release amount in this period accounted for the largest share of the total release, despite the release intensity was not high. A slight increase in alkali release was observed at a higher CO_2 concentration in this stage, while an opposite tendency was observed at a higher O_2 concentration.

The work of He et al. [24] was conducted in premixed-flame conditions. This kind of setup provides convenience to optical measurements, but the reaction atmosphere differs from that of real industrial facilities. Li et al. [184] and Dong et al. [185] studied the influences of O_2/N_2, O_2/CO_2, and original potassium forms on the alkali release from coal pellets using the AES method. The sample was placed in a quartz chamber where gas compositions could be flexibly adjusted. A

Table 7
A comparison of gas components between combustion with air and oxygen [183].

Gaseous species	Air-fuel combustion (wet basis)	Oxy-fuel combustion (wet basis)
O_2	21 vol%	21−30 vol%
N_2	79 vol%	0−10 vol%
CO_2	0 vol%	40−50 vol%
H_2O	Small	10−20 vol%
Others		NO_x, SO_x

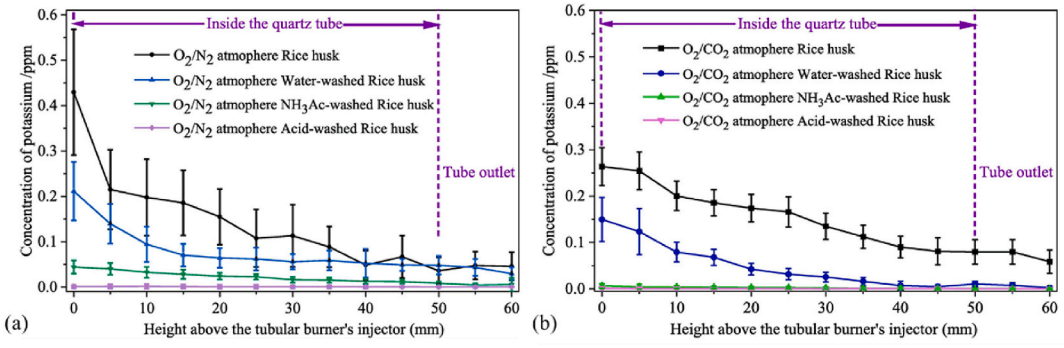

Fig. 41. The atomic K concentration along the burner height direction during rice husk (a) O_2/N_2 combustion and (b) O_2/CO_2 combustion. Reproduced from Sun et al. [182] Copyright (2022): Elsevier.

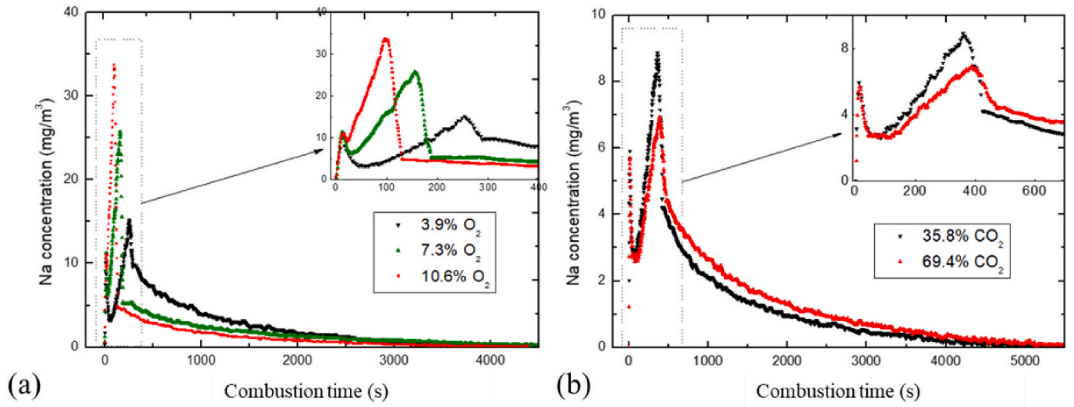

Fig. 42. Effects of (a) O_2 and (b) CO_2 concentration on the total sodium release during oxy-fuel combustion of Zhundong coal using LIBS. Reproduced from He et al. [24] Copyright (2013): ACS.

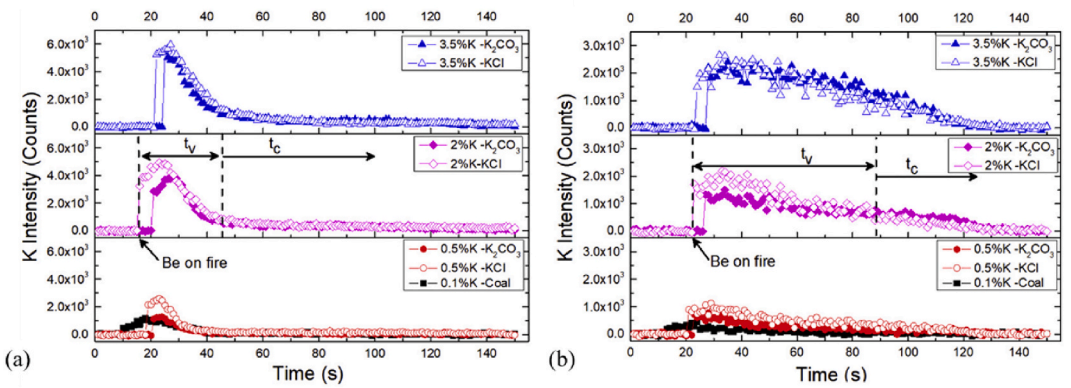

Fig. 43. Release profiles of atomic potassium under (a) O_2/N_2 atmosphere and (b) O_2/CO_2 atmosphere. Note: t_v represents the devolatilization stage and t_c represents the char combustion stage. Reproduced from Dong et al. [185] Copyright (2020): Elsevier.

high-power laser was adopted for ignition and the heating rate was changed through varying laser power to mimic the realistic combustor. The real-time emission spectrum of alkali metals was monitored by a spectrometer. It should be noted that, due to the lack of a calibration procedure, the spectrum results couldn't be used for quantitative measurement of alkali release. The experimental results showed that the increasing O_2 concentration dramatically enhanced the observed sodium and potassium signal intensity, which implied more alkali metals were released at higher O_2 concentrations. However, compared with O_2/N_2 cases, the O_2/CO_2 cases showed a relatively weaker spectral intensity with the same O_2 fraction, demonstrating the inhibition of alkali metals in these cases. Besides, the inhibition effect varied with O_2 content and exhibited a trend of first increasing and then decreasing. To investigate the impact of original chemical form of potassium on the release behaviors, two potassium species, i.e., K_2CO_3 and KCl, were added to the coal sample, respectively. As shown in Fig. 43, with the same additive amount, the emission intensity of potassium with KCl additive was stronger than that with K_2CO_3 additive in both O_2/N_2 and O_2/CO_2 cases. However, the difference became smaller with increasing additive amounts. The release rate of potassium was faster in an O_2/N_2 atmosphere than in an O_2/CO_2 atmosphere. The potassium release profile in the O_2/CO_2 atmosphere had a longer devolatilization duration. The main reason was explained by the substitution of CO_2 for N_2 reduced the heating rate of volatiles and suppressed radical reactions which could promote the combustion rate. The diffusion rate of O_2 and volatiles was also slowed down in CO_2 atmosphere, causing the volatiles to burn longer.

3.2. Alkali release modeling

3.2.1. Kinetics modeling of alkali release

The fate of potassium and sodium release from biomass and coal during different thermochemical conversion processes is essential to understand corrosion and deposition phenomena and ensure the safe operation of power-generation facilities. Release models are valuable to quantitatively depict the alkali release fate. An appropriate modeling expression of the alkali release procedure relies on accurate real-time alkali release data and comprehension of release mechanisms. The rapid development of optical diagnostic techniques makes it possible to obtain time-resolved quantitative data and the release rate of alkali metals can then be calculated. By combining the experimental results and kinetic release model, kinetic parameters of alkali release can be derived. Generally, the rate constant of alkali release is assumed to obey the Arrhenius expression with the pellet temperature. Various optical diagnostic techniques as well as several thermochemical conversion models are employed to derive the kinetic parameters of this expression for different fuels and stages. A summary of rate constants of alkali release is shown in Table 8.

Jones et al. [121] investigated the potassium release behavior from biomass particles within a flame environment. The hot flue gas generated from a CH_4/air premixed flame provided a rapid heating rate and high temperature. According to the spontaneous emission signal of potassium, they divided the potassium release into three stages, i.e. volatile combustion, char combustion, and ash stages (cf. Fig. 44(a)). In the first stage, considering the relatively lower temperature, they assumed that potassium was bounded to or entrained in the decomposing volatiles.

Table 8
Summary of rate constants of alkali release in an Arrhenius form: $k = A\ \exp(-E/RT)$.

Authors	Ref.	Fuel	Reactor	Particle size or weight	Measured alkali species	Reaction stage	A (s^{-1})	E (kJ/mol)
Jone et al.	[121]	Willow	Laminar flame	2–4 mm	Atomic K	Devolatilization stage	2.2×10^{13}	170
van Eyk et al.	[135]	Loy Yang coal	Laminar flame	10–50 mg	Atomic Na	Char and ash combustion	$10^{5.2\pm0.4}$	214
Zhang et al.	[10]	Pinewood	Laminar flame	3–4 mm	Elemental K	Char combustion	12.5	89.9
Fatehi et al.	[156]	Swedish wood	Laminar flame	8 × 4 mm	Elemental K	Char and ash combustion	$2.5 \times 10^{5\pm0.2}$	238–292
Fatehi et al.	[38]	Swedish wood	Laminar flame	8 × 4 mm	Elemental Na	Pyrolysis stage	3×10^{12}	218–248
					Elemental K		2.3×10^{12}	168–198
Zhang et al.	[15]	Sawdust	Fluidized bed reactor	0.18–0.85 mm	Elemental Na	Gasification	3.22×10^{23}	504.7
						Pyrolysis	1.90×10^{34}	733.5
Liu et al.	[157]	Zhundong coal	Laminar flame	4–6 mm	Elemental Na	k_1[a]	$10^{6.083}$	279.3
						k_2[b]	$10^{6.118}$	287.8
Liu et al.	[11]	Corn straw	Laminar flame	4 mm	Elemental K	k_1[a]	2.24	64.8
						k_2[b]	15.3	62.8
Liu et al.	[11]	Poplar	Laminar flame	4 mm	Elemental K	k_1[a]	4.64	84.6
						k_2[b]	20.5	55.4
Zhang et al.	[16]	Sawdust	Fluidized bed reactor	0.18–0.85 mm	Elemental K	Gasification	4.79×10^{10}	207.5
						Pyrolysis	6.58×10^{13}	276.2

[a] Reaction rate k_1 represents reaction rate of volatile alkali during the whole process in a two-step kinetics model [157].
[b] Reaction rate k_2 represents reaction rate of organic alkali during the whole process in a two-step kinetics model [157].

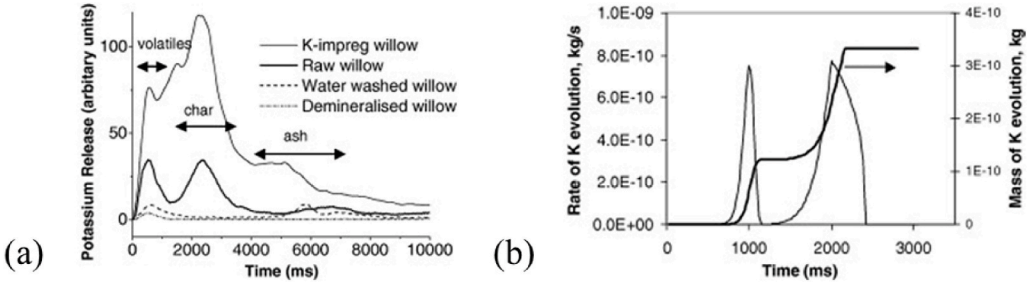

Fig. 44. (a) Comparison of potassium evolution profiles from differently treated particles in experiments and (b) Potassium evolution modeling with a linear heating rate of 500 K/s. Reproduced from Jones et al. [121] Copyright (2007): Elsevier.

Thus, the release rate of potassium is described by a first-order Arrhenius expression:

$$k_v = A_K e^{-E_K/RT} \tag{10}$$

The activation energy E_K and pre-exponential factor A_K was not directly determined from a plot of $\ln(k_v)$ versus $1/T$ since quantitative data of potassium release was not obtained in their work. Instead, the kinetic parameters of oxygenated volatile release [186] during the devolatilization stage were utilized to estimate the kinetic parameters of potassium release in this stage. This is feasible since oxygenated volatiles are the dominant products of biomass component decomposition during the devolatilization stage. As for the char burnout stage, the evaporation model developed in Ref. [187] was used to depict potassium release. They assumed that the main potassium salts released in char combustion were potassium hydroxides. The impact of the char burning rate was incorporated through the resultant particle temperature (Equation (11)). Hence, the release rate of potassium was given by dQ_{KOH}/dt as follows:

$$\frac{dQ_{KOH}}{dt} = 2\pi\Gamma_t \left(\frac{d_o^3 - 6Q_{KOH}}{\rho\pi}\right)^{\frac{1}{3}} \frac{p_{KOH,t}}{RT_t} M_{KOH} \tag{11}$$

where Q_{KOH} is the total mass of KOH released, t represents time, r is the mass diffusivity of KOH in the medium, d_o is the initial diameter of particle, ρ is density, M_{KOH} is the molecular weight of KOH, p_{KOH} is the vapor pressure of KOH, T is the particle temperature, and R is the universal gas constant. Some parameters are accompanied by a subscript t, which means it is a function of time. A comparison of potassium evolution profiles between experiments and models is shown in Fig. 44. The general shape of the potassium release curve was well reproduced with the proposed models (Equation (10) and (11)).

Different from the work by Jones et al. [121], which attributed the release of potassium during char combustion to the evaporation of alkali hydroxides, van Eky et al. [135] investigated the sodium release behavior of Loy Yang brown coal and interpreted the release of sodium during char combustion stage mainly as char-Na decomposition. Then they established the relationship between the sodium release and char surface temperature [135]. A shrinking core model [188] was employed to predict char burnout behavior. Combined with the heat transfer model, the particle temperature at various times during char combustion was determined. The predicted temperatures agreed well with the experimental data measured using two-color pyrometry [134]. The rate constant of sodium release was then calculated using the following equation:

$$k_{Na}(t) = \frac{W_{Na,at}(t)}{\left[\int_0^\infty W_{Na,at}(t)dt - \int_0^t W_{Na,at}(t)dt\right]} \tag{12}$$

where $W_{Na,at}(t)$ is the total flow of atomic sodium, which is obtained from the experimental data of van Eyk et al. [25,134]. An important assumption in their work is that the temperature of the char particle is uniform, which was validated by the value of Biot number (Bi). Another significant assumption is that all sodium contained in coal is eventually fully released, which was concluded from the work of Gallagher [172] and Lindner et al. [189]. Hence it is possible to determine the activation energy and pre-exponential factor by plotting $\ln(k_{Na})$ versus $1/T$. The Arrhenius expression of sodium release during the char combustion stage was derived as follows:

$$k_{c,Na} = 10^{5.2\pm0.4} e^{\frac{-214\ kJ/mol}{RT}} \tag{13}$$

The release rate of sodium was found independent of particle size, which means that an intrinsic reaction rate rather than diffusion is dominant during char combustion. This also implies Equation (13) will be valid for both pulverized coal and fluidized bed combustion.

The kinetics model of van Eyk et al. [135] is insufficient to predict the rate of atomic release at the devolatilization stage. The release of alkali in this stage is governed by not only the coal burning rate but also alkali salt evaporation. Liu et al. [11,157] took this influence into account and divided alkali metals into two types, i.e., alkali compounds bonded with volatile and alkali compounds bonded with char. Then they improved the kinetic model of van Eyk et al. [135] using a two-step model (taking Na as an example):

$$\begin{cases} \mathrm{Na}_{\mathrm{flux},t} = Q_{\mathrm{Na,devol}}\, k_1 + Q_{\mathrm{Na,C\&A}}\, k_2 \\ Q_{\mathrm{Na,devol}} = Q_{\mathrm{Na}}\, V_d \\ Q_{\mathrm{Na,C\&A}} = Q_{\mathrm{Na}}\,(FC_d + A_d) \\ k_v = A_v \exp\left(-\dfrac{E_1}{RT}\right) \\ k_c = A_c \exp\left(-\dfrac{E_2}{RT}\right) \end{cases} \tag{14}$$

where $Q_{\mathrm{Na,devol}}$ is the amount of sodium bonded with volatile and $Q_{\mathrm{Na,C\&A}}$ is the amount of sodium bonded with char, which are calculated from the product of total released sodium (Q_{Na}) and date from the proximate analysis. To solve Equation (14), the kinetic parameters of the dominant process (char combustion stage of coal and the devolatilization stage of biomass) was determined first using the method of van Eky et al. [135] and then these parameters were substituted into Equation (14) to obtain the other pair of kinetic parameters. The simulation results from a two-step model successfully predict the alkali release of the entire combustion period of biomass (Fig. 45(a)) and coal (Fig. 45(b)).

Zhang et al. [10] proposed a kinetic model to depict the potassium release during the char combustion stage of pinewood. They found that the kinetic parameters of potassium release were influenced by the initial partitioning between the inorganic K and char-K. According to their potassium release mechanism [10], the main potassium released during char combustion is from inorganic K, which is inherent to pinewood or generated through the char-K oxidation process. Hence, the conversion fraction of oxidation of char-K to inorganic K was taken into consideration. The shrinking core model [188] was employed to calculate the char conversion fraction. Assuming all of the potassium was released from inorganic K and the temperature dependence of potassium release rate by an Arrhenius expression, the pre-exponential factor A_{K} and activation energy E_{K} during pinewood char combustion stage were obtained (Table 8).

Fatehi et al. [38,156] measured the quantitative potassium and sodium release from a burning biomass particle at different ambient conditions. The data was used to calculate the kinetic rate constants of alkali metals during biomass gasification and pyrolysis process in succession. A one-dimensional model [190] was employed to predict biomass thermal conversion under the experimental conditions. According to their analysis, the release of alkali species during char and ash stage was due to the decomposition of carboxylic acid groups and the relationship between the release rate constant and temperature following a first-order Arrhenius expression was derived from LIBS results and biomass conversion model. However, during biomass pyrolysis stage, the large temperature gradient between surface and center of particles restricted the development of the release model. Thus, temperature at the potassium and sodium "reaction front" was adopted instead of surface temperature. A comparison of potassium release between LIBS results and kinetics modeling is shown in Fig. 46. The model shows a good capacity to predict the peak of alkali release in both pyrolysis and gasification conditions. However, at the early stage of pyrolysis, there is a large discrepancy between the simulation and LIBS results. This is due to ignoring the alkali release at low temperatures when estimating the kinetics constants. Recently, Zhang et al. [15,16] also developed the alkali release model of sawdust pyrolysis and gasification, respectively. The quantitative gaseous potassium and sodium release at different temperatures in fluidized bed was measured by ICP-OES. The results showed that the peak of alkali release rose with increasing reaction temperature. Besides, the rate of alkali release under pyrolysis conditions was slightly higher than that of gasification. These results indicate that temperature and atmosphere have an impact on alkali release kinetics. Then, the overall kinetic parameters of potassium and sodium release during pyrolysis and gasification processes were obtained. The pre-exponential factor and activation energy are shown in Table 8.

3.2.2. CFD modeling of alkali release

The final forms of alkali species in post-flame gases can be modelled with well-established reaction mechanisms that has been reviewed by Glarborg and Marshall et al. [191]. However, the dynamic release and reaction characteristics of alkali metals during complex reaction conditions, such as turbulent combustion, are still very rare. The existing online optical methods are difficult to implement under those situations. Full-scale three-dimensional simulations of alkali metal release through high-precision numerical simulation can be an alternative. To carry out computational fluid dynamics (CFD) simulation methods, two major points need to be considered. The first one is to predict the release of alkali metals from biomass and coal. The amount of the alkali volatiles released from fuels and their exact chemical composition need to be determined to provide initial conditions for further simulation in gas phase. This needs a comprehensive understanding of alkali release mechanisms and kinetics. Second, the chemical kinetics of various alkali species in the gas phase is indispensable to simulate the reaction process and their final states. In addition, deposition models are required if the deposition process is taken into account. To date, the various optical measurements of alkali release behavior can provide information on the

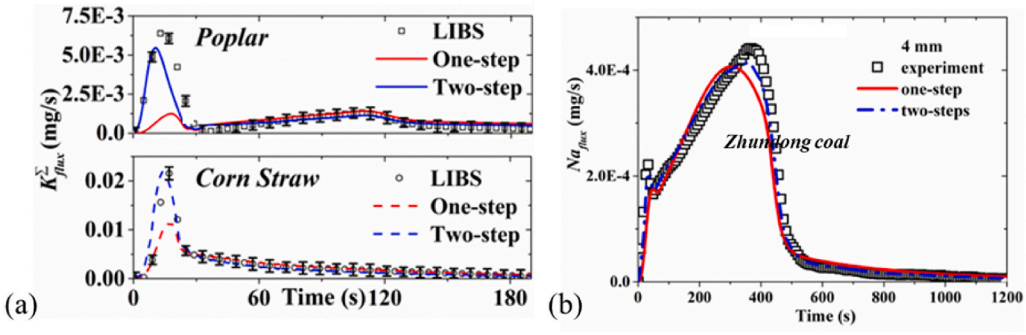

Fig. 45. (a) Comparison of kinetics model of potassium release against measurement results for biomass. Reproduced from Liu et al. [11] Copyright (2019): Elsevier. (b) Comparison of kinetics model of alkali release against measurement results for coal. Reproduced from Liu et al. [157] Copyright (2018): Elsevier.

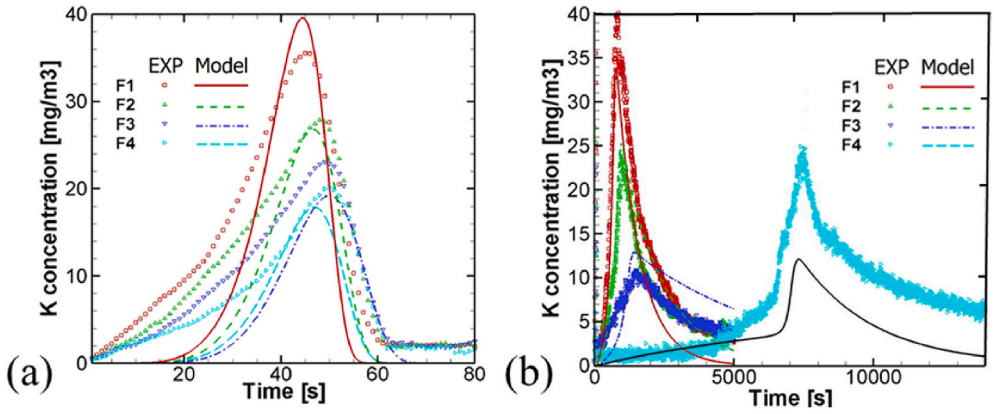

Fig. 46. (a) Results from experiments and model predictions for biomass pyrolysis. Reproduced from Fatehi et al. [38] Copyright (2017): Elsevier. (b) Results from experiments and model predictions for biomass gasification stage. Reproduced from Fatehi et al. [156] Copyright (2015): Elsevier.

release compositions and release kinetic parameters of alkali metals, which combined with the understanding of alkali chemistry as well as aerosol formation mechanisms makes it possible to improve the designs of biomass and coal boilers through CFD simulation methods.

Akbar et al. [192] simulated potassium release and its effect on the deposition for coals with different chlorine by a three-dimensional CFD program. The adopted potassium release mechanisms were the models for sodium proposed by Srinivasachar [193], while the reaction kinetics and thermal dynamic databases for potassium were taken from the work of Glarborg et al. [191]. To take into account the influence of turbulence on chemistry, an Eddy Dissipation Concept (EDC) model described in the work of Han [194] was also implemented. A deposit formation model [195] was extended to take into account the effect of condensable potassium species. In order to predict the deposition rate, two major deposition mechanisms, i.e., condensation and inertial impaction was considered in the model. Simulations were performed on an atmospheric-pressure drop tube reactor [194] and the results were compared with experimental results for high chlorine content coal [196] and low chlorine content coal [197], respectively. Good agreements were achieved between simulations and experimental data as shown in Fig. 47. Obviously, the occurrence of high content chlorine facilitates potassium release during coal thermal conversion process. Subsequently, simulations of different chlorine content biomass at the 0.5 MW semi-industrial pulverized-fuel combustion facility were performed and the results showed in Fig. 48 exhibited a similar deposition tendency, i.e., higher chlorine content leads to higher deposition rates [192]. The first attempt to combine the kinetic model for alkali sulfation with an ash deposition model using CFD was reported by Garba et al. [198]. A reduced reaction mechanism from a detailed alkali mechanism [199] and an ash deposition model [200] was integrated in the CFD model to

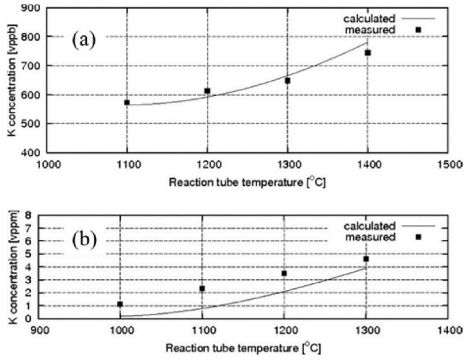

Fig. 47. Simulation and experimental results of potassium release for (a) coal with low chlorine content and (b) coal with high chlorine content, respectively. Reproduced from Akbar et al. [192] Copyright (2010): Elsevier.

simulate the initial stage of deposit buildup in a 10 MW industrial test furnace. CFD results were compared to the experimental data obtained in the literature [201] (Fig. 49). The comparison showed that the model was able to adequately reproduce the deposit position and shape in a 10 MW test furnace, but requires improvements for quantitative predictions.

Wan et al. performed high-fidelity simulation of laboratory-scale pulverized-coal flames to investigate alkali emissions in turbulent gas-solid two-phase flames [202–206]. The numerical modeling of alkali metal reacting dynamics in turbulent pulverized-coal combustion was evaluated using tabulated sodium chemistry in three-dimensional (3D) large eddy simulation (LES) [203]. A lookup table was constructed from a detailed sodium chemistry mechanism [191] including five sodium species, i.e., Na, NaO, NaO_2, NaOH, and $Na_2O_2H_2$, and 24 elementary reactions. This sodium chemistry table contains four coordinates, i.e., equivalence ratio, mass fraction of the sodium element, gas-phase temperature, and a progress variable. The table was first validated against the detailed sodium chemistry mechanism by zero-dimensional simulations. Then, LES simulation of a turbulent pulverized-coal jet flame was performed and major coal-flame parameters were compared against experiments [207]. The chemical percolation devolatilization (CPD) [208] model and the partially stirred reactor (PaSR) [209,210] model were employed to predict coal pyrolysis and gas-phase combustion, respectively. The response of the five sodium-species in the pulverized-coal jet flame was subsequently examined. Finally, a systematic global sensitivity analysis of the sodium lookup table was performed and the accuracy of the proposed tabulated sodium chemistry approach has been calibrated. As shown in Figs. 50 and 51, the results demonstrate that Na and NaOH are the two major sodium species in the pulverized-coal turbulent jet flame. The atomic sodium, Na, has a high concentration in fuel-rich regions; while the highest NaOH concentration was found in regions close to the stoichiometric condition. The fluctuations of the five sodium-species can achieve the same order of magnitude as the corresponding mean values at the jet centerline, indicating that the distribution of the sodium species is considerably affected by the turbulence of the jet flow.

In their following work [204], direct numerical simulation (DNS) was performed to evaluate the possibility of modeling the dynamics of sodium species using one-dimensional premixed flamelet generated manifolds (FGM). The DRM22 skeletal mechanism [211] was employed for volatile-gas combustion. A sodium chemistry lookup table was constructed from laminar one-dimensional premixed flames at various mixture fractions and enthalpy levels, thus following an FGM tabulation strategy. Three-dimensional simulations were performed with the lookup table for sodium species. The predictions of sodium emissions were compared between tabulation based on one-dimensional premixed flamelets and DNS results as shown in Fig. 52. Both major and minor

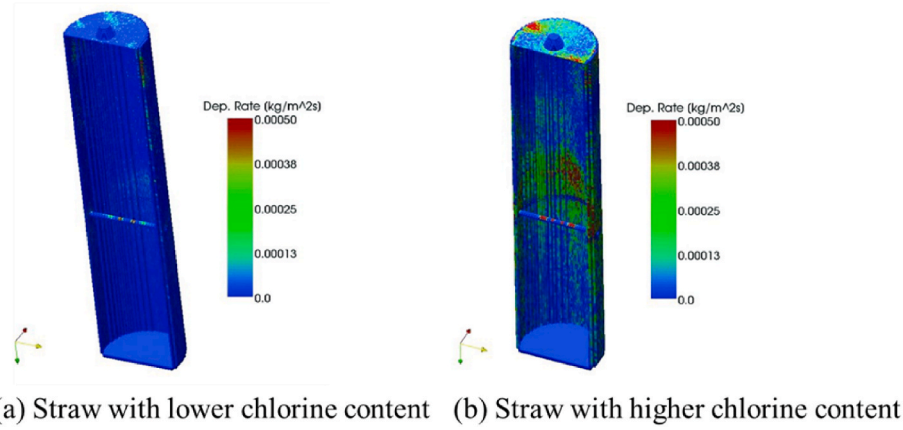

Fig. 48. 3D simulation of deposition rate for straw with (a) lower chlorine content and (b) higher chlorine content at a 0.5 MW semi-industrial pulverized-fuel combustion facility. Reproduced from Akbar et al. [192] Copyright (2010): Elsevier.

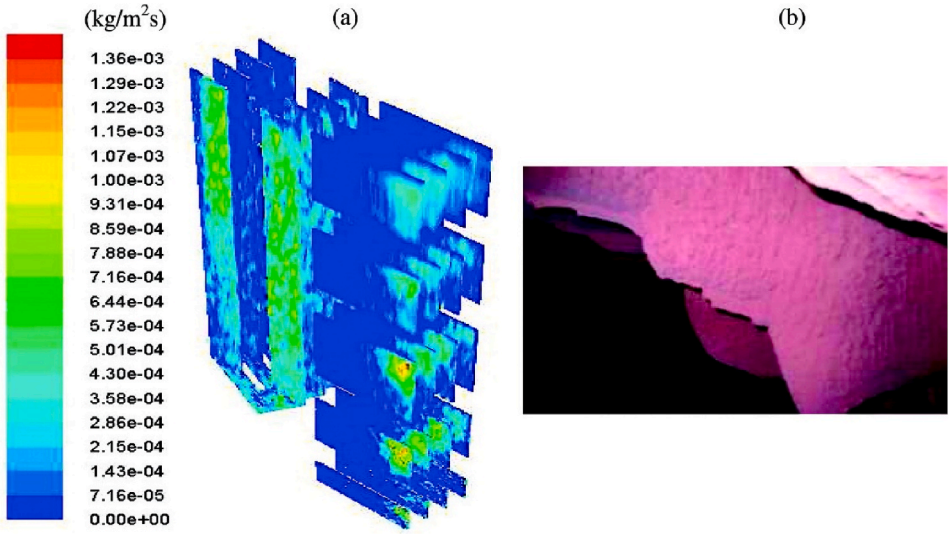

Fig. 49. Deposit formation on the vertical surface of the superheaters: (a) predicted contour of the deposition rate in terms of the position and shape and (b) photo of the deposition formed on the vertical section of the secondary superheater. Reproduced from Garba et al. [198] Copyright (2012): ACS.

sodium species predicted by FGM tabulation method closely follows the reference direct numerical simulation, with a Pearson correlation coefficient larger than 0.9.

Wan et al. [205,206] also investigated the effect of HCl and SO_2 on the alkali emissions in gas-solid two-phase flames. Sodium emissions were simulated in both one-dimensional (1D) premixed/diffusion flames of the coal volatile and an early-stage two-dimensional (2D) pulverized-coal flame (Loy Yang brown coal). In the same way, potassium emissions for the combustion of biomass (corn straw) were simulated. The initial species of Na, K, Cl, and S in the volatile gas was set to be NaOH, KOH, HCl, and SO_2, respectively. The transformation characteristics of alkali species were numerically investigated in both the 1D and 2D flames. The response of the alkali chemistry to volatile-gas combustion was analyzed under fuel-lean, stoichiometric and fuel-rich conditions. As shown in Fig. 53, for the sodium-enriched coal, Na, NaOH and NaCl were found to be the major sodium species during the combustion. $NaHSO_4$ and Na_2SO_4 are the two main sulfated sodium species which were formed mainly in the fuel-lean region, but their concentrations were much lower than that of NaCl. For the biomass, simulations support that KOH is the most significant potassium product under fuel-lean, stoichiometric and fuel-rich conditions, while the productions of sulfurous and chloric potassium species are secondary. Parametric studies with HCl, SO_2 or both species removed from the volatile are then performed to investigate their effects on the alkali transformation characteristics in both the 1D and 2D flames. The parametric study shows that HCl has a stronger tendency to react with alkali species than SO_2.

4. Industrial applications

In situ optical measurements are required in industries to monitor the fates of alkali components contained in fuels. Conventional sampling method can only provide time-averaged point data, which is obviously insufficient especially during plant start-up or on changing the fuel or operating conditions. *In situ* measurements using a variety of optical techniques can realize real-time data acquisition, which is of great significance for industrial processes. Fig. 54 shows the real-time potassium concentration monitoring in a 250 kW coal-fired combustor. A, B, and C correspond to time periods where the combustor was co-fired with oil. As can be seen, the variations in atomic potassium concentration caused by fuel have been observed quantitatively and sensitively. This feature will benefit the safe and efficient operation of industrial facilities, where the time-consuming sampling method is still the dominant analysis tool. However, despite the great development and widespread utilization of optical methods for measurements of alkali release in laboratory-scale facilities, there are still technical barriers limiting the application in

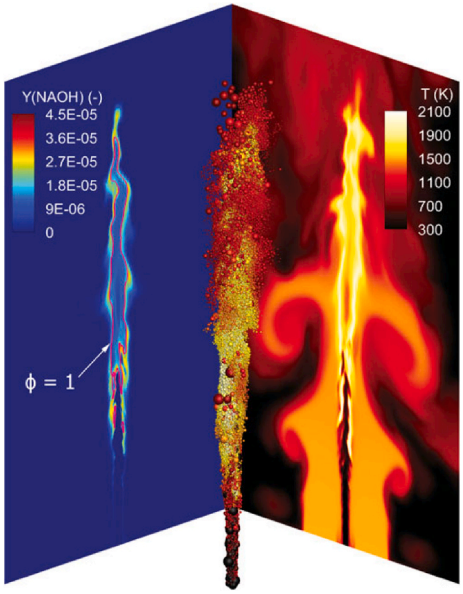

Fig. 50. Instantaneous pulverized-coal particle distribution. Mass fraction of NaOH (left) and gas-phase temperature (right), 2D snapshot through the jet centerline. The pulverized-coal particles are colored by the particle temperature. The size of coal particles is also illustrated. The diameter of the largest particle is 180 μm. Reproduced from Wan et al. [203] Copyright (2018): Elsevier.

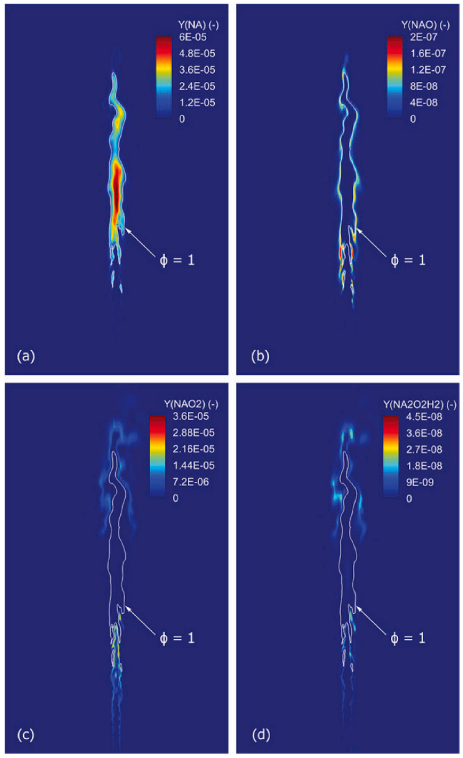

Fig. 51. 2D snapshots of the mass fractions of (a) Na, (b) NaO, (c) NaO_2, and (d) $Na_2O_2H_2$ in the turbulent pulverized-coal combustion. Reproduced from Wan et al. [203] Copyright (2018): Elsevier.

industrial conditions. The need for optical access to achieve optical measurement is one of the biggest challenges. Modifications of the furnace are needed as laser and optical components are indispensable to realize *in situ* measurements based on laser techniques [109,212–214].

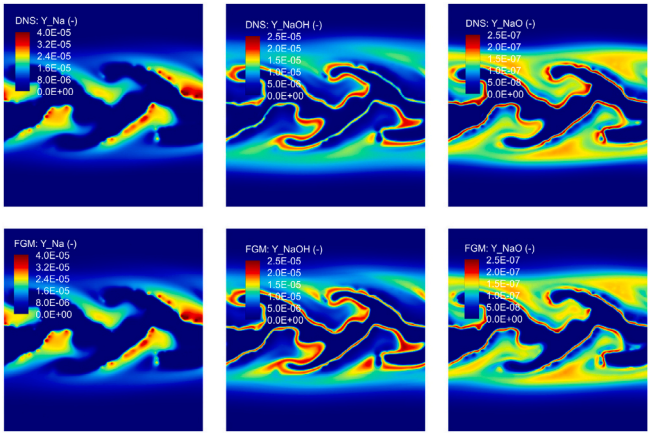

Fig. 52. Comparison of Na, NaOH and NaO predicted by the DNS (top) and the FGM (bottom) sodium tabulation approach at $t = 10$ ms. Reproduced from Wan et al. [204] Copyright (2019): Elsevier.

In addition, optical devices generally have rigorous requirements to the surrounding environments while in the field the environment is usually very harsh. Calibration is another big barrier since quantitative measurements require precise calibration procedures which are not easy to realize in industrial applications. To date, many efforts have been made to overcome those difficulties.

Tunable diode laser absorption spectroscopy is one of the most promising optical techniques to be used in industrial applications since it is in principle a calibration-free method. Besides, the equipment needed in this technique, e.g. diode lasers, detectors, and digitizers, are usually small and portable, making it becomes an ideal method for applications in industry. Schlosser et al. [78] employed TDLAS to measure potassium atom concentration in two pulverized-coal-fired (PCF) plants. One of the PCF plants was at atmospheric pressure with a total power of 250 kW, the other plant was at 10–16 bar with a total power of 1 MW. Under high pressure conditions, broadening and shift of K-line were observed and the pressure-dependent coefficients of pressure-induced broadening and shift were determined. Comparisons of potassium concentrations obtained under different pressures as well as different oxygen contents were discussed in their work to understand the K release characteristics. Qu et al. [93] also measured atomic potassium concentration during the softwood thermochemical conversion process using TDLAS. However, they employed a research-scale entrained flow reactor (EFR) to resemble the industrial reactor. Simultaneous measurements of gas temperature and water vapor (H_2O) were also conducted, which provide useful data on understanding of potassium reactions. The results showed that fuel composition has a higher impact on potassium release compared with flame equivalence ratio.

Optical emission spectroscopy is one of the most convenient techniques used in industries since it employs spontaneous emission from excited alkali atoms generated in flames and does not need an extra light source. Hensel et al. [215] designed and tested a real-time alkali monitor device named fiber-optic alkali monitor (FOAM). The FOAM system consists of a fiber optic, light-filtering background correction part and high sensitivity photodiode detector. The motivation of their work was to acquire real-time alkali data in the exhaust of a pressurized combustor fired with coal-water slurry. Alkali species in flame emit specific fluorescence at the characteristic wavelengths of sodium and potassium and the consequent emissions were transferred to the detection by the fiber optic. The detection limits of the FOAM system were determined to be 380 and 800 ppt for sodium and potassium, respectively, with a dynamic range of four orders of magnitude, which was adequate to monitor alkali species. Validation experiments of field monitoring of alkali levels in the exhaust stream of the combustor indicated that this system was capable of *in situ* monitoring alkali level under high temperature and pressure

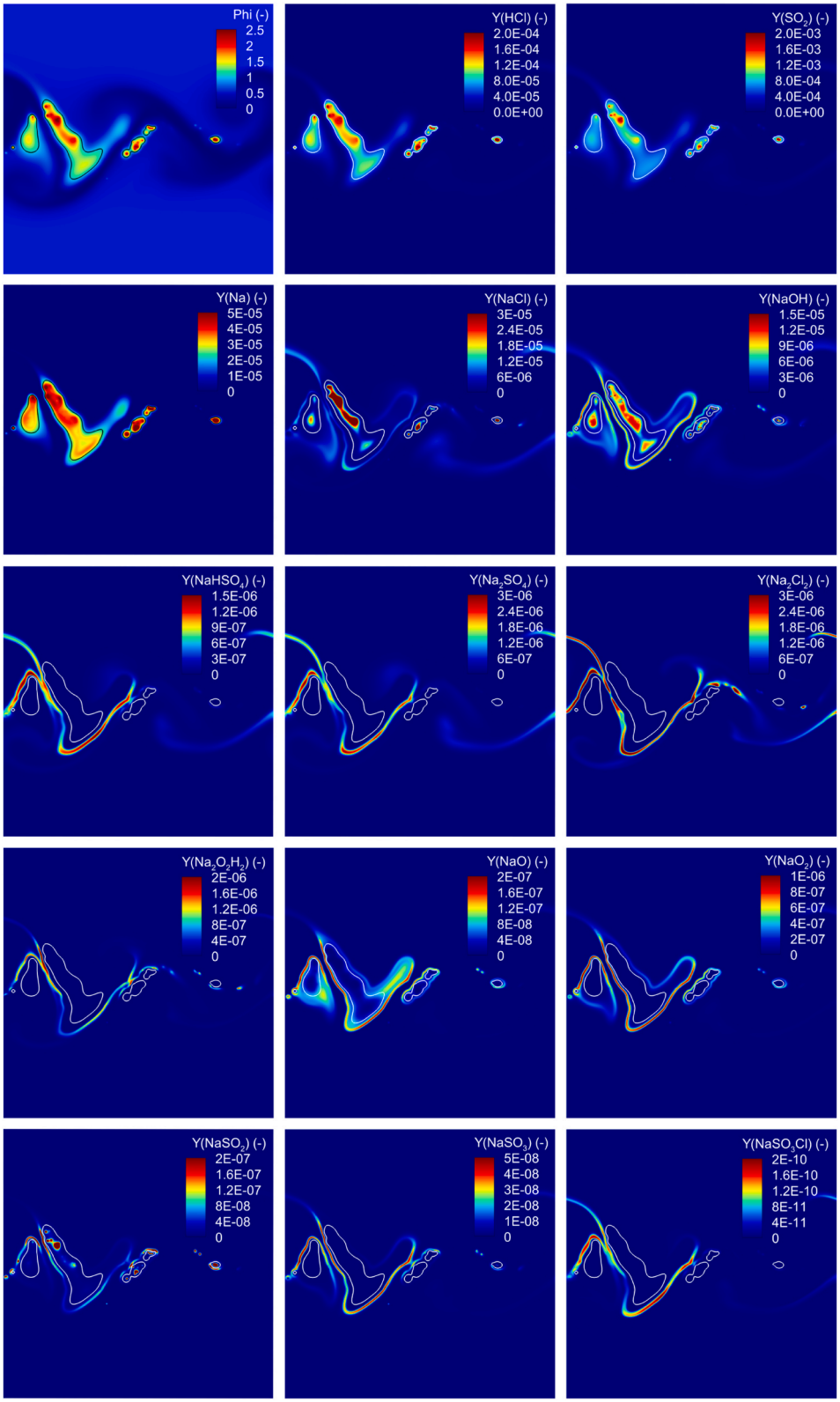

Fig. 53. Instantaneous distributions of the equivalence ratio (φ), the mass fractions of HCl, SO_2 and all the twelve sodium-species at $t = 20$ ms during the combustion of sodium-enriched Loy Yang brown coal. Reproduced from Wan et al. [206] Copyright (2019): Elsevier.

situations. Yan et al. [216] adopted flame emission spectroscopy to measure the alkali release in an industrial grate municipal solid waste incinerator. In their work, a linear polynomial fitting method was employed to uncouple the overlap of the continuous spectrum and the characteristic line. Thus, both temperatures and emission intensity of alkali metals are derived. The emission intensity of alkali metals gave a straight insight into the effects of operating parameters on alkali release and can be regarded as an indicator to adjust the air flow rate and fuel feeding in order to control the alkali level inside the incinerator. Lim et al. [217] utilized optical emission spectroscopy to analyze the

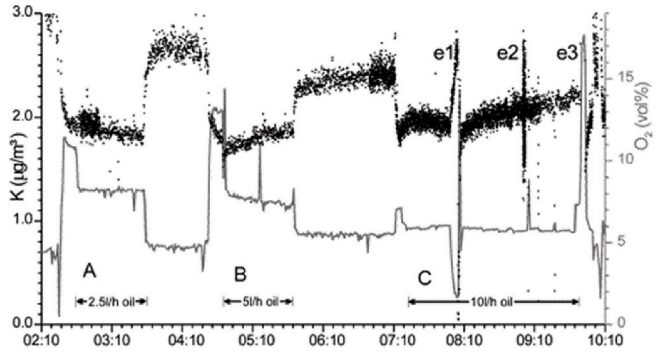

Fig. 54. *In situ* detection of the concentration of atomic potassium in the flue gas duct of a 250-kW coal-combustor using TDLAS method. Reproduced from Schlosser et al. [78]. Copyright (2002): Elsevier.

speciation of alkali species in a 150 kW_{th} biomass furnace fired with sawdust. The emission intensities of Na D lines and K D lines were related to the number density of Na and K in the excited state. Thus, the relative number density of Na and K in the ground state was derived through the Boltzmann law, respectively. The authors thought that those de-excited alkali metals were in the form of compounds in ash, so the ratio of the ground-state relative number density of Na and K could be compared to the ratio of the alkali metal oxides ($[Na_2O]/[K_2O]$) in the ash. The comparison revealed speciation of alkali metals to some extent. Both ratios were larger than a unity, which indicated that there was more Na in ash than K. Considering that K content of biomass is significantly larger than Na, this phenomenon explained that a large amount of K might released as vapor phase and exited through the stack. Chemiluminescence emission spectroscopy is a simple method to monitor real-time alkali behavior since there are no rigorous requirements before implementing this method. However, it is not simple to achieve quantitative measurement since independent calibration is needed as well as a mass of calculations.

Laser-induced breakdown spectroscopy is applied to monitor alkali metals as well. Like the atomic emission spectroscopy method, spectral and temporal resolved measurements are achieved. However, a Nd:YAG laser is needed to provide powerful laser light. Blevins et al. [218] measured concentration of K and Na as well as other metals using LIBS in three different industrial situations i.e., near the superheater of a 10 MW electric power generation boiler fired with biomass and coal, at the exit of a glass-melting furnace burning natural gas with oxygen and near the nose arches of two paper mill recovery boilers burning black liquor. Both an echelle spectrometer and linear spectrometers coupled to intensified CCD cameras were used as detectors. It is worth noticing that discrimination between gaseous and solid alkali metals was not achieved in their work and the measured concentration of elemental alkali represent both gas phase and solid phase. Deguchi et al. [219] realized long-term Na and K monitoring of a 20000 ton/day cement plant using LIBS. The system has been working continuously for over a year without any major problems. The results agreed well with off-line measurement results using conventional sampling method. The normal level of Na and K concentration was 10–50 ppb at the measurement point while several sharp peaks occur indicating corresponding operating condition changes of the plant. The system showed good capacity of monitoring total alkali elements with reliable results and good temporal discrimination. Although LIBS is also base on emission spectroscopy which means calibration procedure is needed, the calibration process is not as difficult as chemiluminescence emission. The relationship of concentration and emission signal intensity generated from the objective excited atoms in the plasma can be described by the following equation:

$$I_i = A_i n_i \sum_j \left(g_i^{(j)} \, exp\left\{ -\frac{E_i^{(j)}}{kT} \right\} \right) \tag{15}$$

where I_i is the emission intensity of species i, A_i is a variable which refers to species i, n_i represent the concentration of species i, $g_i^{(j)}$ is the statistical weight of species i at upper energy level j, $E_i^{(j)}$ is the upper-level energy of species *i*, *k* is the Boltzmann constant, and *T* is the plasma temperature. In addition, Blevins et al. [218] assumed that the LIBS instrument responds in the field was as the same way as its responds in the laboratory. Then, calibrations were performed in laboratory using a nebulizer to generate known concentrations of alkali metals and detected emissions by LIBS to derive the calibration curve, as discussed in 2.4.1.

Another emission technique, namely, laser-induced photofragmentation fluorescence has been applied to *in situ* temporal monitoring of alkali molecules. Monkhouse and co-workers measured the release of Na and K compounds in pulverized [148,150] and fluidized bed [140,145–147,149,220,221] boilers fed with biomass and coal. Optical access is essential to realize *in situ* laser techniques. Gottwald and Monhouse et al. [145] designed an optical access to industrial-scale flue-gas ducts under high pressure. They tested the reliability of this system in a pressurized circulating fluidized bed (PCFB) combustor. Alkali release was monitored using LIPF and the results validated the capability for industrial applications. Later, they investigated the effects of coal composition [146], operating conditions and additives [147] on alkali release during fluidized bed combustion. Meanwhile, they achieved phase discrimination of alkali species in PCFB combustion flue gas [149]. In this case, the laser energy density was kept below the vaporization energy of sodium chlorides, thus only gaseous alkali species was detected and the gas/particle phase partitioning in the flue gas of a PFBC pilot facility was obtained. A simultaneous measurement of potassium and nickel using LIPF was also realized for the first time under flue gas conditions [220]. The results suggest that the release of both metal species was affected by both the amount of chlorine and clay minerals in the system. Glazer et al. [221] further investigated the effects of operating conditions and additives on the combustion of biomass and coal, and the effects of Cl and Si on those two fuels were also discussed. Besides, effects of gas composition, operating conditions and additives were analyzed during pulverized particle combustion [148,150]. Erbel et al. [151] measured the potassium release from gasification process, in which understanding was lacking. A slow release of potassium was observed after stopping feeding, which indicates that alkali species had been taken up in the bed material. Analysis of the bed material proves this assumption. Furthermore, given the re-release of alkali metals while the bed was still hot, alkali-containing layers could have formed on the bed particles but appeared not to form crystalline phases.

One of the greatest progress of alkali measurement in industry-scale facilities achieved in recent years was the simultaneous measurement of KOH, KCl and atomic K by PF-TDLAS. Although LIPF can be used to measure KCl and KOH concentrations, it cannot distinguish one from the other, since the fluorescence they emit after photolysis is at the same wavelength. Thus the measured concentration was the sum of KOH and KCl. Recently, Thorin et al. [117] applied PF-TDLAS to monitor the concentration of KOH, KCl, and atomic K in a 140 kW entrained flow reactor operated under gasification and combustion conditions. The results are shown in Fig. 55. A continuous increase in KOH concentrations as well as a decrease in K-atom concentrations was monitored. Meanwhile, the KCl concentration kept stable. The drifts in concentrations were probably related to the process of reaching a steady state in the reactor. The concentration variations caused by the period variation of fuel feeding were also observed (Fig. 55(b)). These results showed the sensitivity of the PF-TDLAS method, and this feature is crucial for industrial applications.

5. Conclusion and outlook

A big progress in optical methods used to measure the alkali release behavior in thermochemical conversion processes has been made over

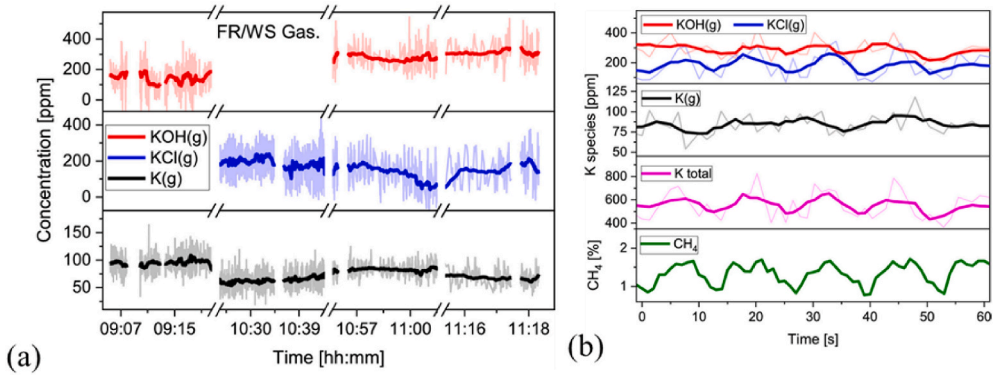

Fig. 55. (a) K species concentrations measured in real-time during a mixture of forest wood and wheat straw gasification at an air-to-fuel ratio of 0.5 in a 140 kW EFR. (b) One minute of real-time data showing potassium species and CH_4 concentrations shows periodic changes due to variations in fuel feed. Reproduced from Thorin et al. [117] Copyright (2023): Elsevier.

the past decade. Currently, the quantitative monitoring of alkali atoms, alkali chlorides, alkali hydroxides, and elemental alkali during the whole thermochemical conversion process of biomass and coal has been achieved. This covers almost all major forms of alkali metals released into the gas phase. The development of these optical techniques creates new possibilities for further exploring the alkali release mechanisms and kinetics. However, as shown in Chapter 3, only a few mechanisms and release models were developed. Besides, those mechanisms and models were all derived from the release behaviors of elemental alkali or alkali atoms. Release characteristics of alkali compounds were absent during the model developing process. Clearly, this cannot meet our needs for a comprehensive alkali release model. Additionally, when comparing the existing release mechanisms, we have observed significant differences among them. The underlying reason for these differences is the varying in multiple factors like the fuel composition, original alkali chemical forms, and reaction conditions, etc. Therefore, it is crucial to understand the specific impacts of these factors on alkali metal releases. However, studies on these issues using optical methods are still desired.

Applications of optical techniques in new combustion technology, e.g., oxy-fuel combustion and chemical looping combustion, are still very scarce. As shown in Table 7, the reaction atmosphere in oxy-fuel combustion is totally different from that in air-fuel combustion, this is manifested not only by the absence of nitrogen but also by a significant increase in vapor amount and SO_x levels compared to conventional combustion atmosphere. These differences may result in a distinct alkali metal release behavior, which should be further investigated. As for chemical looping combustion, the alkali release behavior is crucial since a high alkali release level may cause the agglomeration of the oxygen carrier. However, there have been no reports on the measurement of alkali species using optical techniques yet.

In addition, despite the techniques based on photofragmentation can effectively measure KCl and KOH, monitoring of some key alkali species, such as alkali sulfates, is still challenging. With the presence of sulfur in the fuel or in the atmosphere, alkali sulfates may account for a large proportion of the released alkali metals. Photofragmentation-based techniques may also be capable to measure the alkali sulfates. However, the measurement needs knowledge of the spectroscopic information on alkali sulfates.

Applications of optical techniques in industrial processes are still rare especially 2D measurements of alkali species due to the requirements of proper optical access and operating environments, which is not easy to realize in the industry field. Improvements in the existing techniques to better fit those harsh environments are essential for further utilization of those techniques in industrial applications. TDLAS as well as TDLAS-based methods like PF-TDLAS are the most promising optical method. Although the industrial applications of TDLAS for alkali metal measurements are limited, TDLAS technique has been widely used in industrial applications for measuring other components like CH_4, CO_2, O_2, etc [75]. It is even possible to achieve three-dimensional distribution measurement through applying tomographic reconstruction. Therefore, TDLAS method has great potential in the industrial application of alkali release monitoring. In addition, alkali-induced slagging and corrosion limit the utilization of biomass and high-alkali coal. *In situ* measurement of alkali distribution near the slagging layer, which is rarely reported, is of great importance to understand the slagging mechanism. This requires phase-discrimination ability of the optical technique. To date, there have been investigations that have achieved this requirement by adjusting the laser power and we can be optimistic that this utilization will be fulfilled in the near further.

Declaration of competing interest

The authors declare that they have no known competing financial interests or personal relationships that could have appeared to influence the work reported in this paper.

Data availability

Data will be made available on request.

Acknowledgement

This work was supported by the National Natural Science Foundation of China (52125605), Zhejiang Provincial Natural Science Foundation (LZ21E06003), the Fundamental Research Funds for the Central Universities (2022ZFJH04), the Swedish Energy Agency through the Sweden-China collaboration project, the KC-CECOST biomass project, and the Knut & Alice Wallenberg foundation (COCALD).

References

[1] Energy institute statistical review of world energy. https://www.energyinst.org/statistical-review/home; 2023.
[2] BP Energy Outlook. https://www.bp.com/content/dam/bp/business-sites/en/global/corporate/pdfs/energy-economics/energy-outlook/bp-energy-outlook-2023.pdf; 2023.
[3] Cherubini F, Peters GP, Berntsen T, Strømman AH, Hertwich E. CO_2 emissions from biomass combustion for bioenergy: atmospheric decay and contribution to global warming. GCB Bioenergy 2011;3:413–26.
[4] Moreira D, Pires JCM. Atmospheric CO_2 capture by algae: negative carbon dioxide emission path. Bioresour Technol 2016;215:371–9.
[5] Kemper J. Biomass and carbon dioxide capture and storage: a review. Int J Greenh Gas Control 2015;40:401–30.
[6] Weng W. Optical diagnostics for quantitative potassium chemistry in biomass thermochemical conversion processes. Lund University; 2020.
[7] Hupa M, Karlström O, Vainio E. Biomass combustion technology development – it is all about chemical details. Proc Combust Inst 2017;36:113–34.

[8] Song G, Qi X, Song W, Yang S, Lu Q, Nowak W. Slagging behaviors of high alkali Zhundong coal during circulating fluidized bed gasification. Fuel 2016;186:140–9.
[9] Kleinhans U, Wieland C, Frandsen FJ, Spliethoff H. Ash formation and deposition in coal and biomass fired combustion systems: progress and challenges in the field of ash particle sticking and rebound behavior. Prog Energy Combust Sci 2018;68:65–168.
[10] Zhang ZH, Song Q, Alwahabi ZT, Yao Q, Nathan GJ. Temporal release of potassium from pinewood particles during combustion. Combust Flame 2015;162:496–505.
[11] Liu Y, Wang Z, Xia J, Vervisch L, Wan K, He Y, et al. Measurement and kinetics of elemental and atomic potassium release from a burning biomass pellet. Proc Combust Inst 2019;37:2681–8.
[12] Zhao H, Wakil MA, Viljanen J, Song Q, Yao Q, Kwong CW, et al. In situ measurement of potassium release during biomass combustion using laser-induced breakdown spectroscopy: effect of silicate on potassium release. Energy Fuel 2020;34:3262–71.
[13] Moilanen A. Thermogravimetric characterisations of biomass and waste for gasification processes. Espoo, Finland: Åbo Akademi University; 2006.
[14] Jung S-H, Kang B-S, Kim J-S. Production of bio-oil from rice straw and bamboo sawdust under various reaction conditions in a fast pyrolysis plant equipped with a fluidized bed and a char separation system. J Anal Appl Pyrol 2008;82:240–7.
[15] Zhang Z, Liu J, Shen F, Yang Y, Liu F. On-line measurement and kinetic studies of sodium release during biomass gasification and pyrolysis. Fuel 2016;178:202–8.
[16] Zhang Z, Liu J, Shen F, Wang Z. Temporal release behavior of potassium during pyrolysis and gasification of sawdust particles. Renew Energy 2020;156.
[17] Zhao HB, Song Q, Wu XY, Yao Q. Study on the transformation of inherent potassium during the fast-pyrolysis process of rice straw. Energy Fuel 2015;29:150917122402004.
[18] Zhang Y, Xie X, Zhao J, Wei X. The alkali metal occurrence characteristics and its release and conversion during wheat straw pyrolysis. Renew Energy 2020;151:255–62.
[19] Lane DJ, van Eyk PJ, Ashman PJ, Kwong CW, de Nys R, Roberts DA, et al. Release of Cl, S, P, K, and Na during thermal conversion of algal biomass. Energy Fuel 2015;29:2542–54.
[20] Dayton DC, French RJ, Milne TA. Direct observation of alkali vapor release during biomass combustion and gasification. 1. Application of molecular beam/mass spectrometry to switchgrass combustion. Energy Fuel 1995;9:855–65.
[21] Wei X, Schnell U, Hein KRG. Behaviour of gaseous chlorine and alkali metals during biomass thermal utilisation. Fuel 2005;84:841–8.
[22] He J, Li J, Huang Q, Yan J. Release characteristics of potassium and sodium during pellet combustion of typical MSW fractions using the FES method. Combust Flame 2022;244:112233.
[23] Liu Y, Wang Z, Wan K, Lv Y, Xia J, He Y, et al. In situ measurements of the release characteristics and catalytic effects of different chemical forms of sodium during combustion of Zhundong coal. Energy Fuel 2018;32:6595–602.
[24] He Y, Zhu J, Li B, Wang Z, Li Z, Aldén M, et al. In-situ measurement of sodium and potassium release during oxy-fuel combustion of lignite using laser-induced breakdown spectroscopy: effects of O_2 and CO_2 concentration. Energy Fuel 2013;27:1123–30.
[25] van Eyk PJ, Ashman PJ, Alwahabi ZT, Nathan GJ. Quantitative measurement of atomic sodium in the plume of a single burning coal particle. Combust Flame 2008;155:529–37.
[26] Butler CJ, Green AM, Chaffee AL. Remediation of mechanical thermal expression product waters using raw Latrobe Valley brown coals as adsorbents. Fuel 2007;86:1130–8.
[27] Bryers RW. Fireside slagging, fouling, and high-temperature corrosion of heat-transfer surface due to impurities in steam-raising fuels. Prog Energy Combust Sci 1996;22:29–120.
[28] Vassilev SV, Baxter D, Andersen LK, Vassileva CG. An overview of the chemical composition of biomass. Fuel 2010;89:913–33.
[29] van Eyk PJ, Ashman PJ, Alwahabi ZT, Nathan GJ. The release of water-bound and organic sodium from Loy Yang coal during the combustion of single particles in a flat flame. Combust Flame 2011;158:1181–92.
[30] Benson SA, Holm PL. Comparison of inorganics in three low-rank coals. Ind Eng Chem Prod Res Dev 1985;24:145–9.
[31] Zhang J, Han CL, Yan Z. The varying characterization of alkali metals (Na, K) from coal during the initial stage of coal combustion. Energy Fuel 2001;15:786–93.
[32] Nielsen HP, Frandsen F, Dam-Johansen K, Baxter L. The implications of chlorine-associated corrosion on the operation of biomass-fired boilers. Prog Energy Combust Sci 2000;26:283–98.
[33] Baxter LL, Miles TR, Miles TR, Jenkins BM, Milne T, Dayton D, et al. The behavior of inorganic material in biomass-fired power boilers: field and laboratory experiences. Fuel Process Technol 1998;54:47–78.
[34] Werkelin J, Skrifvars B-J, Zevenhoven M, Holmbom B, Hupa M. Chemical forms of ash-forming elements in woody biomass fuels. Fuel 2010;89:481–93.
[35] Vassilev SV, Vassileva CG. Water-soluble fractions of biomass and biomass ash and their significance for biofuel application. Energy Fuel 2019;33:2763–77.
[36] Monkhouse P. On-line spectroscopic and spectrometric methods for the determination of metal species in industrial processes. Prog Energy Combust Sci 2011;37:125–71.
[37] Glarborg P. Hidden interactions—trace species governing combustion and emissions. Proc Combust Inst 2007;31:77–98.
[38] Fatehi H, Li ZS, Bai XS, Aldén M. Modeling of alkali metal release during biomass pyrolysis. Proc Combust Inst 2017;36:2243–51.
[39] Baxter LL. Ash deposition during biomass and coal combustion: a mechanistic approach. Biomass Bioenergy 1993;4:85–102.
[40] Li QH, Zhang YG, Meng AH, Li L, Li GX. Study on ash fusion temperature using original and simulated biomass ashes. Fuel Process Technol 2013;107:107–12.
[41] Niu Y, Zhu Y, Tan H, Hui S, Jing Z, Xu W. Investigations on biomass slagging in utility boiler: criterion numbers and slagging growth mechanisms. Fuel Process Technol 2014;128:499–508.
[42] Morris JD, Daood SS, Chilton S, Nimmo W. Mechanisms and mitigation of agglomeration during fluidized bed combustion of biomass: a review. Fuel 2018;230:452–73.
[43] Bowie D. Operational experience with a high fouling biomass fuel. Carbon 2006;42:38–44.
[44] Wu X, Zhang X, Yan K, Chen N, Zhang J, Xu X, et al. Ash deposition and slagging behavior of Chinese Xinjiang high-alkali coal in 3 MWth pilot-scale combustion test. Fuel 2016;181:1191–202.
[45] Vassilev SV, Baxter D, Andersen LK, Vassileva CG, Morgan TJ. An overview of the organic and inorganic phase composition of biomass. Fuel 2012;94:1–33.
[46] Vassilev SV, Baxter D, Vassileva CG. An overview of the behaviour of biomass during combustion: Part II. Ash fusion and ash formation mechanisms of biomass types. Fuel 2014;117:152–83.
[47] Vassilev SV, Vassileva CG, Vassilev VS. Advantages and disadvantages of composition and properties of biomass in comparison with coal: an overview. Fuel 2015;158:330–50.
[48] Bogush AA, Stegemann JA, Williams R, Wood IG. Element speciation in UK biomass power plant residues based on composition, mineralogy, microstructure and leaching. Fuel 2018;211:712–25.
[49] Niu Y, Tan H, Hui SE. Ash-related issues during biomass combustion: alkali-induced slagging, silicate melt-induced slagging (ash fusion), agglomeration, corrosion, ash utilization, and related countermeasures. Prog Energy Combust Sci 2015;52:1–61.
[50] Wang X, Liu Y, Tan H, Ma L, Xu Tm. Mechanism research on the development of ash deposits on the heating surface of biomass furnaces. Ind Eng Chem Res 2012;51:12984–92.
[51] Bartels M, Lin W, Nijenhuis J, Kapteijn F, Van Ommen JR. Agglomeration in fluidized beds at high temperatures: mechanisms, detection and prevention. Prog Energy Combust Sci 2008;34:633–66.
[52] Miao Z, Jiang E, Hu Z. Review of agglomeration in biomass chemical looping technology. Fuel 2022;309:122199.
[53] Enestam S, Bankiewicz D, Tuiremo J, Mäkelä K, Hupa M. Are NaCl and KCl equally corrosive on superheater materials of steam boilers? Fuel 2013;104:294–306.
[54] Paneru M, Stein-Brzozowska G, Maier J, Scheffknecht G. Corrosion mechanism of alloy 310 austenitic steel beneath NaCl deposit under varying SO_2 concentrations in an oxy-fuel combustion atmosphere. Energy Fuel 2013;27:5699–705.
[55] Theis M, Skrifvars B-J, Zevenhoven M, Hupa M, Tran H. Fouling tendency of ash resulting from burning mixtures of biofuels. Part 2: deposit chemistry. Fuel 2006;85:1992–2001.
[56] Wang Z, Liu Y, Whiddon R, Wan K, He Y, Xia J, et al. Measurement of atomic sodium release during pyrolysis and combustion of sodium-enriched Zhundong coal pellet. Combust Flame 2017;176:429–38.
[57] Hsu L-J, Alwahabi ZT, Nathan GJ, Li Y, Li ZS, Aldén M. Sodium and potassium released from burning particles of Brown coal and pine wood in a laminar premixed methane flame using quantitative laser-induced breakdown spectroscopy. Appl Spectrosc 2011;65:684–91.
[58] Thorin E, Zhang K, Valiev D, Schmidt FM. Simultaneous detection of K, KOH, and KCl in flames and released from biomass using photofragmentation TDLAS. Opt Express 2021;29:42945–61.
[59] Weng W, Brackmann C, Leffler T, Aldén M, Li Z. Ultraviolet absorption cross sections of KOH and KCl for nonintrusive species-specific quantitative detection in hot flue gases. Anal Chem 2019;91:4719–26.
[60] Kaskan WE. The reaction of alkali atoms in lean flames. Symposium (International) on Combustion 1965;10:41–6.
[61] McEwan MJ, Phillips LF. Use of the LiLiOH method for measuring [H] in low-temperature flames. Combust Flame 1965;9:420–1.
[62] Carabetta R, Kaskan WE. Oxidation of sodium, potassium, and cesium in flames. J Phys Chem 1968;72:2483–9.
[63] Carabetta R, Kaskan W. Chemi-excitation of sodium in flames. Symposium (International) on Combustion 1967;11:321–33.
[64] Fenimore CP. Two modes of interaction of NaOH and SO_2 in gasesfrom fuel-lean H_2-air flames. Symposium (International) on Combustion 1973;14:955–63.
[65] Durie RA, Johnson GM, Smith MY. Gas phase reactions of sodium species with sulfur species in hydrocarbon flames. Symposium (International) on Combustion 1975;15:1123–33.
[66] Husain D, Plane JMC. Kinetic investigation of the reaction between Na + O2+ M by time-resolved atomic resonance absorption spectroscopy. J Chem Soc, Faraday Trans 2: Molecular and Chemical Physics 1982;78:163–78.
[67] Husain D, Plane JMC. Kinetic investigation of the third-order rate processes between K + O2+ M by time-resolved atomic resonance absorption spectroscopy. J Chem Soc, Faraday Trans 2: Molecular and Chemical Physics 1982;78:1175–94.
[68] Vinckier C, Dumoulin A, De Jaegere S. Kinetic study of the Na + O_2 + He reaction in the temperature range 392–777 K. J Chem Soc Faraday Trans 1991;87:1075–81.
[69] Husain D, Lee YH, Marshall P. Temperature dependence of the absolute third-order rate constant for the reaction between K + O_2 + N_2 over the range 680–1010 K studied by time-resolved atomic resonance absorption spectroscopy. Combust Flame 1987;68:143–54.

[70] Husain D, Lee YH. Kinetic study of the absolute rate constant for the reaction between K + N2O by time-resolved atomic resonance absorption spectroscopy. Combust Flame 1987;68:177–83.
[71] Husain D, Lee YH. Measurement of absolute rate data for the reaction of atomic potassium, K(4 $^2S_{½}$), with CH_3F, C_2H_5F, C_6H_5F, CH_3Br, C_2H_5Br, HCl and HBr by time-resolved atomic resonance absorption spectroscopy at $\lambda = 404$ nm (K(5 ^2P_J) ← K(4 $^2S_{½}$)). Int J Chem Kinet 1988;20:223–40.
[72] Edelstein SA, Davidovits P. Cross sections for the alkali-metal-halogen molecule reactions: Na, K, Rb, and Cs with I2. J Chem Phys 1971;55:5164–70.
[73] Slack M, Cox JW, Grillo A, Ryan R, Smith O. Potassium kinetics in heavily seeded atmospheric pressure laminar methane flames. Combust Flame 1989;77:311–20.
[74] Sorvajärvi T, DeMartini N, Rossi J, Toivonen J. In situ measurement technique for simultaneous detection of K, KCl, and KOH vapors released during combustion of solid biomass fuel in a single particle reactor. Appl Spectrosc 2014;68:179–84.
[75] Goldenstein CS, Spearrin RM, Jeffries JB, Hanson RK. Infrared laser-absorption sensing for combustion gases. Prog Energy Combust Sci 2017;60:132–76.
[76] Bolshov MA, Kuritsyn YA, Romanovskii YV. Tunable diode laser spectroscopy as a technique for combustion diagnostics. Spectrochim Acta B Atom Spectrosc 2015;106:45–66.
[77] Qu Z, Steinvall E, Ghorbani R, Schmidt FM. Tunable diode laser atomic absorption spectroscopy for detection of potassium under optically thick conditions. Anal Chem 2016;88:3754–60.
[78] Schlosser E, Fernholz T, Teichert H, Ebert V. In situ detection of potassium atoms in high-temperature coal-combustion systems using near-infrared-diode lasers. Spectrochim Acta Mol Biomol Spectrosc 2002;58:2347–59.
[79] Groll H, Niemax K. Multielement diode laser atomic absorption spectrometry in graphite tube furnaces and analytical flames. Spectrochim Acta B Atom Spectrosc 1993;48:633–41.
[80] Schlosser E, Wolfrum J, Hildebrandt L, Seifert H, Oser B, Ebert V. Diode laser based in situ detection of alkali atoms: development of a new method for determination of residence-time distribution in combustion plants. Appl Phys B 2002;75:237–47.
[81] Gustafsson U, Somesfalean G, Alnis J, Svanberg S. Frequency-modulation spectroscopy with blue diode lasers. Appl Opt 2000;39:3774–80.
[82] Gao Q, Weng W-B, Li B, Li Z-S. Quantitative and spatially resolved measurement of atomic potassium in combustion using diode laser. Chin Phys Lett 2018;35.
[83] Tancin RJ, Spearrin RM, Goldenstein CS. 2D mid-infrared laser-absorption imaging for tomographic reconstruction of temperature and carbon monoxide in laminar flames. Opt Express 2019;27:14184–98.
[84] Cai W, Kaminski CF. Tomographic absorption spectroscopy for the study of gas dynamics and reactive flows. Prog Energy Combust Sci 2017;59:1–31.
[85] Thorin E, Paiva EM, Schmidt FM. Quantitative tomographic laser absorption imaging of atomic potassium during combustion of potassium chloride salt and biomass. Anal Chem 2023;95:1140–8.
[86] Leffler T, Brackmann C, Weng W, Gao Q, Aldén M, Li Z. Experimental investigations of potassium chemistry in premixed flames. Fuel 2017;203:802–10.
[87] Weng W, Zhang Y, Wu H, Glarborg P, Li Z. Optical measurements of KOH, KCl and K for quantitative K-Cl chemistry in thermochemical conversion processes. Fuel 2020;271:117643.
[88] Weng W, Li Z, Wu H, Aldén M, Glarborg P. Quantitative K-Cl-S chemistry in thermochemical conversion processes using in situ optical diagnostics. Proc Combust Inst 2021;38:5219–27.
[89] Berdugo Vilches T, Weng W, Glarborg P, Li Z, Thunman H, Seemann M. Shedding light on the governing mechanisms for insufficient CO and H_2 burnout in the presence of potassium, chlorine and sulfur. Fuel 2020;273:117762.
[90] Weng W, Gao Q, Wang Z, Whiddon R, He Y, Li Z, et al. Quantitative measurement of atomic potassium in plumes over burning solid fuels using infrared-diode laser spectroscopy. Energy Fuel 2017;31:2831–7.
[91] Sepman A, Ögren Y, Qu Z, Wiinikka H, Schmidt FM. Real-time in situ multi-parameter TDLAS sensing in the reactor core of an entrained-flow biomass gasifier. Proc Combust Inst 2017;36:4541–8.
[92] Sepman A, Ögren Y, Qu Z, Wiinikka H, Schmidt FM. Tunable diode laser absorption spectroscopy diagnostics of potassium, carbon monoxide, and soot in oxygen-enriched biomass combustion close to stoichiometry. Energy Fuel 2019;33:11795–803.
[93] Qu Z, Holmgren P, Skoglund N, Wagner DR, Broström M, Schmidt FM. Distribution of temperature, H_2O and atomic potassium during entrained flow biomass combustion – coupling in situ TDLAS with modeling approaches and ash chemistry. Combust Flame 2018;188:488–97.
[94] Weng W, Leffler T, Brackmann C, Aldén M, Li Z. Spectrally resolved ultraviolet (UV) absorption cross-sections of alkali hydroxides and chlorides measured in hot flue gases. Appl Spectrosc 2018;72:1388–95.
[95] Koirtyohann SR, Pickett EE. Background corrections in long path atomic absorption spectrometry. Anal Chem 1965;37:601–3.
[96] Culver BR, Surles T. Interference of molecular spectra due to alkali halides in nonflame atomic absorption spectrometry. Anal Chem 1975;47:920–1.
[97] Furuta N, Yoshimura E, Nemoto Y, Haraguchi H, Fuwa K. Photodissociation of sodium halides in the air-acetylene flame as studied by molecular absorption flame spectroscopy. Chem Lett 1976;5:539–42.
[98] Pritchard MW, Reeves RD. Non-atomic absorption from matrix salts volatilized from graphite atomizers in atomic absorption spectrometry. Anal Chim Acta 1976;82:103–11.
[99] Allain P, Mauras Y. A study of background signals in graphite-furnace atomic absorption spectrometry. Anal Chim Acta 1984;165:141–7.
[100] Daminelli G, Katskov DA, Mofolo RM, Tittarelli P. Atomic and molecular spectra of vapours evolved in a graphite furnace. Part 1. Alkali halides. Spectrochim Acta B Atom Spectrosc 1999;54:669–82.
[101] Furuta N, Yoshimura E, Haraguchi H, Fuwa K. The photodissociation of alkali halides in air—acetylene flame as studied by molecular absorption spectroscopy. Spectrochim Acta B Atom Spectrosc 1978;33:715–26.
[102] Daidoji H. Molecular absorption spectra of some sodium salts in flames. Bunseki Kagaku 1979;28:77–82.
[103] Davidovits P, Brodhead DC. Ultraviolet absorption cross sections for the alkali halide vapors. J Chem Phys 1967;46:2968–73.
[104] Leffler T, Brackmann C, Berg M, Aldén M, Li ZS. Development of an alkali chloride vapour-generating apparatus for calibration of ultraviolet absorption measurements. Rev Sci Instrum 2017;88:023112.
[105] Forsberg C, Broström M, Backman R, Edvardsson E, Badiei S, Berg M, et al. Principle, calibration, and application of the in situ alkali chloride monitor. Rev Sci Instrum 2009;80:023104.
[106] Rowland FS, Makide Y. Upper stratospheric photolysis of NaOH. Geophys Res Lett 1982;9:473–5.
[107] Li B, Sun Z, Li Z, Aldén M, Jakobsen JG, Hansen S, et al. Post-flame gas-phase sulfation of potassium chloride. Combust Flame 2013;160:959–69.
[108] Leffler T, Brackmann C, Berg M, Li Z, Aldén M. On-Line alkali measurement for fuel quality control in biomass-Operated boilers. IFRF Combustion Journal 2016;2016:1–19.
[109] Leffler T, Brackmann C, Berg M, Aldén M, Li Z. Online alkali measurement during oxy-fuel combustion. Energy Proc 2017;120:365–72.
[110] Allgurén T, Andersson K. Chemical interactions between potassium, sulfur, chlorine, and carbon monoxide in air and oxy-fuel atmospheres. Energy Fuel 2020;34:900–6.
[111] Sorvajärvi T, Saarela J, Toivonen J. Optical detection of potassium chloride vapor using collinear photofragmentation and atomic absorption spectroscopy. Opt Lett 2012;37:4011–3.
[112] Sorvajärvi T, Toivonen J. Principles and calibration of collinear photofragmentation and atomic absorption spectroscopy. Appl Phys B 2014;115:533–9.
[113] Sorvajärvi T, Viljanen J, Toivonen J, Marshall P, Glarborg P. Rate constant and thermochemistry for $K + O_2 + N_2 = KO_2 + N_2$. J Phys Chem 2015;119:3329–36.
[114] Lehmusto J, Olin M, Viljanen J, Kalliokoski J, Mylläri F, Toivonen J, et al. Detection of gaseous species during KCl-induced high-temperature corrosion by the means of CPFAAS and CI-APi-TOF. Mater Corros 2020;71:222–31.
[115] Viljanen J, Allgurén T, Wang Y, Li X, Toivonen J, Andersson K, et al. In-situ monitoring of transient gas phase K–Cl–S chemistry in a pilot-scale combustor. Proc Combust Inst 2021;38:1823–31.
[116] Thorin E, Schmidt FM. TDLAS-based photofragmentation spectroscopy for detection of K and KOH in flames under optically thick conditions. Opt Lett 2020;45:5230–3.
[117] Thorin E, Sepman A, Ögren Y, Ma C, Carlborg M, Wennebro J, et al. Quantitative real-time in situ measurement of gaseous K, KOH and KCl in a 140 kW entrained-flow biomass gasifier. Proc Combust Inst 2023;39:1337–45.
[118] Viljanen J, Gall D, Gogolev I, Allgurén T, Andersson K. Detection of alkali path in a pilot-scale combustor using laser spectroscopy and surface ionization — from vapor to particles. Fuel 2023;343:127900.
[119] Thorin E. Quantitative laser diagnostics of gas-phase potassium species in biomass combustion and gasification. Umeå University; 2023.
[120] Ingle J, J D, Crouch SR. Spectrochemical analysis: old tappan. NJ (US): Prentice Hall College Book Division; 1988.
[121] Jones JM, Darvell LI, Bridgeman TG, Pourkashanian M, Williams A. An investigation of the thermal and catalytic behaviour of potassium in biomass combustion. Proc Combust Inst 2007;31:1955–63.
[122] Mason PE, Darvell LI, Jones JM, Williams A. Observations on the release of gas-phase potassium during the combustion of single particles of biomass. Fuel 2016;182:110–7.
[123] Mason PE, Jones JM, Darvell LI, Williams A. Gas phase potassium release from a single particle of biomass during high temperature combustion. Proc Combust Inst 2017;36:2207–15.
[124] Mason PE, Darvell LI, Jones JM, Pourkashanian M, Williams A. Single particle flame-combustion studies on solid biomass fuels. Fuel 2015;151:21–30.
[125] Clery DS, Mason PE, Rayner CM, Jones JM. The effects of an additive on the release of potassium in biomass combustion. Fuel 2018;214:647–55.
[126] Striūgas N, Sadeckas M, Paulauskas R. Investigation of K*, Na* and Ca* flame emission during single biomass particle combustion. Combust Sci Technol 2019;191:151–62.
[127] Weng W, Costa M, Li Z, Aldén M. Temporally and spectrally resolved images of single burning pulverized wheat straw particles. Fuel 2018;224:434–41.
[128] Weng W, Costa M, Aldén M, Li Z. Single particle ignition and combustion of pulverized pine wood, wheat straw, rice husk and grape pomace. Proc Combust Inst 2019;37:2663–71.
[129] He Z, Lou C, Fu J, Lim M. Experimental investigation on temporal release of potassium from biomass pellet combustion by flame emission spectroscopy. Fuel 2019;253:1378–84.
[130] Daily JW. Laser induced fluorescence spectroscopy in flames. Prog Energy Combust Sci 1997;23:133–99.
[131] Smith B, Winefordner JD, Omenetto N. Atomic fluorescence of sodium under continuous-wave laser excitation. J Appl Phys 1977;48:2676–80.
[132] Hynes AJ, Steinberg M, Schofield K. The chemical kinetics and thermodynamics of sodium species in oxygen-rich hydrogen flames. J Chem Phys 1984;80:2585–97.

[133] Weiland KJR, Wise ML, Smith GP. Laser-induced fluorescence detection strategies for sodium atoms and compounds in high-pressure combustors. Appl Opt 1993; 32:4066.
[134] van Eyk PJ, Ashman PJ, Alwahabi ZT, Nathan GJ. Simultaneous measurements of the release of atomic sodium, particle diameter and particle temperature for a single burning coal particle. Proc Combust Inst 2009;32:2099–106.
[135] van Epj, Ashman PJ, Nathan GJ. Mechanism and kinetics of sodium release from brown coal char particles during combustion. Combust Flame 2011;158:2512–23.
[136] Oldenborg RC, Baughcum SL. Photofragment fluorescence as an analytical technique: application to gas-phase alkali compounds. Conference: international laser science conference. Dallas, TX, USA: Los Alamos National Lab., NM (USA); 1985. p. 3. Medium: ED; Size.
[137] Leffler T, Brackmann C, Alden M, Li Z. Laser-induced photofragmentation fluorescence imaging of alkali compounds in flames. Appl Spectrosc 2017;71: 1289–99.
[138] Chadwick BL, Domazetis G, Morrison RJS. Multiwavelength monitoring of photofragment fluorescence after 193 nm photolysis of NaCl and NaOH: application to measuring the sodium species released from coal at high temperatures. Anal Chem 1995;67:710–6.
[139] Chadwick BL, Griffin PG, Morrison RJS. Quantitative detection of gas-phase NaOH using 355-nm multiple-photon absorption and photofragment fluorescence. Appl Spectrosc 1997;51:990–3.
[140] Monkhouse P. On-line diagnostic methods for metal species in industrial process gas. Prog Energy Combust Sci 2002;28:331–81.
[141] Helble JJ, Srinivasachar S, Boni AA, Charon O, Modestino A. Measurement and modeling of vapor-phase sodium chloride formed during pulverized coal combustion. Combust Sci Technol 1992;81:193–205.
[142] Chadwick BL, Morrion RJS. Monte Carlo simulation of radiation trapping and quenching of photofragment fluorescence after 193 nm photolysis of NaCl. J Chem Soc, Faraday Trans 1995;91:1931–4.
[143] Chadwick BL, Ashman RA, Campisi A, Crofts GJ, Godfrey PD, Griffin PG, et al. Development of techniques for monitoring gas-phase sodium species formed during coal combustion and gasification. Int J Coal Geol 1996;32:241–53.
[144] Hartinger K, Nord S, Monkhouse P. Quenching of fluorescence from Na (3 ^{2}P) and K (4 ^{2}P) atoms following photodissociation of NaCl and KCl at 193 nm. Appl Phys B 1997;64:363–7.
[145] Gottwald U, Monkhouse P. Single-port optical access for spectroscopic measurements in industrial flue gas ducts. Appl Phys B 1999;69:151–4.
[146] Gottwald U, Monkhouse P, Bonn B. Dependence of alkali emissions in PFB combustion on coal composition. Fuel 2001;80:1893–9.
[147] Gottwald U, Monkhouse P, Wulgaris N, Bonn B. In-situ study of the effect of operating conditions and additives on alkali emissions in fluidised bed combustion. Fuel Process Technol 2002;75:215–26.
[148] Schürmann H, Unterberger S, Hein K, Monkhouse P, Gottwald U. The influence of fuel additives on the behaviour of gaseous alkali-metal compounds during pulverised coal combustion. Faraday Discuss 2002;119:433–44.
[149] Monkhouse PB, Gottwald UA, Davidsson KO, Lönn B, Engvall K, Pettersson JBC. Phase discrimination of alkali species in PCFB combustion flue gas using simultaneous monitoring by surface ionisation and photofragmentation fluorescence. Fuel 2003;82:365–71.
[150] Schürmann H, Monkhouse P, Unterberger S, Hein KRG. In situ parametric study of alkali release in pulverized coal combustion: effects of operating conditions and gas composition. Proc Combust Inst 2007;31:1913–20.
[151] Erbel C, Mayerhofer M, Monkhouse P, Gaderer M, Spliethoff H. Continuous in situ measurements of alkali species in the gasification of biomass. Proc Combust Inst 2013;34:2331–8.
[152] Weng W, Li S, Costa M, Li Z. Quantitative imaging of potassium release from single burning pulverized biomass char particles. Fuel 2020;264.
[153] He Y, Qiu K, Whiddon R, Wang Z, Zhu Y, Liu Y, et al. Release characteristic of different classes of sodium during combustion of Zhun-Dong coal investigated by laser-induced breakdown spectroscopy. Sci Bull 2015;60:1927–34.
[154] He Y, Whiddon R, Wang Z, Liu Y, Zhu Y, Liu J, et al. Inhibition of sodium release from Zhundong coal via the addition of mineral additives: online combustion measurement with laser-induced breakdown spectroscopy (LIBS). Energy Fuel 2017;31:1082–90.
[155] Liu Y, Wan K, He Y, Wang Z, Xia J, Cen K. Experimental study of potassium release during biomass-pellet combustion and its interaction with inhibitive additives. Fuel 2020;260:116346.
[156] Fatehi H, He Y, Wang Z, Li ZS, Bai XS, Aldén M, et al. LIBS measurements and numerical studies of potassium release during biomass gasification. Proc Combust Inst 2015;35:2389–96.
[157] Liu Y, He Y, Wang Z, Wan K, Xia J, Liu J, et al. Multi-point LIBS measurement and kinetics modeling of sodium release from a burning Zhundong coal particle. Combust Flame 2018;189:77–86.
[158] Viljanen J, Zhao H, Zhang Z, Toivonen J, Alwahabi ZT. Real-time release of Na, K and Ca during thermal conversion of biomass using quantitative microwave-assisted laser-induced breakdown spectroscopy. Spectrochim Acta B Atom Spectrosc 2018;149:76–83.
[159] Yuan Y, Li S, Yao Q. Dynamic behavior of sodium release from pulverized coal combustion by phase-selective laser-induced breakdown spectroscopy. Proc Combust Inst 2015;35:2339–46.
[160] Liu Y, Wang Z, Lv Y, Wan K, He Y, Xia J, et al. Inhibition of sodium release from Zhundong coal via the addition of mineral additives: a combination of online multi-point LIBS and offline experimental measurements. Fuel 2018;212: 498–505.
[161] He Y, Liu S, Liu Y, Wang Z, Sun Z, Xia J, et al. Dynamic zinc and potassium release from a burning hyperaccumulator pellet and their interactions with inhibitive additives. Fuel 2021;286:119365.
[162] van Lith SC, Alonso-Ramírez V, Jensen PA, Frandsen FJ, Glarborg P. Release to the gas phase of inorganic elements during wood combustion. Part 1: development and evaluation of quantification methods. Energy Fuel 2006;20: 964–78.
[163] van Lith SC, Jensen PA, Frandsen FJ, Glarborg P. Release to the gas phase of inorganic elements during wood combustion. Part 2: influence of fuel composition. Energy Fuel 2008;22:1598–609.
[164] Johansen JM, Jakobsen JG, Frandsen FJ, Glarborg P. Release of K, Cl, and S during pyrolysis and combustion of high-chlorine biomass. Energy Fuel 2011;25: 4961–71.
[165] Knudsen JN, Jensen PA, Dam-Johansen K. Transformation and release to the gas phase of Cl, K, and S during combustion of annual biomass. Energy Fuel 2004;18: 1385–99.
[166] Jensen PA, Frandsen F, Dam-Johansen K, Sander B. Experimental investigation of the transformation and release to gas phase of potassium and chlorine during straw pyrolysis. Energy Fuel 2000;14:1280–5.
[167] Davidsson K, Stojkova B, Pettersson JB. Alkali emission from birchwood particles during rapid pyrolysis. Energy Fuel 2002;16:1033–9.
[168] Olsson JG, Jäglid U, Pettersson JB, Hald P. Alkali metal emission during pyrolysis of biomass. Energy Fuel 1997;11:779–84.
[169] Davidsson K, Korsgren J, Pettersson JB, Jäglid U. The effects of fuel washing techniques on alkali release from biomass. Fuel 2002;81:137–42.
[170] Davidsson K, Pettersson JB, Nilsson R. Fertiliser influence on alkali release during straw pyrolysis. Fuel 2002;81:259–62.
[171] Li CZ, Sathe C, Kershaw JR, Pang Y. Fates and roles of alkali and alkaline earth metals during the pyrolysis of a Victorian brown coal. Fuel 2000;79:427–38.
[172] Gallagher NB, Peterson TW, Wendt JOL. Sodium partitioning in a pulverzed coal combustion environment. Symposium (International) on Combustion 1996;26: 3197–204.
[173] Pearce W, Hill J. The mode of occurrence and combustion characteristics of chlorine in British coal. Prog Energy Combust Sci 1986;12:117–62.
[174] Quyn DM, Wu H, Bhattacharya SP, Li C-Z. Volatilisation and catalytic effects of alkali and alkaline earth metallic species during the pyrolysis and gasification of Victorian brown coal. Part II. Effects of chemical form and valence. Fuel 2002;81: 151–8.
[175] Quyn DM, Wu H, Li C-Z. Volatilisation and catalytic effects of alkali and alkaline earth metallic species during the pyrolysis and gasification of Victorian brown coal. Part I. Volatilisation of Na and Cl from a set of NaCl-loaded samples. Fuel 2002;81:143–9.
[176] Kosminski A, Ross DP, Agnew JB. Transformations of sodium during gasification of low-rank coal. Fuel Process Technol 2006;87:943–52.
[177] Zhang Z-H, Song Q, Yao Q, Yang R-M. Influence of the atmosphere on the transformation of alkali and alkaline earth metallic species during rice straw thermal conversion. Energy Fuel 2012;26:1892–9.
[178] Bayarsaikhan B, Hayashi J-i, Shimada T, Sathe C, Li C-Z, Tsutsumi A, et al. Kinetics of steam gasification of nascent char from rapid pyrolysis of a Victorian brown coal. Fuel 2005;84:1612–21.
[179] Chansa O, Luo Z, Eddings EG, Yu C. Determination of alkali release during oxyfuel co-combustion of biomass and coal using laser-induced breakdown spectroscopy. Fuel 2021;289:119658.
[180] Liu Y, He Y, Wang Z, Xia J, Wan K, Whiddon R, et al. Characteristics of alkali species release from a burning coal/biomass blend. Appl Energy 2018;215: 523–31.
[181] Weng W, Aldén M, Li Z. Insight into KOH and KCl release behavior of burning wood and straw pellets using quantitative in situ optical measurements. Proc Combust Inst 2023;39:3239–48.
[182] Cen S, Xiaolin W, Teng L, Li Z, Qinzheng T, Sen L. Potassium release during pulverized biomass combustion in a tubular burner investigated by TDLAS. Fuel 2022;317:123570.
[183] Wang F, Shen B, Yang J, Singh S. Review of mercury formation and capture from CO2-enriched oxy-fuel combustion flue gas. Energy Fuels 2017;31:1053–64.
[184] Li S, Dong M, Lu J, Tian Z, Hou Z, Lin W, et al. Study on the alkali release from the combustion products of a single coal particle by laser ignition. Energy Fuels 2017; 31:4452–60.
[185] Dong M-R, Luo F-S, Huang M, Li S-S, Zhao W-H, Lu J-D. Study on the ignition characteristics and alkali release of single coal particles with additional different forms of potassium. Fuel Process Technol 2020;203:106385.
[186] Chen Y, Charpenay S, Jensen A, Wójtowicz MA, Serio MA. Modeling of biomass pyrolysis kinetics. Symposium (International) on Combustion 1998;27:1327–34.
[187] Yu C, Zhang W. Modeling potassium release in biomass pyrolysis. Progress in Thermochemical Biomass Conversion 2001:1107–15.
[188] Laurendeau NM. Heterogeneous kinetics of coal char gasification and combustion. Prog Energy Combust Sci 1978;4:221–70.
[189] Lindner ER, Wall TF. Sodium ash reactions during combustion of pulverised coal. Symposium (International) on Combustion 1991;23:1313–21.
[190] Fatehi H, Bai XS. A comprehensive mathematical model for biomass combustion. Combust Sci Technol 2014;186:574–93.
[191] Glarborg P, Marshall P. Mechanism and modeling of the formation of gaseous alkali sulfates. Combust Flame 2005;141:22–39.
[192] Akbar S, Schnell U, Scheffknecht G. Modelling potassium release and the effect of potassium chloride on deposition mechanisms for coal and biomass-fired boilers. Combust Theor Model 2010;14:315–29.

[193] Srinivasachar S, Helble JJ, Ham DO, Domazetis G. A kinetic description of vapor phase alkali transformations in combustion systems. Prog Energy Combust Sci 1990;16:303–9.
[194] Han X. Modeling and simulation of SOx and NOx reduction processes in pulverized coal furnaces. Cuvillier Verlag; 2003.
[195] Richter S, Ströhle J, Schnell U, Hein K. Application of the 3D combustion simulation code AIOLOS to the prediction of ash deposition in a pulverised coal-fired utility boiler. In: Proceedings of the 4th international symposium on coal combustion; 1999. p. 18–21.
[196] Schürmann H, Monkhouse P, Unterberger S, Hein K. In situ parametric study of alkali release in pulverized coal combustion: effects of operating conditions and gas composition. Proc Combust Inst 2007;31:1913–20.
[197] Reichelt T. Freisetzung gasformiger Alkaliverbindungen bei atmospharischer und druckaufgeladener Verbrennung. Stuttgart Univ 2001.
[198] Garba MU, Ingham DB, Ma L, Porter RTJ, Pourkashnian M, Tan HZ, et al. Prediction of potassium chloride sulfation and its effect on deposition in biomass-fired boilers. Energy Fuel 2012;26:6501–8.
[199] Hindiyarti L, Frandsen F, Livbjerg H, Glarborg P, Marshall P. An exploratory study of alkali sulfate aerosol formation during biomass combustion. Fuel 2008;87:1591–600.
[200] Tomeczek J, Wacławiak K. Two-dimensional modelling of deposits formation on platen superheaters in pulverized coal boilers. Fuel 2009;88:1466–71.
[201] Niu Y, Tan H, Ma L, Pourkashanian M, Liu Z, Liu Y, et al. Slagging characteristics on the superheaters of a 12 MW biomass-fired boiler. Energy Fuel 2010;24:5222–7.
[202] Wan K, Wang Z, Vervisch L, Xia J, Liu Y, He Y, et al. Large-eddy simulation of alkali metal reacting dynamics in a preheated pulverized-coal jet flame using tabulated chemistry. ASME 2017 power conference joint with ICOPE-17 collocated with the ASME 2017 11th international conference on energy sustainability, the ASME 2017 15th international conference on fuel cell science, engineering and technology, and the ASME 2017 nuclear forum. 2017.
[203] Wan K, Xia J, Vervisch L, Liu Y, Wang Z, Cen K. Modelling alkali metal emissions in large-eddy simulation of a preheated pulverised-coal turbulent jet flame using tabulated chemistry. Combust Theor Model 2018;22:203–36.
[204] Wan K, Vervisch L, Xia J, Domingo P, Wang Z, Liu Y, et al. Alkali metal emissions in an early-stage pulverized-coal flame: DNS analysis of reacting layers and chemistry tabulation. Proc Combust Inst 2019;37:2791–9.
[205] Wan K, Wang Z, Xia J, Vervisch L, Domingo P, Lv Y, et al. Numerical study of HCl and SO_2 impact on potassium emissions in pulverized-biomass combustion. Fuel Process Technol 2019;193:19–30.
[206] Wan K, Wang Z, Xia J, Vervisch L, Domingo P, Lv Y, et al. Numerical study of HCl and SO2 impact on sodium emissions in pulverized-coal flames. Fuel 2019;250:315–26.
[207] Taniguchi M, Okazaki H, Kobayashi H, Azuhata S, Miyadera H, Muto H, et al. Pyrolysis and ignition characteristics of pulverized coal particles. J Energy Resour Technol 2001;123:32–8.
[208] Grant DM, Pugmire RJ, Fletcher TH, Kerstein AR. Chemical model of coal devolatilization using percolation lattice statistics. Energy Fuel 1989;3:175–86.
[209] Berglund M, Fedina E, Fureby C, Tegnér J, Sabel'Nikov V. Finite rate chemistry large-eddy simulation of self-ignition in supersonic combustion ramjet. AIAA J 2010;48:540–50.
[210] Wan K, Xia J, Wang Z, Pourkashanian M, Cen K. Large-eddy simulation of pilot-assisted pulverized-coal combustion in a weakly turbulent jet. Flow, Turbul Combust 2017;99:531–50.
[211] Kazakov A, Frenklach M. Reduced reaction sets based on GRI-Mech 1.2. Berkeley, CA: University of California at Berkeley; 1994. http://www.me.berkeley.edu/drm.
[212] Yahya A, Sye CP, Ishola TA, Suryanto H. Effect of adding palm oil mill decanter cake slurry with regular turning operation on the composting process and quality of compost from oil palm empty fruit bunches. Bioresour Technol 2010;101:8736–41.
[213] Hsieh K, Wang H, Locke BR. Analysis of a gas-liquid film plasma reactor for organic compound oxidation. J Hazard Mater 2016;317:188–97.
[214] Vainio E, Kinnunen H, Laurén T, Brink A, Yrjas P, DeMartini N, et al. Low-temperature corrosion in co-combustion of biomass and solid recovered fuels. Fuel 2016;184:957–65.
[215] Hensel JP, Goff DR, Logan RG, Pineault R, Romanosky Jr RR, Wachter JK. On-line, real-time alkali monitor for process stream analysis. Rev Sci Instrum 1987;58:1647–54.
[216] Yan W, Lou C, Cheng Q, Zhao P, Zhang X. In situ measurement of alkali metals in an MSW incinerator using a spontaneous emission spectrum. Appl Sci 2017;7:263.
[217] Lim M, Matsuoka L. Quantitative analysis and speciation of alkali metal emissions from biomass combustion in a 150 kWth furnace by optical emission spectroscopy. Chem Eng Commun 2019:1–10.
[218] Blevins LG, Shaddix CR, Sickafoose SM, Walsh PM. Laser-induced breakdown spectroscopy at high temperatures in industrial boilers and furnaces. Appl Opt 2003;42:6107–18.
[219] Deguchi Y, Noda M, Fukuda Y, Ichinose Y, Endo Y, Inada M, et al. Industrial applications of temperature and species concentration monitoring using laser diagnostics. Meas Sci Technol 2002;13:R103.
[220] Gottwald U, Monkhouse P, Wulgaris N, Bonn B. Simultaneous detection of nickel and potassium in the flue gas of a fluidised bed coal combustor by excimer laser-induced fragmentation fluorescence. Fuel Process Technol 2003;80:143–53.
[221] Glazer MP, Khan NA, de Jong W, Spliethoff H, Schürmann H, Monkhouse P. Alkali metals in circulating fluidized bed combustion of biomass and coal: measurements and chemical equilibrium analysis. Energy Fuel 2005;19:1889–97.

Prof. Zhihua Wang is a Qiushi distinguished professor of Zhejiang University, vice director of the State Key Laboratory of Clean Energy Utilization. He graduated and got his PhD degree from Department of Energy Engineering at Zhejiang University of China in 2005. As visiting scholar, he studied in the Division of Combustion Physics, Lund University of Sweden with Prof. Marcus Aldén from 2008 to 2010. After back to China, he got the professor title since end of 2011. He got support of Distinguished Young Scholars Fund (2021) and Outstanding Youth Fund (2014) from the National Natural Science Foundation of China, Top-notch Young Professionals support from central government. Director of the Zhejiang University-Lund University Laser Diagnostic Center in Energy Science. His research interesting focused on the clean and efficient combustion of solid fuels with advanced laser diagnostic tools. For release of alkali metal from biomass and coal, his group has developed multi-point LIBS alkali elements measurement and K/Na PLIF atomic measurement technologies. With new developed K/Na release kinetic model, combined with solid fuel combustion, comprehensive reaction flow simulation works has been done with LES and DNS method.

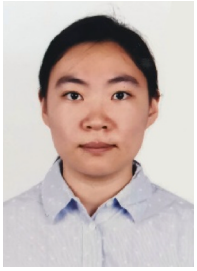

Miss. Siyu Liu is a PhD candidate of the State Key Laboratory of Clean Energy Utilization, Zhejiang University, China. She has completed her undergraduate study from Zhejiang University, China. Her research interests lie in the area of alkali metals release measurement during combustion processes with advanced laser diagnostic tools and kinetics modeling. Her current research is focused on simultaneous measurement of alkali compounds by photolysis.

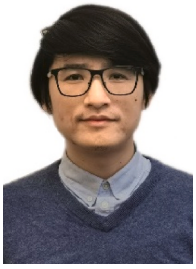

Dr. Wubin Weng is a Researcher at Zhejiang University, China. He graduated and got his PhD degree from Division of Combustion Physics, Department of Physics, at Lund University of Sweden in 2020. He works on the topic of optical diagnostics for quantitative chemistry in biomass thermochemical conversion processes. His research interest is focused on the development and application of different advanced laser-based diagnostics for species and temperature measurement in harsh combustion environments. For the alkali research field, he achieved quantitative detection of major alkali species, including sodium/potassium hydroxide, chloride and atom, in biomass and coal thermochemical conversion processes, through broadband UV absorption spectroscopy, TDLAS, laser-induced photofragmentation and PLIF, and had insight into the fate of alkali species in combustion and gasification processes and the interaction between alkali species and other minor species (chlorine, sulfur, nitrogen).

Prof. Yong He is a full Professor in the College of Energy Engineering at Zhejiang University, China. He graduated from Zhejiang University where he also did his PhD studies and post-doctoral research. He has spent two years in Lund University (Sweden) as a joint PhD student during the PhD study. His research interests include solid fuel combustion, coal gasification, alkali release and control, laser diagnostics and pollutant emission control. He has worked in the field of *in situ* measurement of alkali metals since his PhD study, specifically using the methods of laser induced breakdown spectroscopy (LIBS) and planar laser induced fluorescence (PLIF).

Prof. Marcus Aldén got his PhD in Physics at Lund University in 1983. He was the Head of the Division of Combustion Physics between 1991 and 2019 and he became Professor within the Physics Department at Lund University in 1992. Between 1997 and 2021 Prof. Aldén was Program director of the National Swedish Centre in Combustion Science and Technology, CECOST, and he was part-time visiting professor at Technical University of Eindhoven between 2005 and 2009. Prof. Aldén has been Chairman of the Gordon Conference on *Laser Diagnostics of Combustion* in 2003 and served as Program co-Chair of the 31st International Symposium on Combustion in Heidelberg 2006. He has got several awards, e.g. the ASEA Energy Award, the Akzo Nobel Science Award Sweden, the Håkan Friesinger VOLVO Transportation Award and the 2019 AIAA Aerodynamic Measurement Technology Award. In 2022 Prof. Aldén was awarded the Jürgen Warntatz Gold Medal from the Combustion Institute and the same year he was asked to deliver the Hottel Lecure at the Introduction of the 39th International Symposium on Combustion in Vancouver.

The scientific activities have ranged from very fundamental studies of laser-matter interactions to industrially real-world applications. Of his scientific contributions could be mentioned the first multiple-point spatially-resolved LIF measurements in flames, the first detection of oxygen atoms and CO molecules in flames, the development of dual-broadband rotational CARS, spatially resolved polarization spectroscopy applied in flames and the development of a high repetition rate laser/detector system for studies of flames and engines and the development of thermographic phosphors for combustion applications. Prof Aldén is member of the Royal Swedish Academy of Engineering Sciences, IVA, the Royal Swedish Academy of Sciences, KVA, and of The Royal Physiographic Society in Lund. In 2009 and in 2015 he got Advanced Investigators Grants from the European Research Council, ERC. He has Honorary Professorships at Xian Jiaotong University and at Tianjin University and is Guest professor at Zhejiang University, all in China.

Prof. Zhongshan Li is a full professor in the Division of Combustion Physics of Lund University (LU), Sweden. He performed his undergraduate study in Jilin University, China and earned his PhD of physics in the Division of Atomic Physics of LU at 2000. He joined the Division of Combustion Physics in the same year and for the last twenty years he has supervised 12 PhD students in the field of combustion research. He has been adjoint professor of Zhejiang University and Tianjin University.

His research interests cover laser combustion diagnostics, turbulent combustion, plasma assistant combustion and carbon-neutral/free fuels. In relation to alkali metal thermochemical processes in biomass utilization, his group has recently achieved *in situ* quantitative optical measurements in practical combustion environments, which enable quantitative analysis of the detail kinetics related to alkali atoms, chlorine and hydroxide compounds.